View Article Online
View Journal

Dalton Transactions

An international journal of inorganic chemistry

Accepted Manuscript

This article can be cited before page numbers have been issued, to do this please use: A. Kasprzak and P. A. Guka, *Dalton Trans.*, 2020, DOI: 10.1039/D0DT01366H.

ROYAL SOCIETY OF CHEMISTRY

rsc.li/dalton

View Article Online
DOI: 10.1039/D0DT01366H

COMMUNICATION

Ferrocene-Templated Pd-Bearing Molecular Reactor

Artur Kasprzak* and Piotr A. Guńka

Received 00th January 20xx,
Accepted 00th January 20xx

DOI: 10.1039/x0xx00000x

The high-yield, chromatography-free syntheses of the ferrocene-templated molecular cage and its Pd-bearing derivative, are presented. The formation of the symmetric cage-type structure was confirmed by single-crystal X-ray diffraction analysis. The Pd-bearing cage was used as an innovative catalyst for the efficient synthesis of 1,1'-biphenyls at mild conditions. The presented catalyst is reusable and 1,1'-biphenyl can be obtained efficiently in a gram scale process.

The design of supramolecular systems comprising π-conjugated building blocks draws an unflagging interest in the supramolecular chemistry.[1-9] An important example of application of supramolecular frameworks is their use as catalysts.[10-15] Such machines, termed as molecular reactors, may enable the acceleration of the catalytic reaction or may induce stereo- or regioselectivity of the process. Commonly, the driving force responsible for this feature is the ability to recognize aromatic molecules.

1,3,5-Triphenylbenzene framework or its nitrogen-containing derivatives are the widely used motifs for the construction of the supramolecular frameworks possessing various prospective applications.[16-19] In the recent years, an emerging field of application of 1,3,5-triphenylbenzene-type motifs is the synthesis of the symmetric molecular cages.[20-28] Such structures are characterized by the organized cavity. In fact, the synthesis of such symmetric molecular cages may be challenging; reported reaction yields vary between 15-80%. However, the efforts are worthwhile, because the proper selection of the building blocks results in a tuneable cavity size and properties. For example, in 2019 Stoddart et al. reported the synthesis of a triazine-templated cage.[20] This cage was obtained with a combined yield of 14%. The specific inter-platform distance of 11.0 Å enabled accommodation of several molecules within confined space.

Faculty of Chemistry, Warsaw University of Technology, Noakowskiego Str. 3, 00-664 Warsaw, Poland; e-mail: akasprzak@ch.pw.edu.pl

† Electronic Supplementary Information (ESI) available: Experimental section and compounds characterization data, crystal data, molecular recognition experiments, calculation of binding parameters, reaction kinetics data. See DOI: 10.1039/x0xx00000x

We envisioned that the 1,1'-ferrocene motif is the ideal candidate for the construction of the novel symmetric molecular cage bearing the 1,3,5-triphenylbenzene moiety. Herein, we report the high-yield and chromatography-free methods for the construction of such cage compound and its Pd-bearing derivative, exhibiting the ability to bind aromatic molecules. The Pd-decorated cage was employed as the innovative catalyst for the fast and efficient synthesis of 1,1'-biphenyls. We envision that our findings will stimulate the progress in the design, chemistry and applications of supramolecular frameworks.

The synthesis of the ferrocene-templated cage (**3**) is presented in **Fig. 1a, step I**. Acid-catalysed imine-bond formation between 1,1'-diformylferrocene (**1**) and 1,3,5-tris(4-aminophenyl)benzene (**2**) afforded **3** in 95% yield.[29] Such high synthesis yield is an exceptional value in the molecular cages chemistry. Additionally, pure **3** was obtained by filtration, without the need to perform further chromatographic purification. The selective formation of **3** was confirmed with a series of characterization techniques; combination of NMR spectroscopy, Fourier-transform infrared spectroscopy (FT-IR), UV-Vis spectroscopy, high-resolution mass spectrometry (HRMS) and elemental analysis confirmed the formation of pure cage **3**.[30] The ^{1}H NMR spectrum of **3** (**Fig. 2c**) comprises six groups of signals, only. It suggested that the obtained molecular cage is highly symmetric (average D_{3h} symmetry in solution).

Cage **3** crystallizes in the rhombohedral $R\bar{3}$ space group with a third of the molecule in the asymmetric unit (**Fig. 1b-c**).[31] The molecule exhibits the symmetry of C_3 point group and the imine moieties are in the *E* configuration. The central benzene ring is practically coplanar with peripheral cyclopentadienyl rings on one side of the molecule with root mean square displacement of carbon atoms from the average plane of only 0.081 Å. A root mean square displacement (RMSD) of carbon atoms from an average plane of the rings on the other side of the molecule is significantly larger (0.270 Å). Similarly as in 1,3,5-triphenylbenzene, the middle phenyl rings are twisted out of the planes of the central rings. This is due to steric repulsion between hydrogen atoms of the middle rings and that of the central ring as well as imine-type hydrogen atoms, as evidenced by the dihedral angles between average ring planes the top

(27.89(12)º) and bottom (23.06(12)º) sides of **3**. The middle phenyl rings from the top and bottom parts are close to being parallel with a dihedral angle of 4.88(12)º which maximizes π stacking interactions as well as minimizes steric repulsion between hydrogen atoms. The central benzene rings are parallel with a dihedral angle of 0.00(11)º. The separation between their centres equals 3.7342(17) Å. This value is larger than the interlayer separation of graphene layers in graphite (3.354 Å). The distance between imine nitrogen atoms is shorter (3.680(3) Å).[33] Molecules pack in layers via dispersion interactions and C–H···N hydrogen bonds, forming two symmetry-independent types of smaller and larger voids in 1:3 ratio.[34] The layers in turn form 3D crystal via dispersion and π stacking interactions.[35]

We envisaged that **3** might be capable to bind aromatic molecules by means of non-covalent forces. This hypothesis was based on the presence of two, π-conjugated 1,3,5-triphenylbenzene motifs that may induce non-covalent interactions with other π-electron systems. We did not anticipate the formation of host-guest complexes with the inclusion of guest molecules within the cavity of **3**, since its X-ray structure revealed that there is no space to entrap the aromatic molecules there. Thus, we considered arrangements of the aromatic molecules on the cage or along the rim of triphenylbenzene moiety, *e.g.*, a parallel displaced π-π stacking and/or aromatic-aromatic interactions at peripheral parts of the cage.[37] To uncover binding modes, interactions between **3** and various aromatics (**G-1**-**G-6**, **Fig. 2a**) were tracked with NMR spectroscopy (the spectra for the representative interactions between **3** and **G-1** are presented in **Fig. 2**[36a]). Upon the addition of the aromatic molecule (800 mol%), the upfield shifts for the H_a, H_b and H_c were observed in the ^{1}H NMR spectrum of **3** (**Fig. 2c**). This feature was ascribed to the π-π interactions between **3** and aromatic molecules.[20] Simple benzene derivatives (**G-1**, **G-2**) underwent higher upfield shifts in comparison to the highly conjugated, unsubstituted aromatics (**G-3**–**G-5**).[38] The presence of the electron withdrawing substituent in the pyrene skeleton (**G-6**) provided stronger binding with **3** than for the native pyrene (**G-5**). The interactions with **G-2** and **G-6** were also tracked with ^{1}H-^{1}H ROESY NMR and ^{1}H DOSY NMR (**Fig. 2d-e** for representative **G-1**[39]). The cross-correlations between H_a, H_b and H_c and the protons of **G-1** – **G-6** were observed in the ^{1}H-^{1}H ROESY NMR spectrum (**Fig. 2d**). It means that the distance between the interacting protons ($H_{\{G\text{-}1\text{–}G\text{-}6\}}$ ↔ H_a, H_b and H_c) is shorter than 4-4.5 Å. Thus, we anticipate that the aromatic molecules were accommodated near {H_a, H_b and H_c}-oriented sites of **3** and were located further (>4.5 Å) from Fc moiety. We anticipate that this binding mode follows a parallel displaced π-π stacking geometry.[37] The lowering of the diffusion coefficient for **3** after the addition of the aromatic molecule was observed in the ^{1}H DOSY NMR spectra (**Fig. 2e**). These features were previously reported to stand for the non-covalent interactions.[20,40] DOSY NMR experiments suggested the formation of a single non-covalent systems (all peaks showed the same diffusion coefficient).

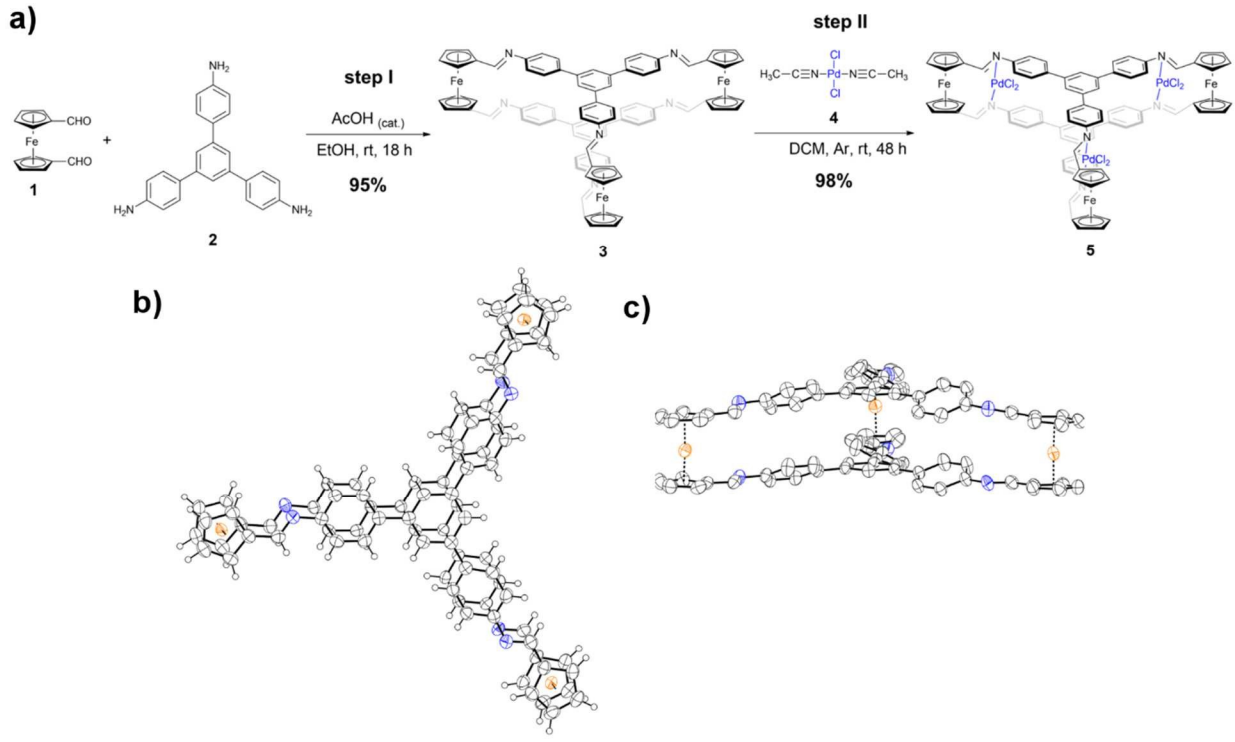

Fig. 1. (**a**) Synthesis of 3 (step I) and 5 (step II); Molecular structure of 3: (**b**) top view, (**c**) side view. Thermal ellipsoids are drawn at 50% probability level. Hydrogen atoms were omitted for clarity in (**c**)

View Article Online
DOI: 10.1039/D0DT01366H

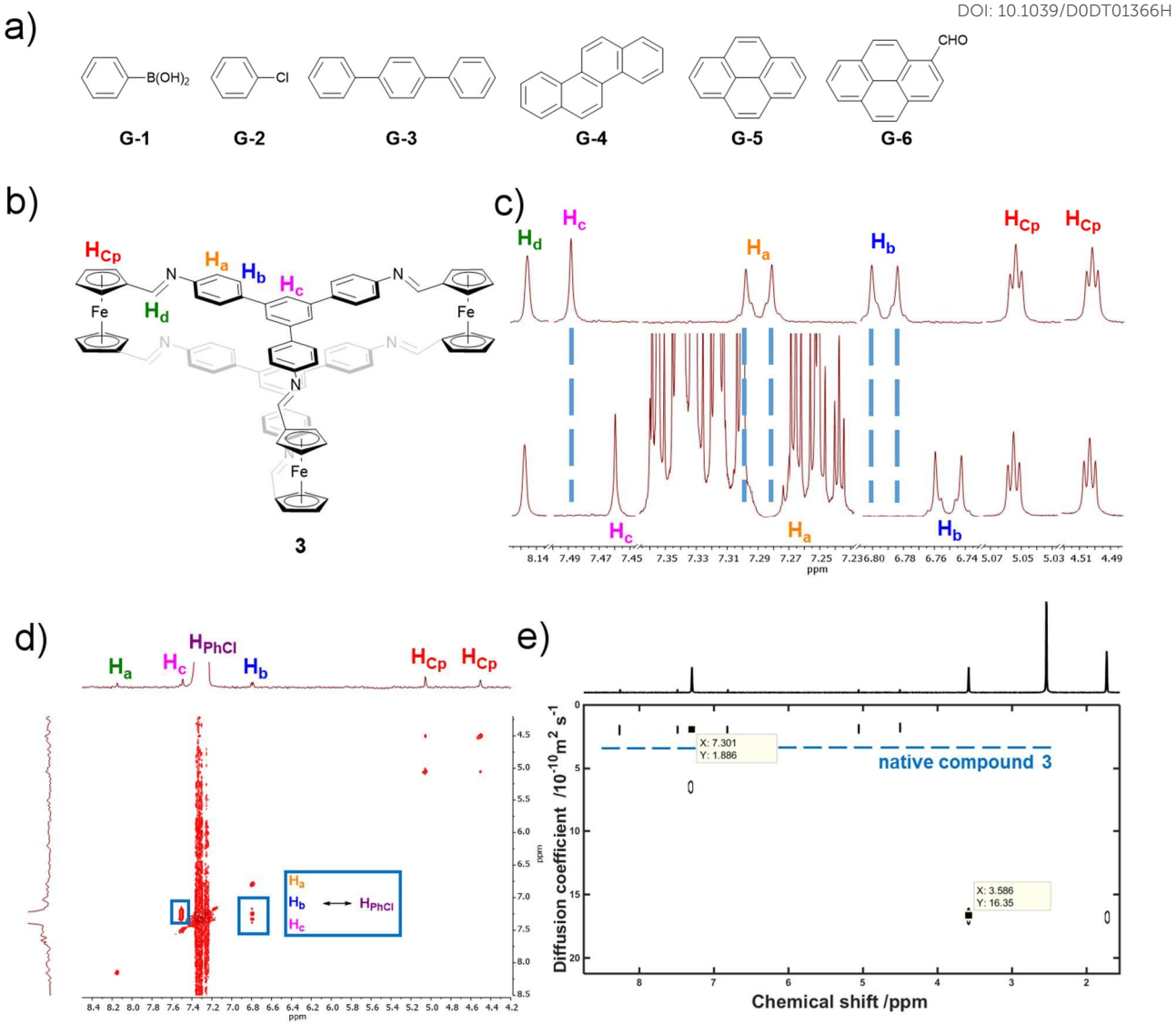

Fig. 2. (**a**) Structures of the aromatic molecules tested; (**b**) atom labels for NMR investigations with **3**; (**c**) ^{1}H NMR spectrum of **3** (top) and **3** in the presence of **G-2** (800 mol%; bottom); (**d**) inset of the ^{1}H-^{1}H ROESY NMR spectrum of **3** in the presence of **G-2** (800 mol%; crucial-cross correlations are marked); (**e**) ^{1}H DOSY NMR spectrum of **3** in the presence of **G-2** (800 mol%)

To get an insight into the binding parameters of these non-covalent systems, association constants (K_{app}) and free energies (ΔG) were estimated based on PL experiments (UV-Vis and PL titration experiments were performed, PL was found as the more sensitive technique).[36b] The studied non-covalent systems featured the lowering of the emission intensity for **3** after addition of further portions of an aromatic molecule. The change in the emission intensity differed between the systems. It was a result of different K_{app} and ΔG. The association constant values were estimated.[36b-c] The non-covalent systems exhibited good binding parameters with ΔG equal to −16.1 – −14.2 kJ·mol^{-1} at 298.15 K (**Table 1**). **G-6** exhibited the highest binding parameters (**Table 1**, entry 6). For the non-covalent system of **G-6** exhibiting the highest K_{app} and the lowest ΔG, these parameters evaluated from PL experiments were also compared with the respective values obtained from ^{1}H DOSY NMR experiment. These results were highly consistent (PL analysis: 650 M^{-1}, ^{1}H DOSY NMR analysis: 658 M^{-1}).[36b] **G-1** and **G-2** were characterized by lower ΔG values than **G-3**-**G-5** (**Table 1**, entries 1-5). It suggested that simple benzene derivatives were bound stronger by **3** in comparison to unsubstituted, conjugated aromatics. This trend is consistent with the outcomes from ^{1}H NMR assays.

Job's plot analyses suggested 1:3 binding stoichiometry for the interactions between **3** and **G-1** or **G-2**, whilst 1:1 stoichiometry was found for **G-3**–**G-6**.[36b] Following these estimated stoichiometries, the formation of the non-covalent systems was further confirmed with ESI-MS analysis.[41a,b] The mixtures of **3** and **G-1**–**G-6** were analysed. Beside the peaks coming from the native cage **3** and unbound **G-1**–**G-6**, the peaks

originating from the presence of the non-covalent systems were clearly found.[41c] It is noteworthy that ESI-MS studies supported the systems' stoichiometries estimated from PL (1:1 stoichiometry for **G-3**–**G-6** and 1:3 stoichiometry for **G-1** and **G-2**).

In order to exclude any possible non-covalent interaction between an aromatic molecule and a 1,3,5-triphenylbenzene-templated compound, the ^{1}H NMR, ^{1}H-^{1}H ROESY NMR and ^{1}H DOSY NMR spectra of 1,3,5-tris(4-aminophenyl)benzene (**2**) were measured in the presence of **G-6** (800 ml%). No significant changes between the spectra of native **2** and after addition of **G-6**, were found.[41d] These findings revealed that the cage-type architecture of **3** is essential for providing the binding property. To further support this claim, ESI-MS spectrum of the mixture of **2** and **G-6** (300 mol%) was measured.[41c] If a non-covalent system was formed, the significant peak of m/z > 580 shall be observed. The peaks that were ascribed to native **2** (m/z = *ca*. 230) and native **G-6** (m/z = *ca*. 352) were found, only. No peak coming from the non-covalent system (m/z > 580) was found.

Table 1. Binding parameters for the studied systems

Entry	Aromatic molecule	Non-covalent system stoichiometry (**3** : aromatic molecule)	K_{app}[a,b]	ΔG /kJ·mol^{-1}
1	**G-1**	1:3	6.1(1)·10^2 M^{-3}	−15.9
2	**G-2**	1:3	5.9(2)·10^2 M^{-3}	−15.8
3	**G-3**	1:1	3.1(2)·10^2 M^{-1}	−14.2
4	**G-4**	1:1	3.5(3)·10^2 M^{-1}	−14.5
5	**G-5**	1:1	4.0(3)·10^2 M^{-1}	−14.9
6	**G-6**	1:1	6.5(2)·10^2 M^{-1}	−16.1

[a] because of some complexity of the studied non-covalent systems, K_{app} values should be treated as the approximate ones and they elucidate the trend of these interactions; [b] standard errors were estimated based on the outcomes from least squares regression method for the I_0/I = f(C_{ar}) linear fits (standard error of slope of curve)

Cage **3** comprises the imine-type nitrogen atoms located in a vertical orientation. We envisioned that this part of **3** might play a role of a metal coordination site.[43-48] Due to the importance of Pd in many fields of applied science, *e.g*., catalysis, our goal was to incorporate three Pd residues to **3**. The chromatography-free protocol for the synthesis of Pd-decorated cage (**5**) was successfully developed (**Fig. 1a, step II**). Treatment of **3** with bis(acetonitrile)dichloropalladium(II) (**4**) afforded **5** in high yield (98%).[29] Pure **5** was obtained by means of filtration and was fully characterized.[30] NMR spectroscopy revealed that the symmetric cage-type structure of cage was retained after the incorporation of the $PdCl_2$ residues; similarly to the ^{1}H NMR spectrum of **3**, the ^{1}H NMR spectrum of **5** comprises six groups of signals, indicating the average D_{3h} symmetry in solution.[42]

With the Pd-bearing cage **5** at hand, we began to engineer its application. A breakthrough at this point of our project occurred when we had noted the structural similarity between **5** and [1,1'-bis(diphenylphosphino)ferrocene]dichloropalladium(II), commercially used catalyst for the Suzuki-Miyaura reaction[43-45]. Inspired by this resemblance, we decided to study the pioneering application of **5** as the catalyst for 1,1'-biphenyl synthesis. The optimization experiments gave remarkable results.[49] These trials revealed that 1,1'-biphenyl can be obtained in 99% yield at mild conditions (room temperature) in 20 minutes, only (**Table 2**, entry 1).[50] Importantly, 0.5 mol% of **5** was used, only. Having achieved for the first time such exceptional results of the Suzuki-Miyaura reaction employing easy-to-perform procedure without a use of a sophisticated instrument (*e.g*., microwave reactor), we were curious whether our method can be applied for other starting materials. To our delight, the substituted 1,1'-biphenyls were efficiently obtained (96-98%) in very short reaction times (**Table 2**, entries 2-5). We believe that the designed cage architecture is a new class of good ligand of Pd catalyst. Secondly, we showed above that the designed cage non-covalently interacts with aromatic molecules. In the light of calculated binding parameters, one might also consider the influence of non-covalent interactions with aromatic molecules on providing encouraging reaction parameters. We hypothesised that the designed cage architecture giving rise to the non-covalent interaction feature, facilitated the contact between the reagents towards the catalytic process. To support these hypotheses, the reaction rates under ^{1}H NMR conditions were estimated for the reaction between phenylboronic acid and chlorobenzene (**Fig. 3**; Michaelis-Menten method was employed).[50b-c] No reaction was found without a catalyst added. On the contrary, the rate constant for the reaction in the presence of **5** (k_{cage}) was found to be *ca*. 8.5·10^{-3} M^{-1}·s^{-1}. This feature elucidated the usefulness of the designed catalyst and was the first premise of the accelerating effect of non-covalent interactions during the catalytic process. In order to further support this claim, the respective reaction was monitored in the presence of binding competing aromatic molecule **G-6** (**Fig. 3**). We envisioned that **G-6** might prevent the non-covalent interactions between our cage-type catalyst and phenylboronic acid or chlorobenzene, because of the competitive Δ*G* values between these systems (compare the Δ*G* values for **G-1**, **G-2** and **G-6; Table 1**). In other words, **G-6** might "block" the proper arrangement of phenylboronic acid or chlorobenzene in their system with **5**, thus, highly limits the acceleration of catalytic process. Any inhibiting effect of **G-6** shall result in lowering of the reaction rate of the studied catalytic process. With this competing molecule present, reaction rate was indeed *ca*. 100-fold lower ($k_{cage+G-6}$ = *ca*. 8.2·10^{-5} M^{-1}·s^{-1}). This feature was ascribed to the

inhibiting effect of **G-6**; in other words, non-covalent interactions between **5** and **G-6** highly prevented binding of the reactants (chlorobenzene, phenylboronic acid) by **5**. These experiments clearly suggested an influence of aromatic molecule binding on the designed catalytic process. We also anticipate that the presence of three units of Pd per one unit of cage might play a role in this process.

Encouraged by the above-presented results, we further studied the designed methodology towards its prospective offering to industrial users. We found that 1,1'-biphenyl can be obtained in a gram scale reaction (**Table 2**, entry 6). Moreover, the catalyst can be easily recovered from the reaction mixture (after the catalytic reaction **5** was precipitated and filtered[51]) and reused in the next ten reaction cycles without any loss of its high catalytic activity.[52] In general, the process parameters (that is: the reaction yield and time, amount of the catalyst) remain unchanged between the experiments (compare entries 1 and 6 in **Table 2**). These prominent results showed that scaling-up the reaction and the use of recovered catalyst, did not affect its excellent catalytic performance. To the best of our knowledge, such parameters have never been studied before in the molecular cages chemistry.

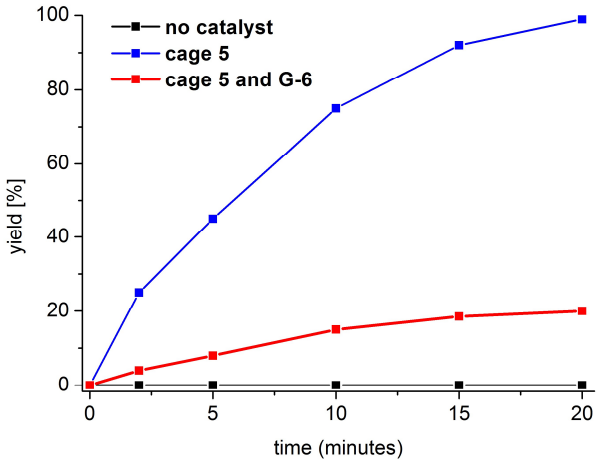

Fig. 3. Kinetic curves for the designed catalytic process

Table 2. The data on the synthesis of 1,1'-biphenyls

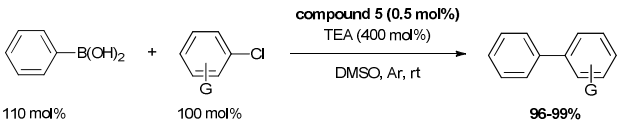

Entry	G	reaction time [minutes]	Yield [%][a]
1	H[b]	20	99
2	4-CH_3[b]	21	98
3	4-NO_2[b]	26	96
4	4-Br[b]	23	97
5	2-Br[b]	25	96
6	H[c]	21	99

[a] isolated yields; [b] reaction scale: 0.50 mmol; [c] reaction scale: 10.00 mmol

View Article Online
DOI: 10.1039/D0DT01366H

Conclusions

In conclusion, the efficient, easy-to-perform and chromatography-free synthesis of the new type of molecular cage comprising the ferrocene and 1,3,5-triphenylbenzene motifs was obtained. The constructed molecular cage exhibits the property to bind aromatic molecules. This cage can be used as the effective ligand of Pd catalyst. The Pd-decorated cage ('molecular reactor') was applied for the very efficient and fast synthesis of various 1,1'-biphenyls at mild conditions. The developed catalyst is also interesting towards its prospective use in industrial practice. We believe this work significantly improves the state-of-the-art of the chemistry of supramolecular systems and sheds a light on applications of such new type of cage compounds.

Acknowledgments

The financial support from Warsaw University of Technology (WUT) is acknowledged. We thank Dr. Magdalena Poplawska (WUT) for helpful discussions, Dr. Krzysztof M. Borys (WUT) for providing 1,1'-diformylferrocene and Dr. Maciej Dranka (WUT) for his assistance in single-crystal X-ray analyses. The Authors would like to thank the Reviewers for their important and constructive comments.

Conflicts of interest

There are no conflicts to declare.

Notes and references

1 F. J. M. Hoeben, P. Jonkheijm, E. W. Meijer and A. P. H. J. Schenning, *Chem. Rev.*, 2005, **105**, 1491.
2 M. Saito, H. Shinokubo and H. Sakurai, *Mater. Chem. Front.*, 2018, **2**, 635.
3 Z.-T. Li, Beilstein J. Org. Chem., 2015, **11**, 2057.
4 T. Ogoshi, T.-a. Yamagishi and Y. Nakamoto, *Chem. Rev.*, 2016, **116**, 7937.
5 M. M. Cetin, Y. Beldjoudi, I. Roy, O. Anamimoghadam, Y. J. Bae, R. M. Young, M. D. Krzyaniak, C. L. Stern, D. Philp, F. M. Alsubaie, M. R. Wasielewski and J. F. Stoddart, *J. Am. Chem. Soc.*, 2019, **141**, 18727.
6 S. R. Scottwell and J. D. Crowley, *Chem. Commun.,* 2016, **52**, 2451.
7 Y. Yakiyama, T. Hasegawa and H. Sakurai, *J. Am. Chem. Soc.* 2019, **141**, 18099.
8 P. Li, P. Li, M. R. Ryder, Z. Liu, C. L. Stern, O. K. Farha and J. F. Stoddart, *Angew. Chem. Int. Ed.*, 2019, **58**, 1664.
9 M. Kołodziejski, A. R. Stefankiewicz and J.-M. Lehn, *Chem. Sci.*, 2019, **10**, 1836.
10 C. J. Easton, S. F. Lincoln, L. Barr and H. Onagi, *Chem. Eur. J.*, 2004, **10**, 3120.
11 A. S. Lubbe, T. van Leeuwen, S. J. Wezenberg and B. L. Feringa, *Tetrahedron,* 2017, **73**, 4837.

12 J. Teyssandier, S. De Feyter and K. S. Mali, *Chem. Commun.,* 2016, **52**, 11465.
13 M. S. Shad, P. V. Santhini and W. Dehaen, *Beilstein J. Org. Chem.,* 2019, **15***,* 2142.
14 L. Barr, S. F. Lincoln and C. J. A. Easton, *Supramolecular Chem.,* 2005, **17**, 547.
15 J. Kang and J. Rebek, *Nature,* 1997, **385**, 50.
16 K. Gontarczyk, W. Bury, J. Serwatowski, P. Wieciński, K. Woźniak, K. Durka and S. Luliński, *ACS Appl. Mater. Interfaces,* 2017, **9**, 31129.
17 M. Taddei, F. Costantino, R. Vivani, S. Sabatini, S.-H. Lim and S. M. Cohen, *Chem. Commun.,* 2014, **50**, 5737.
18 D. Kaleeswaran, P. Vishnoi, R. Murugavel, *J. Mater. Chem. C,* 2015, **3**, 7159.
19 V. K. Maka, A. Mukhopadhyay, G. Savitha and J. N. Moorthy, *Nanoscale,* 2018, **10**, 22389.
20 T. Jiao, K. Cai, Z. Liu, G. Wu, L. Shen, C. Cheng, Y. Feng, C. L. Stern and J. F. Stoddart, H. Li, *Chem. Sci*., 2019, **10**, 5114.
21 Z. Wang, Y. Luo, YT.-L. Zhai, H. Ma, J.-J. Chen, Y. Shu and C. Zhang, *Org. Lett*., 2016, **18**, 4574.
22 C. Mejuto, G. Guisado-Barrios, D. Gusev and E. Peris, *Chem. Commun.,* 2015, **51**, 13914.
23 Q.-Q. Wang, N. Luo, X.-D. Wang, Y.-F. Ao, Y.-F. Chen, J.-M. Liu, C.-Y. Su, D.-X. Wang and M.-X. Wang, *J. Am. Chem. Soc*., 2017, **139**, 635.
24 Z. Wang, H. Ma, T.-L. Zhai, G. Cheng, Q. Xu, J.-M. Liu, J. Yang, Q.-M. Zhang, Q.-P. Zhang, Y.-S. Zheng, B. Tan and C. Zhang, *Adv. Sci.,* 2018, **5**, article no. 1800141 (7 pages).
25 B. M. Schmidt, T. Osuga, T. Sawada, M. Hoshino, M. Fujita, *Angew. Chem. Int. Ed.* **2016**, *55*, 1561.
26 W. Cullen, H. Takezawa and M. Fujita, *Angew. Chem. Int. Ed*., 2019, **58**, 9171.
27 Y. Zhou, H. Li, T. Zhu, T. Gao and P. Yan, *J. Am. Chem. Soc*., 2019, **141**, 19634.
28 F. Beuerle and B. Gole, *Angew. Chem. Int. Ed*., 2018, **57**, 4850.
29 For the experimental details, see Section S1, ESI.
30 For the spectra and data, see Sections S1-S4, ESI.
31 Crystal Data for cage **3**: $C_{84}H_{60}Fe_3N_6$ (M =1320.94 g/mol), trigonal, space group $R\bar{3}$ (no. 148), color dark pink, a = 24.9627(11) Å, c = 20.5795(11) Å, V = 11105.8(11) Å^3, Z = 6, T = 293 K, μ(Mo Kα) = 0.626 mm^{-1}, D_{calc} = 1.185 g/cm^3, 11433 reflections measured (6.778° ≤ 2Θ ≤ 53.998°), 5389 unique (R_{int} = 0.0362, R_{sigma} = 0.0644) which were used in all calculations. The final R_1 was 0.0467 (I >2σ(I)) and wR_2 was 0.1154 (all data); GoF = 0.964. For additional structure determination and crystal packing data, see Section S5, ESI. CCDC 1970365 contains supplementary crystallographic data for this paper. These data can be obtained free of charge from the joint CCDC's and FIZ Karlsruhe's service to view and retrieve structures via https://www.ccdc.cam.ac.uk/structures/.
32 For the crystal structure of 1,3,5-triphenylbenzene, see: M. S. Farag, *Acta Cryst*., 1954, **7**, 117.
33 The separation between centers of cyclopentadienyl anions interacting with iron cations is even shorter (3.306(5) Å).
34 For molecular packing in layers, see Fig. S9, ESI.
35 See Fig. S10, ESI.
36 (**a**) For the NMR data for the interactions of **3** with **G-2** – **G-6**, see Section S5, ESI; (**b**) For the additional discussion, spectra and calculation of binding parameters, see Section S9, ESI; (**c**) Stern-Volmer method was used, for details of this methodology, see for example: A. M. Pyle, J. P. Rehmann, R. Meshoyrer, C. V. Kumar, N. J. Turro and J. C. Barton, *J. Am. Chem. Soc*., 1989, **111**, 3051 or A. Kasprzak and H. Sakurai., *Dalton Trans*., 2019, **48**, 17147.
37 (**a**) R. Thakuria, N. K. Nath and B. K. Saha, Cryst. Growth Des., 2019, **19**, 523; (**b**) R. P. Matthews, T. Welton and P. A. Hunt, *Phys. Chem. Chem. Phys.,* 2014, **16**, 3238; (**c**) S. E. Wheeler, T.J. Seguin, Y. Gua, and A.C. Doney, *Acc. Chem. Res*., 2016, **49**, 1061; (**d**) D. B. Ninković, J. P. Blagojević Filipović, M. B. Hall, E. N. Brothers and S. D. Zarić, *ACS Cent. Sci*., 2020, **6**, 420.
38 See the data in Table S2, ESI.
39 For the spectra on binding studies with **G-6**, see Figs. S17-S18, ESI.
40 A. Kasprzak, K. Borys, S. Molchanov and A. Adamczyk-Wozniak, *Carbohydr. Polym.*, 2018, **198**, 294.
41 (**a**) Q. He, Y.-F. Ao, Z.-T. Huang and D.-X. Wang, *Angew. Chemie Int. Ed.*, 2015, **54**, 11785; (**b**) E. Darii, S. Alves, Y. Gimbert, A. Perret and J.-C. Tabet, *J. Chromatogr. B*, 2017, **1047**, 45; (**c**) For the ESI-MS spectra, see Section S11, ESI; (**d**) For the spectra, see Figs. S19-S23, ESI.
42 See Fig. S13, ESI.
43 T. Hayashi, M. Konishi, Y. Kobori, M. Kumada, T. Higuchi and K. Hirotsu, *J. Am. Chem. Soc.,* 1984, **106**, 158.
44 T. J. Colacot, H. Qian, R. Cea-Olivares and S. Hernandez-Ortega, *J. Organomet. Chem*., 2001, **637–639**, 691.
45 R. S. Chauhan, D. B. Cordes, A. M. Z. Slawin, S. Yadav and C. Dash, *Inorg. Chim. Acta.,* 2018, **478**, 125.
46 J. Wiedermann, K. Mereiter and K. Kirchner, *J. Mol. Cat. A,* 2006, **257**, 67.
47 G. R. Owen, A. J. P. White and R. Vilar, *Organometallics,* 2009, **28**, 5783.
48 H. Hu, D. Chen, H. Gao, L. Zhong and Q. Wu, *Polym. Chem*., 2016, **7**, 529.
49 Optimization experiments: Table S1, ESI.
50 (**a**) For the experimental conditions, see Subsection S1.6, ESI; (**b**) For details of this methodology, see for example: J. Jiao, Z. Li, Z. Qiao, X. Li, Y. Liu, J. Dong, J. Jiang and Y. Cui, *Nat. Commun.,* 2018, **9**, article number 4423, 8 pages; (**c**) For the additional discussions and experimental details, see Section S10, ESI.
51 For details, see Subsection S1.6, ESI.
52 For the data on the reusability studies, see Fig. S31, ESI.

View Article Online
DOI: 10.1039/D0DT01366H

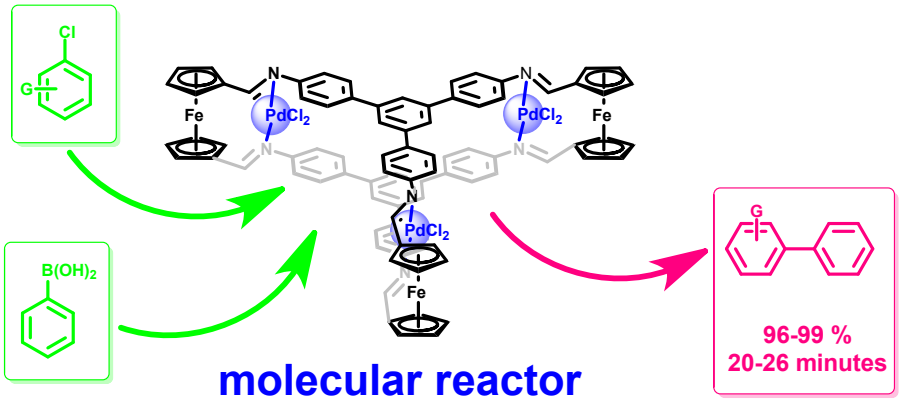

Synthesis of novel ferrocene-templated cage and palladium derivative of this cage, as well as the use of this cage as molecular reactor toward efficient 1,1′-biphenyl synthesis, are presented.

View Article Online
DOI: 10.1039/D0DT01366H

Electronic Supplementary Information (ESI) for

Ferrocene-Templated Pd-Bearing Molecular Reactor

Artur Kasprzak*, Piotr A. Guńka

Faculty of Chemistry, Warsaw University of Technology, Noakowskiego Str. 3, 00-664 Warsaw, Poland

* corresponding author e-mail: akasprzak@ch.pw.edu.pl

Table of contents

S1. Experimental section....2
S1.1 Materials and methods....2
S1.2. Synthesis of the starting materials....2
S1.3 Synthesis of ferrocene-templated molecular cage (**3**)....3
S1.4 Interactions between the ferrocene-templated molecular cage (**3**) and aromatic molecules – ^{1}H NMR....4
S1.5 Synthesis of ferrocene-templated Pd-bearing cage (**5**)....4
S1.6 General procedure for the synthesis of 1,1′-biphenyls using ferrocene-templated Pd-bearing cage (**5**) as the catalyst....5
S2. NMR spectra....9
S3. IR spectra....12
S4. UV-Vis spectra for compound **3** and compound **5**....13
S5. Crystal structure analyses on cage **3**....14
S6. Interactions with aromatic molecules – NMR assays....18
S7. Synthesis of 1,1′-biphenyls – ^{1}H NMR spectra....27
S8. Recyclability studies....30
S9. UV-Vis titration, PL titration spectra, Job's plot analyses and calculation of binding parameters for the studied non-covalent systems....32
S10. Kinetic studies....44
S11. ESI-MS spectra of the mixtures of **3** with **G-1**–**G-6**....49
S12. References....53

View Article Online
DOI: 10.1039/D0DT01366H

S1. Experimental section

S1.1 Materials and methods

Chemical reagents and solvents were commercially purchased and purified according to the standard methods, if necessary. Air- and moisture-sensitive reactions were carried out using commercially anhydrous solvents under an inert atmosphere of argon. The NMR experiments were carried out using a Varian VNMRS 500 MHz spectrometer (^{1}H NMR at 500 MHz or ^{13}C NMR at 125 MHz) equipped with a multinuclear z-gradient inverse probe head. Unless otherwise stated, the spectra were recorded at 25 °C. Standard 5 mm NMR tubes were used. ^{1}H and ^{13}C chemical shifts (δ) were reported in parts per million (ppm) relative to the solvent signals: THF-d_8, δ_H (residual THF) 3.58 ppm, δ_C 67.57 ppm; DMSO-d_6, δ_H (residual DMSO) 2.50 ppm, δ_C 39.52 ppm; $CDCl_3$, δ_H (residual $CHCl_3$) 7.26 ppm, δ_C 77.23 ppm. NMR spectra were analysed with the MestReNova v12.0 software (Mestrelab Research S.L). ^{1}H DOSY (Diffusion Ordered SpectroscopY) NMR experiments were performed using a stimulated echo sequence incorporating bipolar gradient pulses[1] and with convection compensation.[2] The gradient strength was logarithmically incremented in 15 steps from 25% up to 95% of the maximum gradient strength. The DOSY Toolbox software was used for DOSY NMR spectra processing (*The DOSY Toolbox – version 2.5, 2014, Mathias Nilsson, School of Chemistry, University of Manchester, UK*). Fourier-transform infrared (FT-IR) spectra were recorded in a Attenuated Total Reflectance (ATR) mode with the Thermo Nicolet Avatar 370 spectrometer with spectral resolution of 2 cm^{-1} (100 scans). The wavenumbers for the absorption bands *v* were reported in cm^{-1}. UV-Vis and PL measurements were performed with a Cytation 3 Cell Multi-Mode Reader (BioTek Instruments, Inc.). The concentration for all the samples of native compounds was $2 \cdot 10^{-5}$ M. For the UV-Vis measurements, the wavelengths for the absorption maxima λ_{max} were reported in nm. TOF-HRMS (ESI) measurements were performed with a Q-Exactive ThermoScientific spectrometer. Elemental analyses were performed using CHNS Elementar Vario EL III apparatus. Each elemental composition was reported as an average of two analyses. Melting points were determined on Standford Research Systems MPA 100 and were uncorrected. TLC and PTLC analyses were performed using Merck Silica gel 60 F254 plates.

S1.2. Synthesis of the starting materials

Synthesis of 1,3,5-tris(4-aminophenyl)benzene

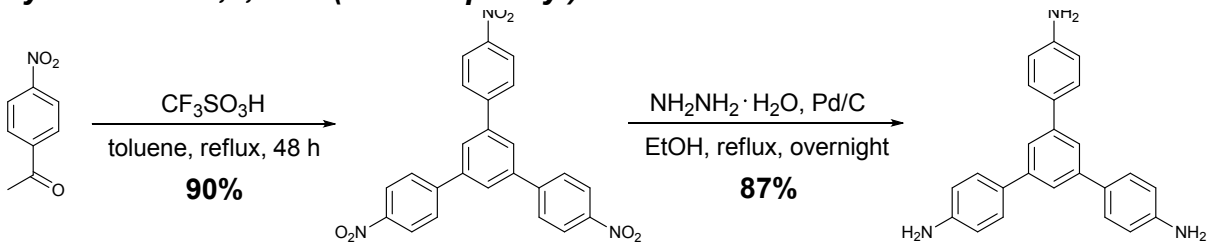

1,3,5-Tris(4-nitrophenyl)benzene and 1,3,5-tris(4-aminophenyl)benzene were synthesized based on the literature procedure.[3] A mixture of 4-nitroacetophenone

(10 g, 60.5 mmol) and triflic acid (400 µL) in toluene (40 mL) was refluxed for 48 hours. The formed black solid was filtered off and washed with toluene (15 mL). The solid was suspended in DMF (60 mL) and refluxed for 20 minutes. Hot solution was filtered off and washed with hot DMF (20 mL). The obtained solid was once again refluxed in DMF (60 mL) for 20 minutes. Filtration, washing with acetone (30 mL) and drying at 45°C for 24 hours, provided 1,3,5-tris(4-nitrophenyl)benzene (8.0114 g, 90%) as a pale-green solid. In order to obtain 1,3,5-tris(4-aminophenyl)benzene, a mixture of 1,3,5-tris(4-nitrophenyl)benzene (3 g, 6.80 mmol) and Pd/C (Pd loading 10 wt.%; 600 mg) in ethanol (60 mL) was heated to reflux and hydrazine hydrate (9 mL) was added dropwise. The resultant mixture was refluxed overnight. The reaction mixture was filtrated off trough celite and it was cooled (at -24°C for 3 hours). The formed precipitate was filtrated off and washed with cold ethanol (10 mL). The solid was dried in air for 24 hours to give 1,3,5-tris(4-aminophenyl)benzene (2.0792 g, 87%) as a bright-yellow solid. ^{1}H NMR (DMSO-d_6, 500 MHz ppm), δ_H 7.48-7.45 (m, 9H), 6.68-6.65 (m, 6H), 5.20 (bs, 6H). The NMR data is consistent with the literature.[3]

Synthesis of bis(acetonitrile)dichloropalladium(II)

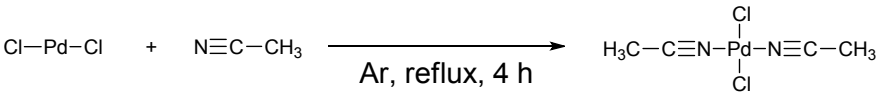

quantitative yield

Bis(acetonitrile)dichloropalladium(II) was synthesized based on the literature procedure.[4] A suspension of $PdCl_2$ (400 mg, 2.26 mmol) in dry acetonitrile (80 mL) was refluxed under argon atmosphere for 4 hours. The solvent was then evaporated on a rotary evaporator and the resultant solid was dried under high vacuum to give bis(acetonitrile)dichloropalladium(II) (586.3 mg; quantitative yield) as a yellow solid.

S1.3 Synthesis of ferrocene-templated molecular cage (3)

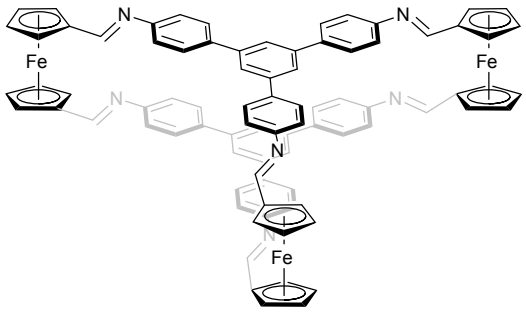

3

A solution of 1,1′-diformylferrocene (145.2 mg, 0.6 mmol) in EtOH (20 mL) was added to a solution of 1,3,5-tris(4-aminophenyl)benzene (95.9 mg, 0.4 mmol) in EtOH (10 mL). Glacial acetic acid (100 µL) was added and the mixture turned turbid. The reaction mixture was stirred at room temperature for 18 hours. Then, the formed solid was filtered off, washed with MeOH (30 mL) and dried at room temperature for 24 hours to give cage **3** (251.0 mg; 95% yield) as a dark pink solid.

Mp: >300°C; ^{1}H NMR (THF-d_8, 500 MHz, ppm), δ_H 8.15 (s, 6H), 7.49 (s, 6H), 7.30-7.28 (m, 12H), 6.81-6.78 (m, 12H), 5.06-5.05 (m, 12H), 4.50-4.51 (m, 12H); ^{13}C{^{1}H} NMR (THF-d_8, 125 MHz, ppm), δ_C 160.6 (6C), 151.2 (3C), 146.7 (3C), 141.3 (6C), 138.2 (6C), 127.5 (12C), 123.8 (6C), 120.6 (12C), 82.3 (6C), 71.7 (12C), 70.3 (12C); FT-IR (ATR), *v* 3085, 3035, 2870, 1625, 1590, 1500, 1375, 1170, 1040, 820 cm^{-1}; Elemental analysis: calculated for $C_{84}H_{60}Fe_3N_6$: C (76.38%), H (4.58%), N (6.36%), found: C (76.42%), H (4.61%), N (6.25%); TOF-HRMS (ESI): calcd. for $C_{84}H_{61}Fe_3N_6$ $[M+H]^+$ = 1321.3000, found: m/z 1321.2998.

S1.4 Interactions between the ferrocene-templated molecular cage (3) and aromatic molecules – ^{1}H NMR

The 1 mM stock solution of the ferrocene-templated molecular cage (**3**) and 8 mM stock solution of the aromatic molecule (phenylboronic acid (**G-1**), chlorobenzene (**G-2**), 1,4-terphenyl (**G-3**), chrysene (**G-4**), pyrene (**G-5**) or 1-pyrenecarboxaldehyde (**G-6**)) in THF-d_8 were prepared. The samples subjected to the NMR experiments comprised 0.5 mM (100 mol%) of the ferrocene-templated molecular cage (**3**) and 4 mM (800 mol%) of an aromatic molecule. Total volume of a sample was 0.6 mL.

S1.5 Synthesis of ferrocene-templated Pd-bearing cage (5)

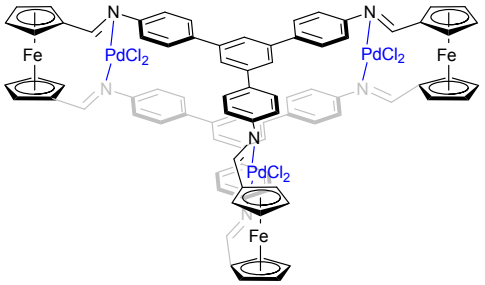

5

A solution of the ferrocene-templated molecular cage (**3**; 198.1 mg, 0.15 mmol) and bis(acetonitrile)dichloropalladium(II) (**4**; 116.8 mg, 0.45 mmol) in dry DCM (20 mL) was stirred under argon atmosphere at room temperature for 48 hours. The formed precipitate was filtered off, washed with dry DCM (30 mL) and dried under high vacuum to give cage **5** (272.4 mg; 98% yield) as a brown solid.

Mp: >300°C; ^{1}H NMR (DMSO-d_6, 500 MHz, ppm), δ_H 8.41 (s, 6H), 7.65 (s, 6H), 7.56-7.54 (m, 12H), 7.26-7.24 (m, 12H), 5.22-5.21 (m, 12H), 4.77-4.76 (m, 12H); ^{13}C{^{1}H} NMR (DMSO-d_6, 125 MHz, ppm), δ_C 168.2 (6C), 157.5 (3C), 153.3 (3C), 149.9 (6C), 142.8 (6C), 135.1 (12C), 133.4 (6C), 128.2 (12C), 90.3 (6C), 79.3 (12C), 77.6 (12C); FT-IR (ATR), *v* 3095, 3020, 2920, 1610, 1590, 1505, 1370, 1250, 1055, 830 cm-1; Elemental analysis: calculated for $C_{84}H_{60}Cl_6Fe_3N_6Pd_3$: C (54.45%), H (3.26%), N (4.54%), found: C (54.62%), H (3.43%), N (4.23%); TOF-HRMS (ESI): calcd. for $C_{84}H_{60}Cl_6Fe_3N_6Pd_3$ $[M+H]^+$ = 1853.9363, found: m/z 1853.9361.

S1.6 General procedure for the synthesis of 1,1′-biphenyls using ferrocene-templated Pd-bearing cage (5) as the catalyst

A mixture of phenylboronic acid (0.55 mmol; 110 mol%), chlorobenzene or its derivative[5] (0.50 mmol; 100 mol%), cage **5** (0.0025 mmol; **0.5 mol%**) and triethylamine (TEA; 2.00 mmol; 400 mol%) in DMSO (6 mL) was stirred at room temperature under argon atmosphere for an appropriate time[5]. The reaction progress was tracked with TLC. The mixture was diluted with hexane (35 mL) and it was cooled (at 4°C for 1 hour). The pale-red precipitate was formed, whilst the other components of the reaction mixture after a catalytic reaction remained dissolved. The solid was filtered off, washed with hexane (10 mL) and dried under high vacuum to recover catalyst as a brown solid. The compound recovered after the catalytic reaction was used as the catalyst in the next reaction cycles[5]. The filtrate was washed with distilled water (3x15 mL), brine (2x15 mL) and dried over $MgSO_4$. After filtration, volatiles were evaporated on a rotary evaporator. The crude product was purified using PTLC (SiO_2, layer thickness of 1 μL; eluents: mixtures of AcOEt/hex) to give pure 1,1′-biphenyls in high yields (96-99%)[5].

For the optimization of the reaction conditions for the synthesis of 1,1′-biphenyl using cage **5** as the catalyst, see **Table S1**, ESI. The proposed mechanism regarding the formation of the recovered catalyst and data for the compound recovered after the catalytic reaction (**a**) and for all the obtained 1,1′-biphenyls (**b**), are provided below. For the spectra, see Sections S7-S8, ESI.

Table S1. Optimization of the reaction conditions for the synthesis of 1,1′-biphenyl (**P-1**) using Pd-bearing cage **5** as the catalyst.

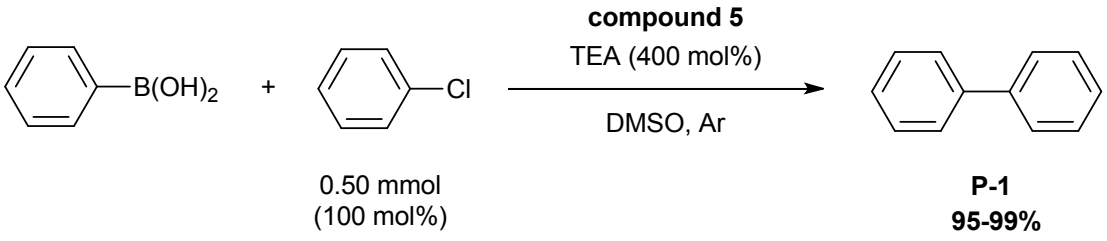

Entry	Phenylboronic acid (mol%)	Catalyst 5 (mol%)	Reaction time [minutes][a]	Reaction temperature [°C]	Yield [%][b]
1	110	10.0	20	rt	99
2	110	5.0	20	rt	99
3	**110**	**0.5**	**20**	**rt**	**99**
4	110	0.1	120	rt	98
5	110	0.5	70	90°C	95
6	130	0.5	20	rt	99

[a] the reaction progress was tracked with TLC; [b] isolated yields.

a) ^{1}H NMR, ^{13}C NMR, elemental analysis and melting point data for the compound recovered after the catalytic reaction (NMR spectra are presented in Section S8, ESI):

The data on the compound recovered after the catalytic reaction are as follows:

Mp: >300°C; ^{1}H NMR (DMSO-d_6, 500 MHz, ppm), δ_H 8.41 (s, 6H), 7.65 (s, 6H), 7.56-7.54 (m, 12H), 7.26-7.24 (m, 12H), 5.22-5.21 (m, 12H), 4.77-4.76 (m, 12H); ^{13}C{^{1}H} NMR (DMSO-d_6, 125 MHz, ppm), δ_C 167.5 (6C), 157.5 (3C), 153.0 (3C), 149.9 (6C), 142.8 (6C), 135.1 (12C), 133.4 (6C), 128.2 (12C), 90.3 (6C), 79.2 (12C), 77.5 (12C); Elemental analysis: found: C (61.68%), H (3.57%), N (5.18%); TOF-HRMS (ESI): found: m/z 1639.0032.

Based on above-presented data, the Pd^0[cage] was isolated after the catalytic process (elemental analysis: calculated for $C_{84}H_{60}Fe_3N_6Pd_3$: C (61.51%), H (3.69%), N (5.12%); HRMS: calcd. for $C_{84}H_{60}Fe_3N_6Pd_3$ $[M]^+$ = 1639.0039).

In fact, the cage comprising the Pd^0 acted the catalyst in the catalytic process. The following mechanism for the generation of Pd^0[cage] from Pd^{II}Cl$_2$[cage] is proposed[5c]:

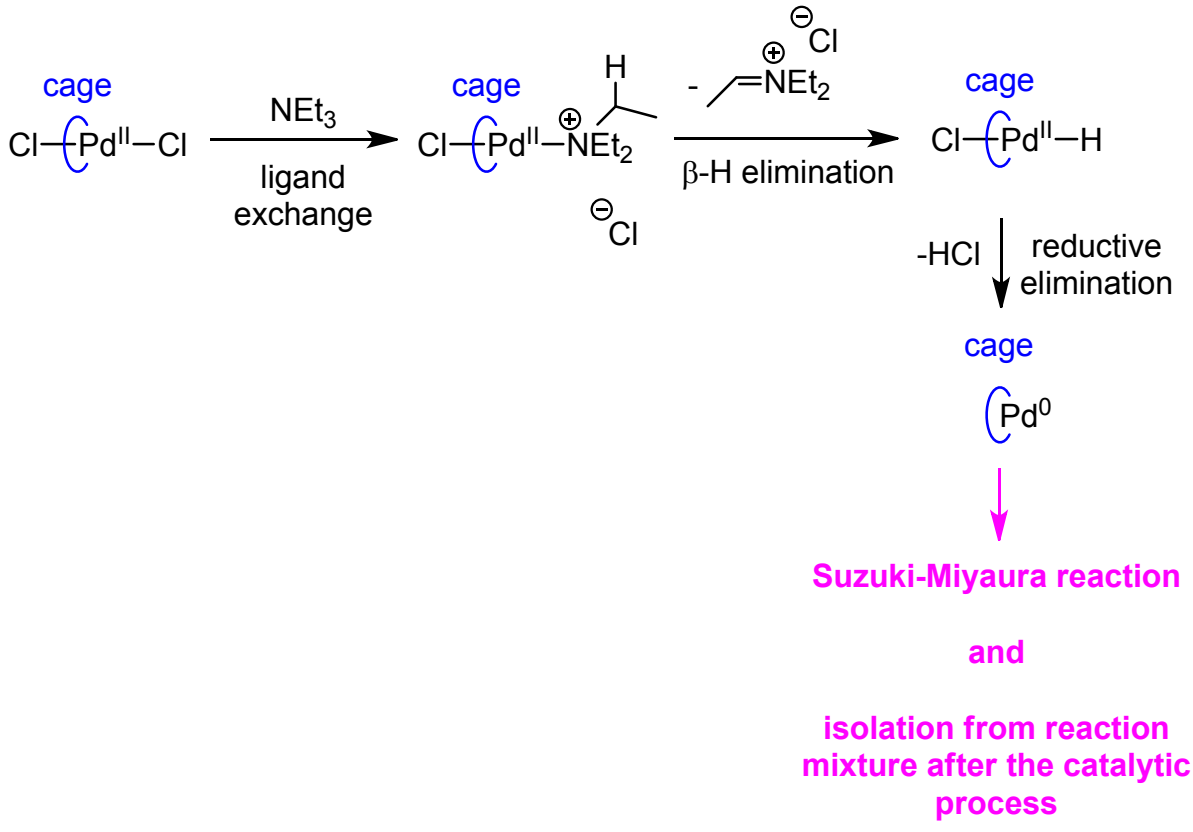

b) ^{1}H NMR, HRMS and melting point data for the 1,1′-biphenyls obtained in the catalytic reaction (^{1}H NMR spectra are presented in Section S7, ESI). The data for all the obtained 1,1′-biphenyls are consistent with the literature.[6],[7]

*1,1'-biphenyl (**P-1**):*

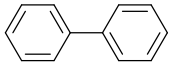

P-1

Yield[8] (0.50 mmol scale): **99 %**; Yield[8] (10.00 mmol scale): **99 %**.
Reaction time (0.50 mmol scale): **20 minutes**; Reaction time (10.00 mmol scale): **21 minutes**.
Mp: 70°C; ^{1}H NMR ($CDCl_3$, 500 MHz, ppm), δ_H 7.63-7.61 (m, 4H), 7.48-7.44 (m, 4H), 7.39-7.35 (m, 2H); TOF-HRMS (ESI): calcd. for $C_{12}H_{10}$ $[M]^+$ = 154.0783, found: m/z 154.0782. No differences between the spectra of 1,1′-biphenyl obtained in 0.50 mmol and 10.00 mmol scale reactions, were found.

*4-methyl-1,1'-biphenyl (**P-2**):*

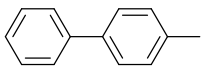

P-2

Yield[8]: **98 %**.
Reaction time: **21 minutes**.
Mp: 46°C; ^{1}H NMR ($CDCl_3$, 500 MHz, ppm), δ_H 7.61-7.58 (m, 2H), 7.53-7.50 (m, 2H), 7.46-7.42 (m, 2H), 7.36-7.32 (m, 1H), 7.28-7.26 (m, 2H), 2.42 (s, 3H); TOF-HRMS (ESI): calcd. for $C_{13}H_{12}$ $[M]^+$ = 168.0939, found: m/z 168.0941.

*4-nitro-1,1'-biphenyl (**P-3**):*

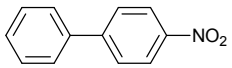

P-3

Yield[8]: **96 %**.
Reaction time: **26 minutes**.
Mp: 113°C; ^{1}H NMR ($CDCl_3$, 500 MHz, ppm), δ_H 8.32-8.30 (m, 2H), 7.75-7.73 (m, 2H), 7.51-7.40 (m, 5H); TOF-HRMS (ESI): calcd. for $C_{13}H_9NO_2$ $[M]^+$ = 199.0633, found: m/z 199.0631.

View Article Online
DOI: 10.1039/D0DT01366H

*4-bromo-1,1'-biphenyl (**P-4**):*

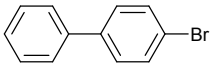

P-4

Yield[8]: **97 %**.
Reaction time: **23 minutes**.
Mp: 89°C; ^{1}H NMR ($CDCl_3$, 500 MHz, ppm), δ_H 7.59-7.56 (m, 4H), 7.48-7.43 (m, 4H), 7.39-7.36 (m, 1H); TOF-HRMS (ESI): calcd. for $C_{12}H_9Br$ $[M]^+$ = 231.9888, found: m/z 231.9885.

*2-bromo-1,1'-biphenyl (**P-5**):*

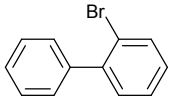

P-5

Yield[8]: **96 %**.
Reaction time: **25 minutes**.
Bright-yellow liquid; ^{1}H NMR ($CDCl_3$, 500 MHz, ppm), δ_H 7.70-7.68 (m, 1H), 7.46-7.34 (m, 7H), 7.24-7.19 (m, 1H); TOF-HRMS (ESI): calcd. for $C_{12}H_9Br$ $[M]^+$ = 231.9888, found: m/z 231.9887.

S2. NMR spectra

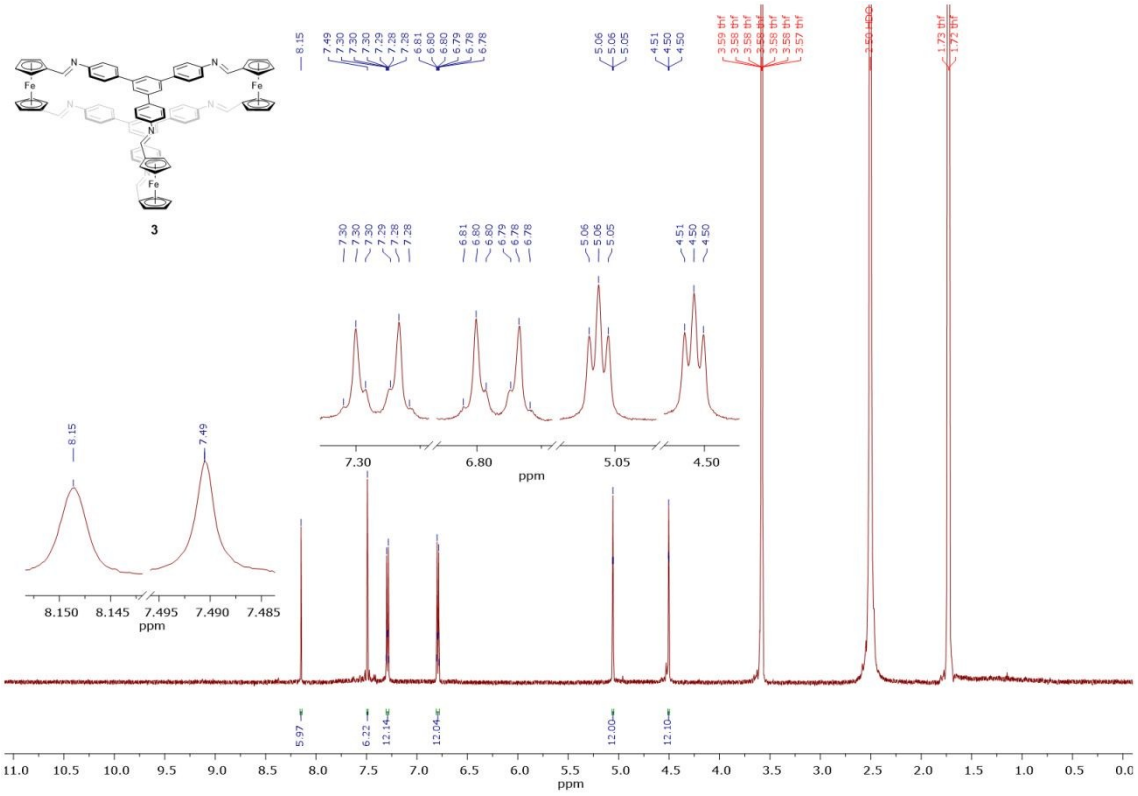

Figure S1. ^{1}H NMR (THF-d_8, 500 MHz) spectrum of cage **3**.

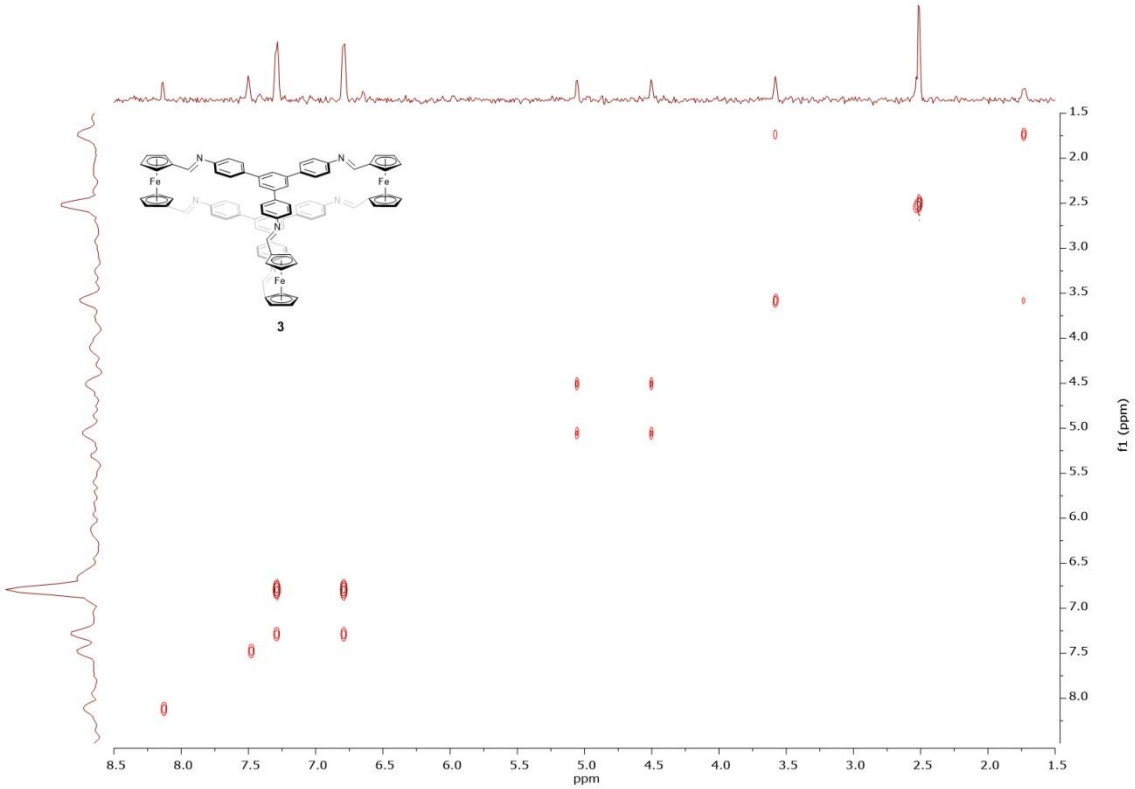

Figure S2. ^{1}H-^{1}H COSY NMR (THF-d_8, 500 MHz) spectrum of cage **3**.

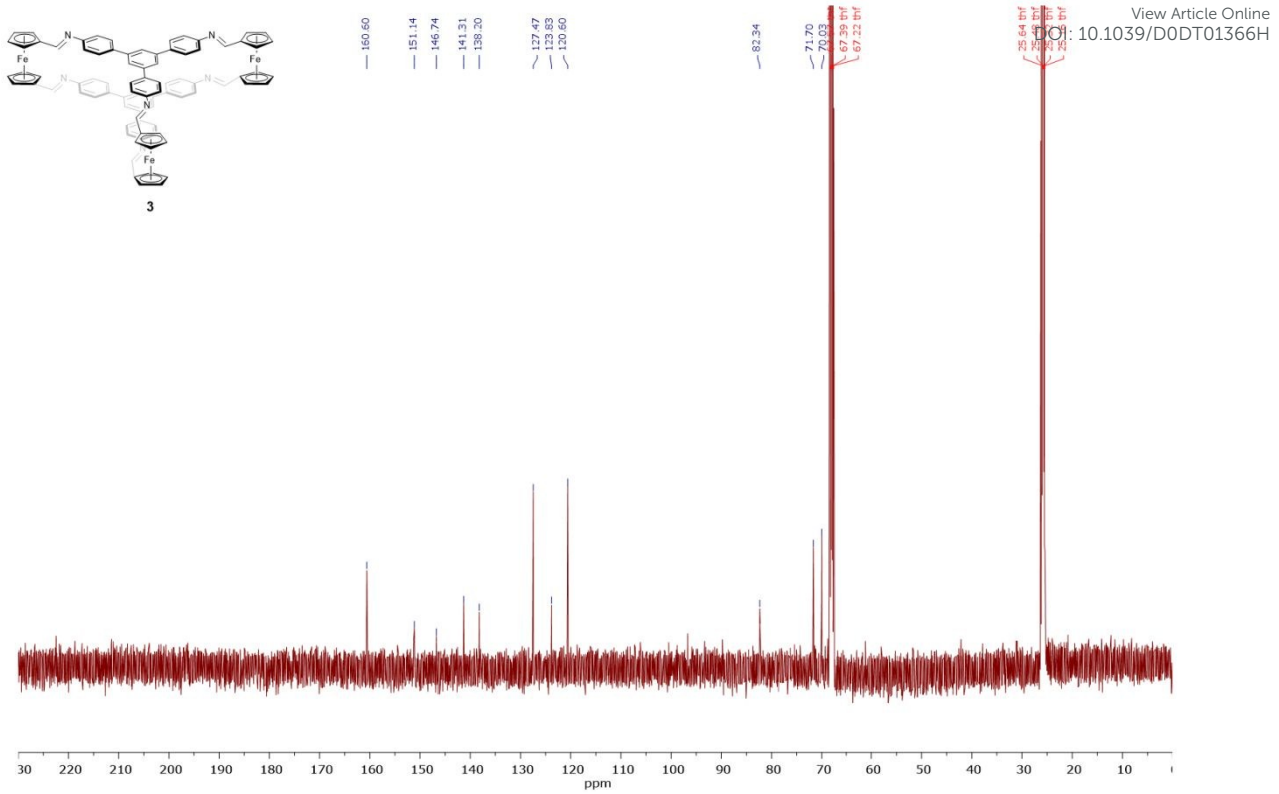

Figure S3. ^{13}C NMR (THF-d_8, 125 MHz) spectrum of cage **3**.

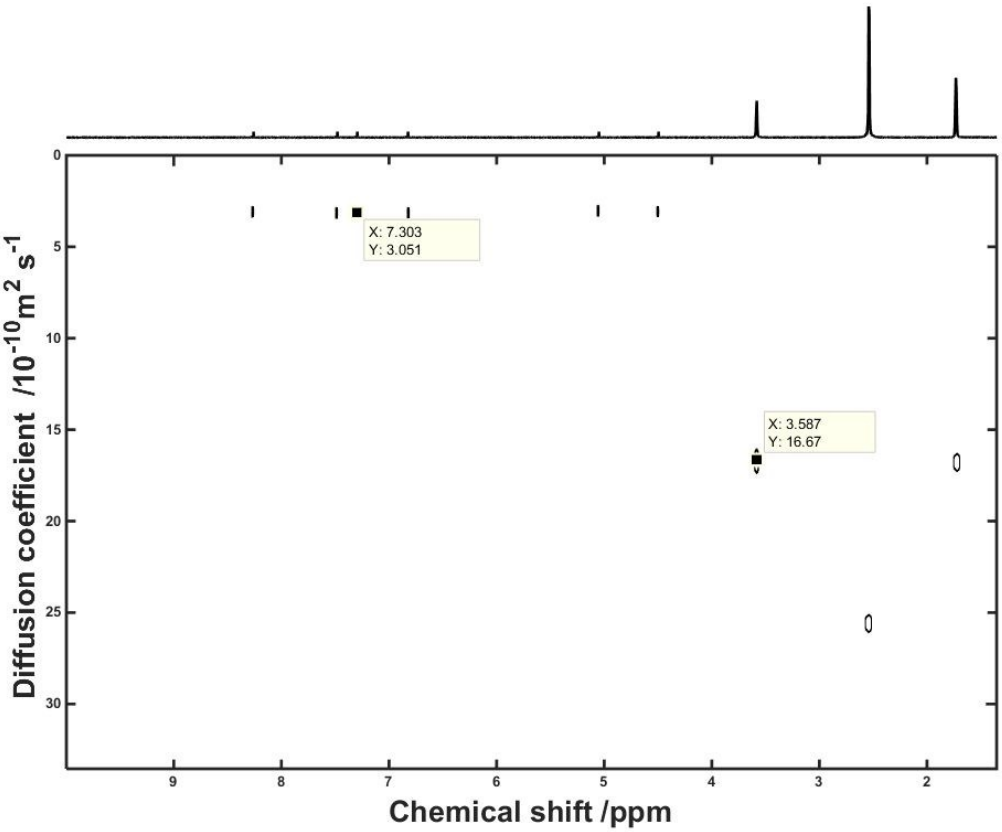

Figure S4. ^{1}H DOSY NMR (THF-d_8, 500 MHz) spectrum of cage **3**.

View Article Online
DOI: 10.1039/D0DT01366H

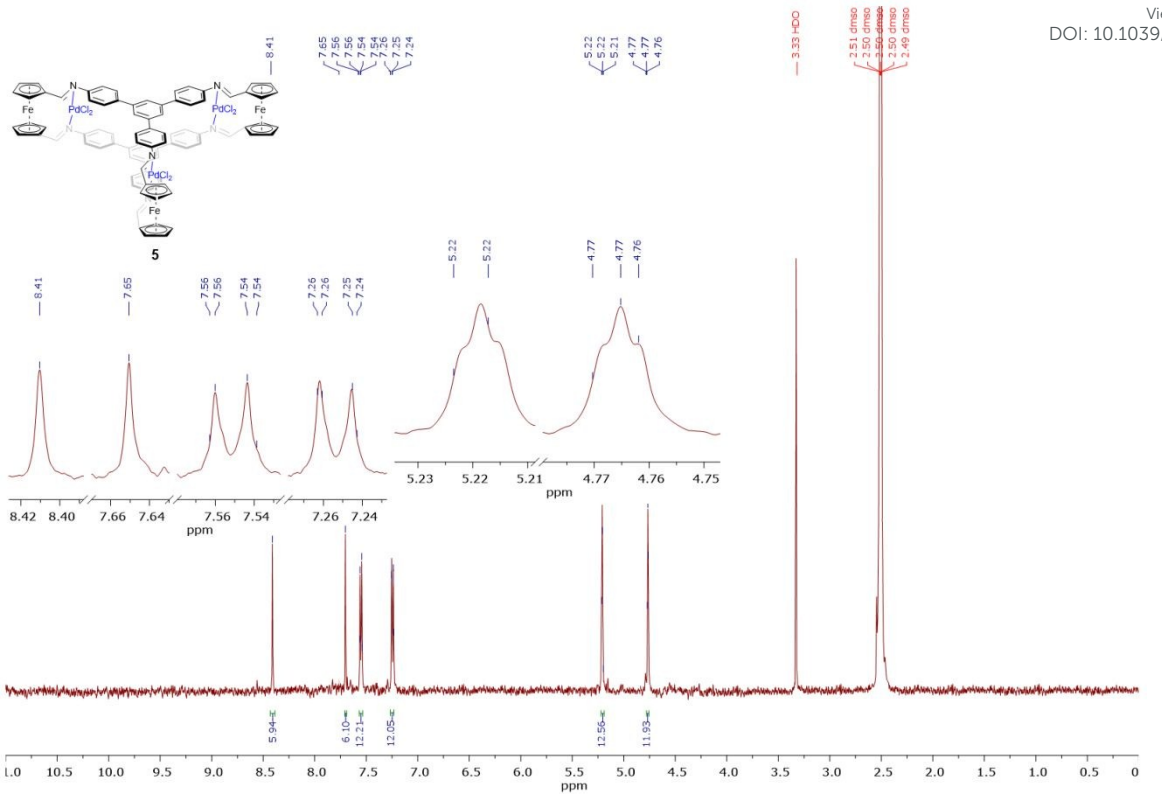

Figure S5. ^{1}H NMR (DMSO-d_6, 500 MHz) spectrum of cage **5**.

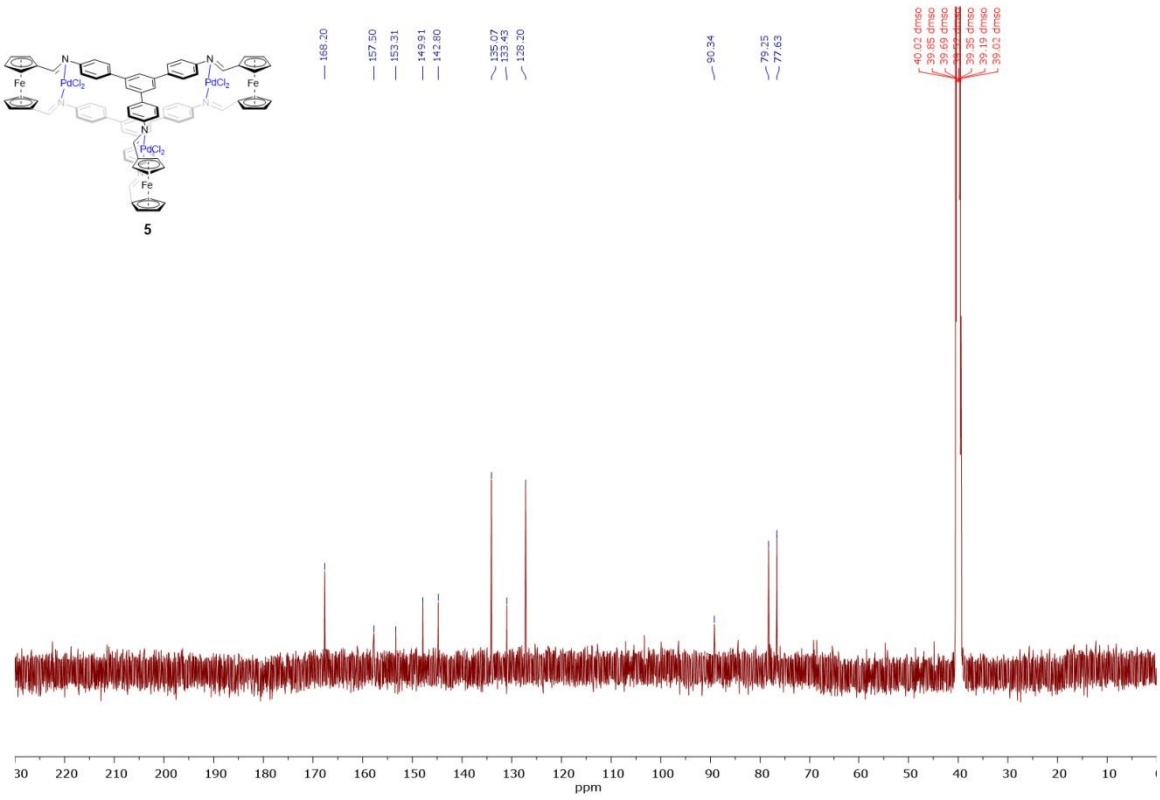

Figure S6. ^{13}C NMR (DMSO-d_6, 125 MHz) spectrum of cage **5**.

View Article Online
DOI: 10.1039/D0DT01366H

S3. IR spectra

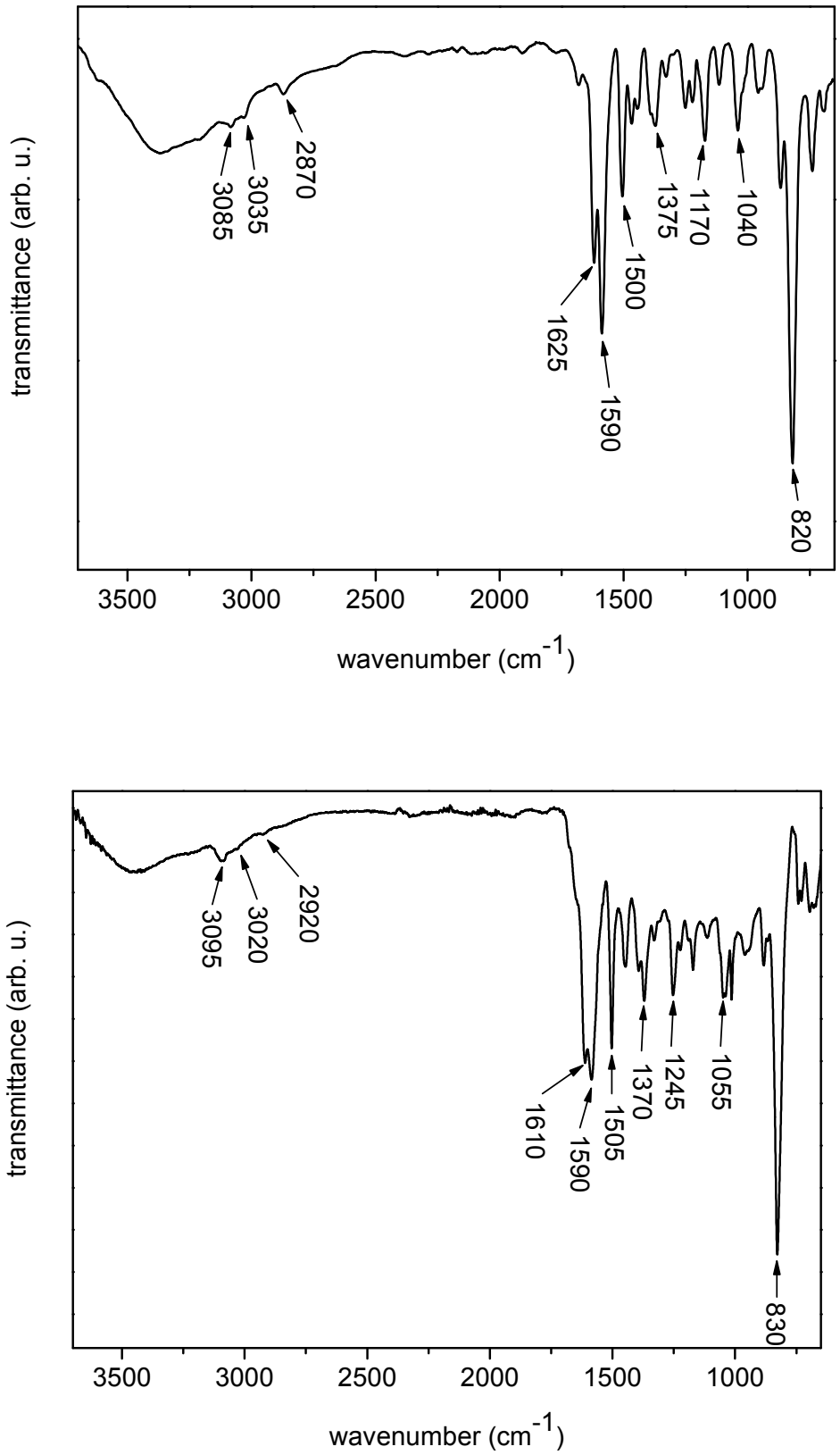

Figure S7. FT-IR spectrum of cage **3** (**top**) and cage **5** (**bottom**).

S4. UV-Vis spectra for compound 3 and compound 5

View Article Online
DOI: 10.1039/D0DT01366H

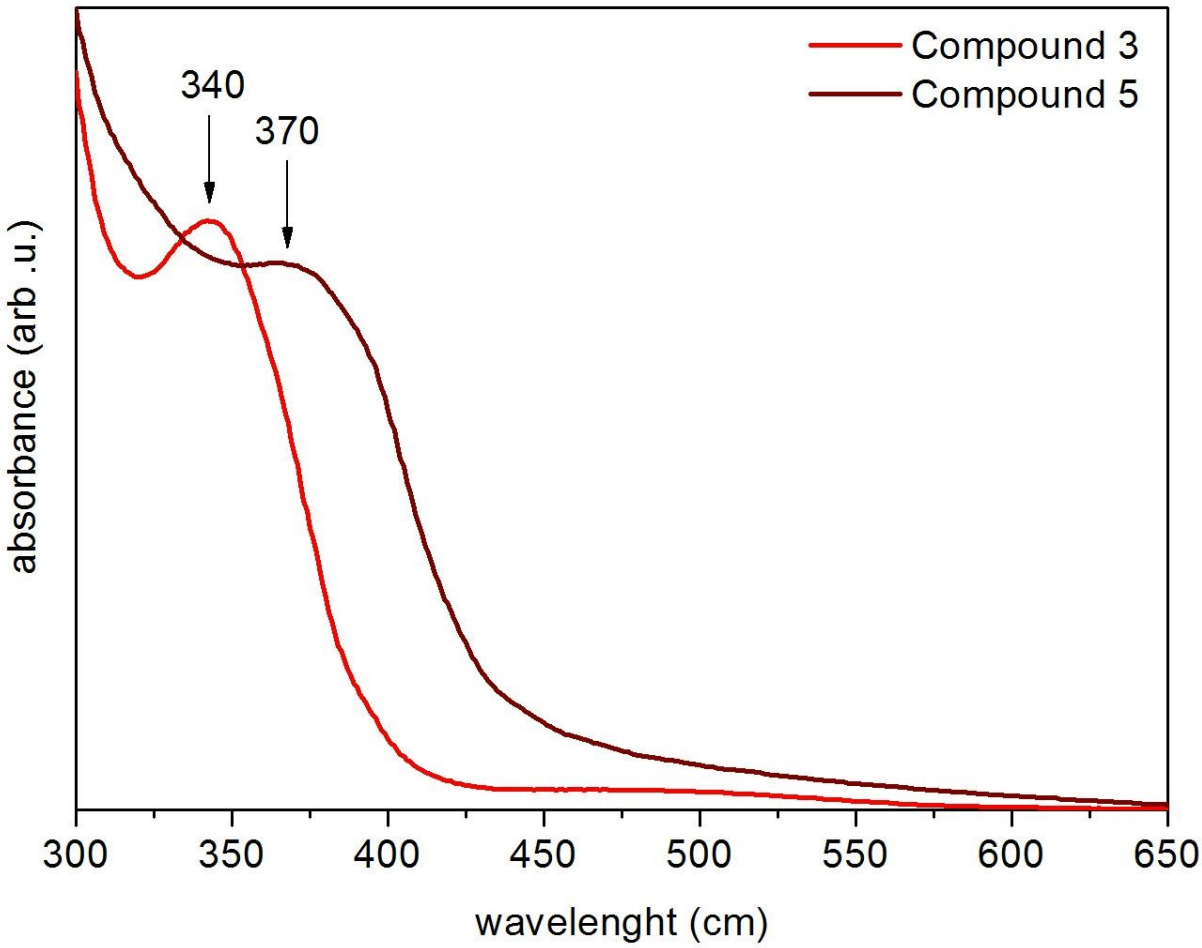

Figure S8. UV-Vis spectra of cage **3** (**red curve:** solvent: THF, concentration: $2 \cdot 10^{-5}$ M) and cage **5** (**brown curve:** solvent: DMSO, concentration: $2 \cdot 10^{-5}$ M).

View Article Online
DOI: 10.1039/D0DT01366H

S5. Crystal structure analyses on cage 3

Single crystals of cage **3** suitable for crystal structure determination were grown after five days of slow evaporation of a dichloromethane solution of cage **3** with a layer of benzene on top of it. Appropriate single crystal for X-ray diffraction experiment was selected under a microscope using polarized light and attached to a cactus needle with a two-component epoxy glue. Diffraction data were collected using graphite-monochromated Mo-Kα X-ray radiation on a Rigaku Oxford Diffraction Gemini A Ultra diffractometer equipped with Atlas CCD detector. CrysAlis^{PRO} software was used for data collection and analysis.[9] Crystal structure was subsequently solved and refined using ShelxT and ShelxL programs, respectively, invoked from within Olex2 suite.[10]-[12] Hydrogen atoms were introduced into calculated positions. The crystal structure contains two types of voids. The smaller ones with a volume of 216 Å^3 are centered at 3*b* Wyckoff position (0, 0, ½; symmetry of $\bar{3}$ point group) and the larger ones (223 Å^3) are located at 9*d* Wyckoff position (½, 0, ½; symmetry of $\bar{1}$ point group). The larger voids are occupied by benzene molecules as evidenced by the Q-peaks in residual density maps whereas the smaller ones are probably occupied by dichloromethane molecules. This is inferred based on the cavities' shape which is more isotropic than that of the larger voids. The final model of the structure was obtained by removing the contribution of all the disordered solvent molecules from scattering factors by the SQUEEZE procedure implemented in PLATON.[13][14] The number of "squeezed" electrons is 62 and 52 for the larger and smaller voids, respectively. This is more than 42 which is the number of benzene and dichloromethane electrons but SQUEEZE is known to overestimate the number of solvent molecule electrons.[14] Details of crystal structure determination are given in **Table S2**. CCDC 1970365 contains supplementary crystallographic data for this paper. These data can be obtained free of charge from the joint CCDC's and FIZ Karlsruhe's service to view and retrieve structures via https://www.ccdc.cam.ac.uk/structures/.

View Article Online
DOI: 10.1039/D0DT01366H

Table S2. Crystal data and structure refinement for cage **3**.

Identification code	Cage **3**
Empirical formula	$C_{84}H_{60}Fe_3N_6$
Formula weight	1320.93
T /K	293.15
Crystal system	trigonal
Space group	$R\bar{3}$
a /Å	24.9627(11)
b /Å	24.9627(11)
c /Å	20.5795(11)
α /°	90
β /°	90
γ /°	120
V /Å^3	11105.8(11)
Z	6
ρ_{calc}/g/cm^3	1.185
μ/mm^{-1}	0.626
F(000)	4104.0
Crystal size/mm^3	0.25 × 0.19 × 0.085
Radiation	MoKα (*λ* = 0.71073)
2Θ range for data collection/°	6.778 to 53.998
Index ranges	−29 ≤ *h* ≤ 27, −24 ≤ *k* ≤ 31, −20 ≤ *l* ≤ 26
Reflections collected	11433
Independent reflections	5389 [R_{int} = 0.0362, R_{sigma} = 0.0644]
Data/restraints/parameters	5389/0/280
Goodness-of-fit on F^2	0.964
Final *R* indexes [*I*>=2*σ* (*I*)]	R_1 = 0.0467, wR_2 = 0.0982
Final *R* indexes [all data]	R_1 = 0.0854, wR_2 = 0.1154
Largest diff. peak/hole / eÅ^{-3}	+0.35/−0.19

View Article Online
DOI: 10.1039/D0DT01366H

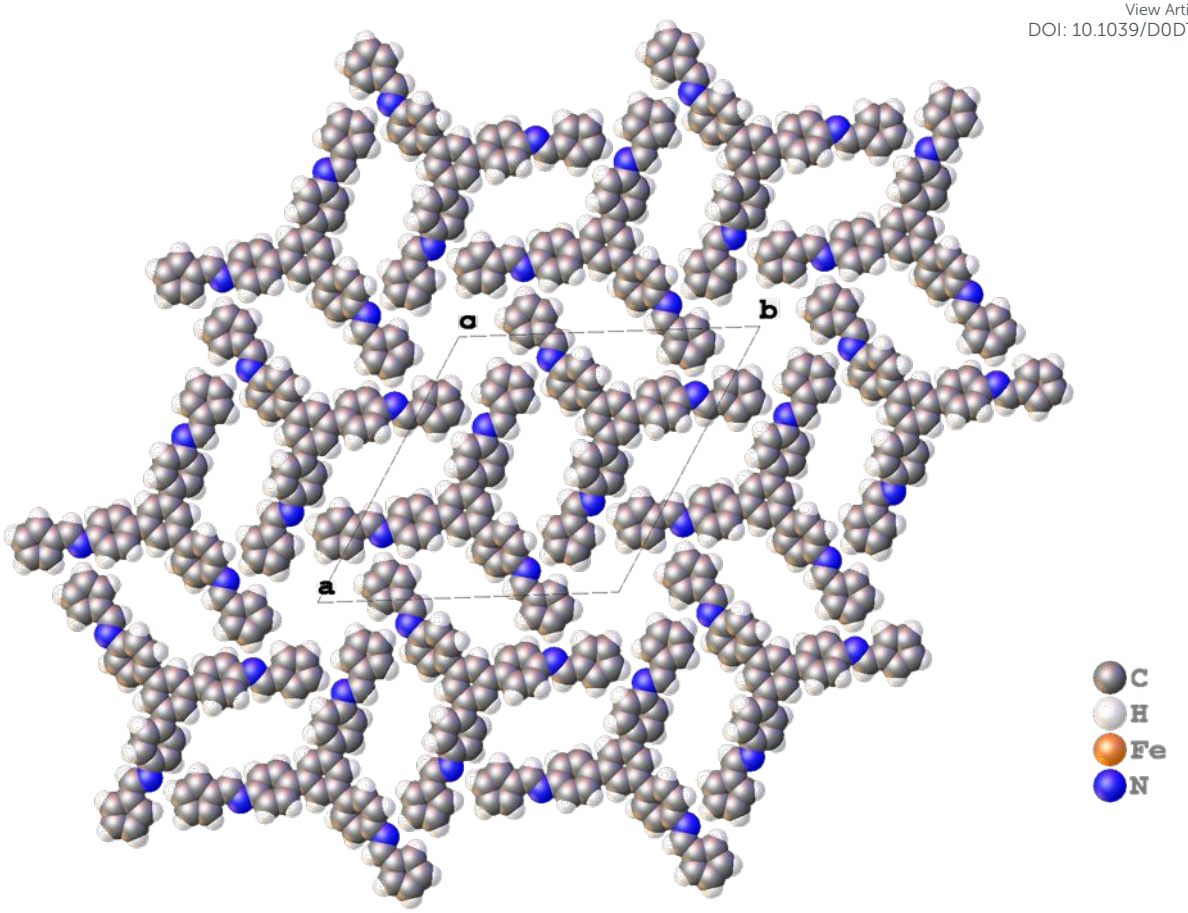

Figure S9. View of one layer of molecules along crystallographic *c* direction in cage **3** crystal structure. Molecules drawn in space-filling model. See legend for colour coding of atoms. The larger and smaller voids contain disordered solvent molecules of benzene and dichloromethane, respectively.

View Article Online
DOI: 10.1039/D0DT01366H

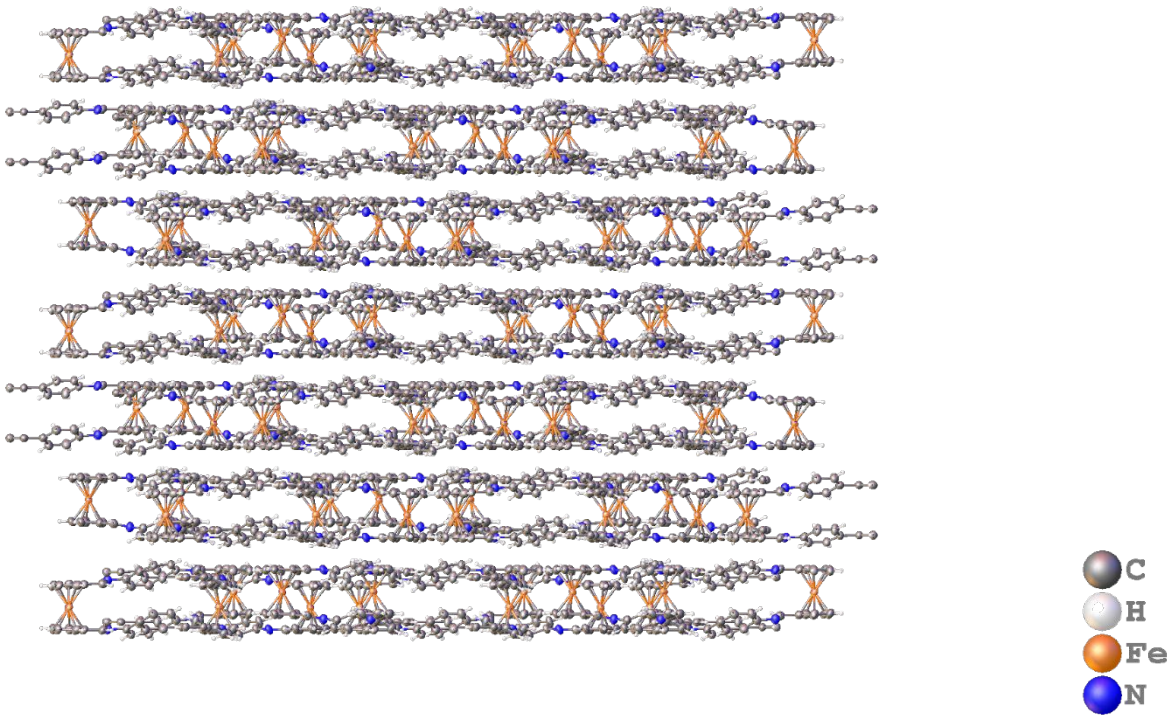

Figure S10. View of 3D packing of molecules along crystallographic *a* direction in cage **3** crystal structure. Molecules drawn ellipsoids representing thermal motion of 50% probability level. See legend for colour coding of atoms. The larger and smaller voids contain disordered solvent molecules of benzene and dichloromethane, respectively.

S6. Interactions with aromatic molecules – NMR assays

View Article Online
DOI: 10.1039/D0DT01366H

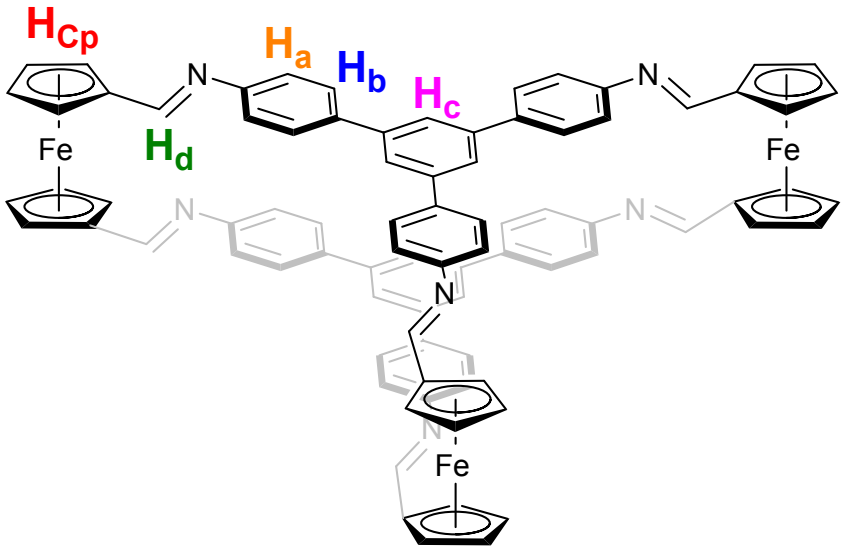

3

Figure S11. Structure of the molecular cage **3** with the atom labels marked.

Table S3. Relative signal shifts for the H_b protons of cage **3** after the addition of 800 mol% of an aromatic molecule. No shift for the H_{cp} and H_d protons were observed (see the spectra below). For the atom labels of cage **3**, see Figure S11. For the structures of the aromatic molecules, see Figure 2 in the main article text.

Entry	Aromatic molecule	Chemical shift for H_b (ppm)	Relative difference in the chemical shift in comparison to native cage 3 (ppm)
1	- (native cage **3**)	6.810	N/A
2	phenylboronic acid (**G-1**)	6.761	-0.049
3	chlorobenzene (**G-2**)	6.763	-0.047
4	1,4-terphenyl (**G-3**)	6.789	-0.021
5	chrysene (**G-4**)	6.782	-0.028
6	pyrene (**G-5**)	6.778	-0.032
7	1-pyrenecarboxaldehyde (**G-6**)	6.732	-0.078

View Article Online
DOI: 10.1039/D0DT01366H

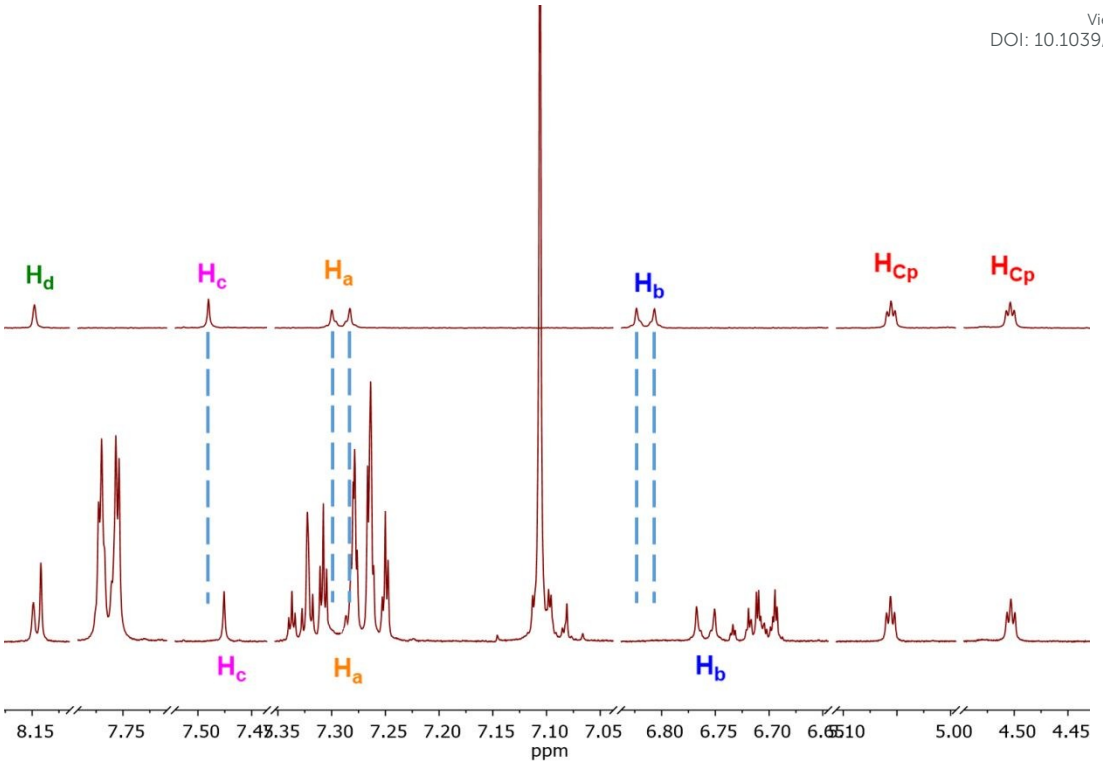

Figure S12. ^{1}H NMR (THF-d_8, 500 MHz) spectrum of cage **3** (**top**) and ^{1}H NMR (THF-d_8, 500 MHz) spectrum of cage **3** with 800 mol% of phenylboronic acid (**G-1**) added (**bottom**). For the atom labels of cage **3**, see Figure S11.

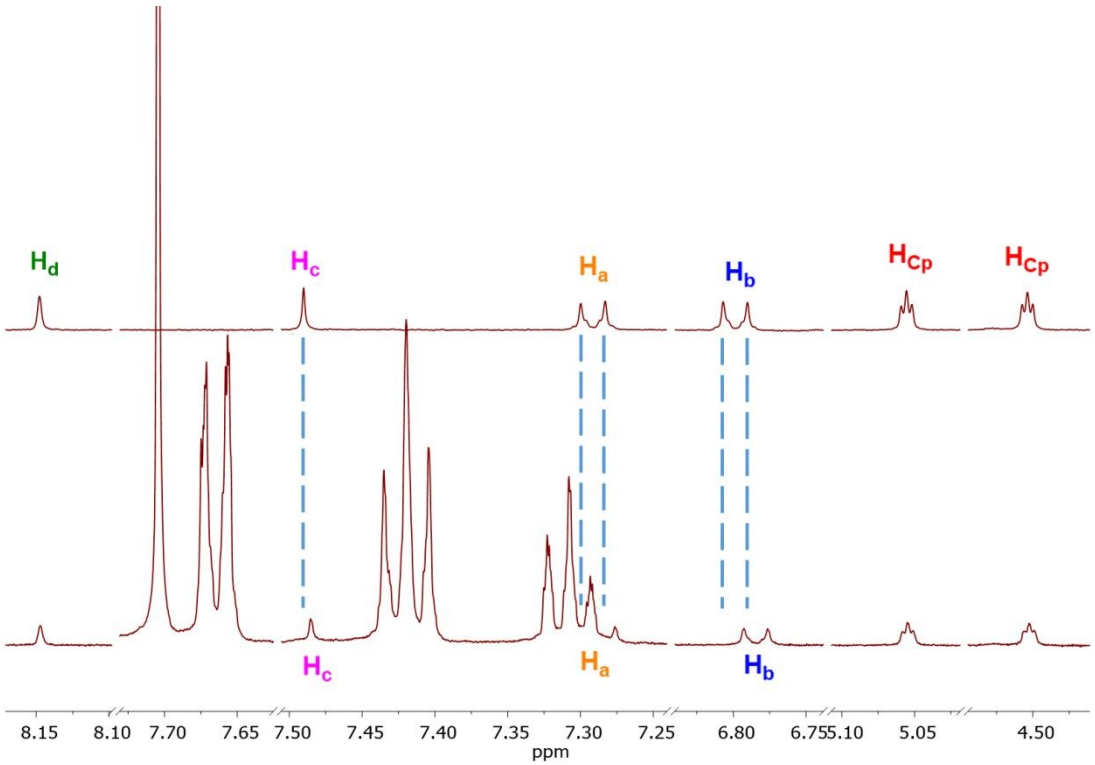

Figure S13. ^{1}H NMR (THF-d_8, 500 MHz) spectrum of cage **3** (**top**) and ^{1}H NMR (THF-d_8, 500 MHz) spectrum of cage **3** with 800 mol% of 1,4-terphenyl (**G-3**) added (**bottom**). For the atom labels of cage **3**, see Figure S11.

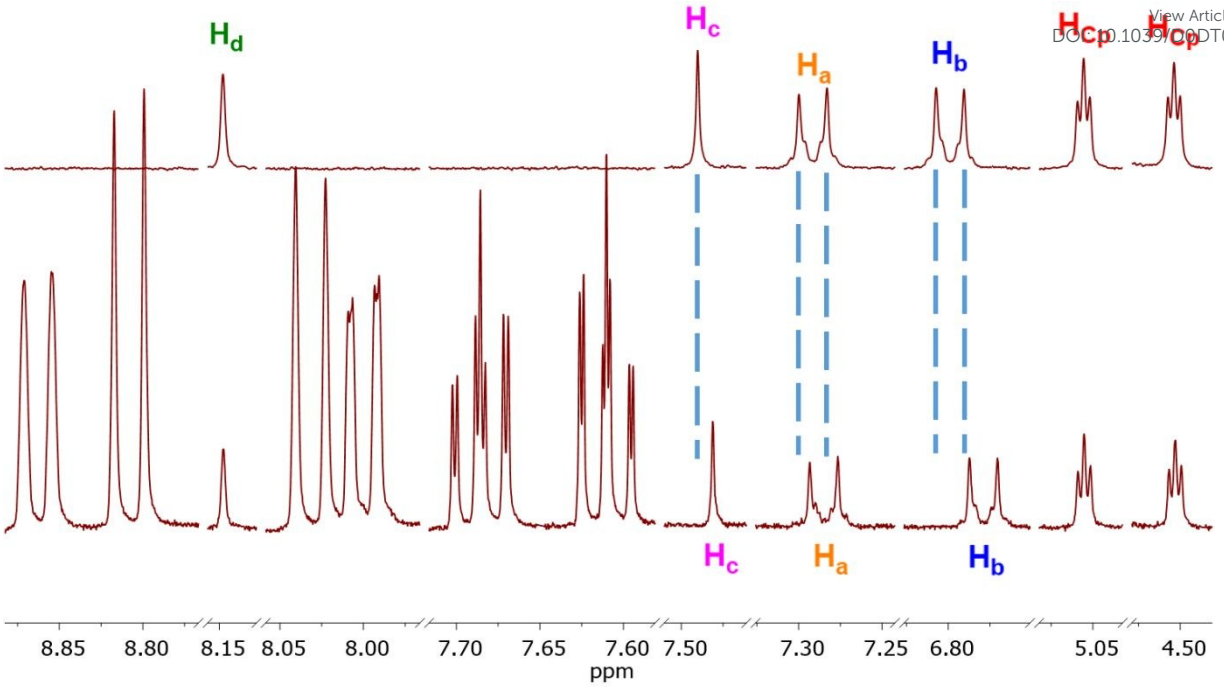

Figure S14. ^{1}H NMR (THF-d_8, 500 MHz) spectrum of cage **3** (**top**) and ^{1}H NMR (THF-d_8, 500 MHz) spectrum of cage **3** with 800 mol% of chrysene (**G-4**) added (**bottom**). For the atom labels of cage **3**, see Figure S11.

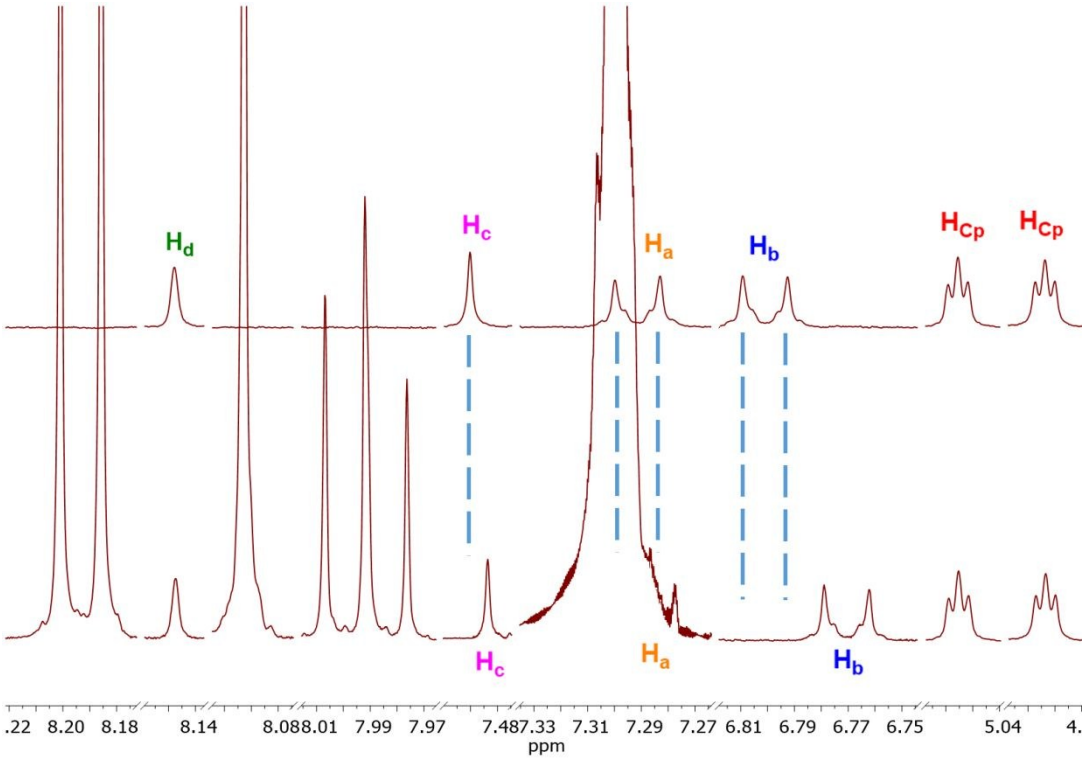

Figure S15. ^{1}H NMR (THF-d_8, 500 MHz) spectrum of cage **3** (**top**) and ^{1}H NMR (THF-d_8, 500 MHz) spectrum of cage **3** with 800 mol% of pyrene (**G-5**) added (**bottom**). For the atom labels of cage **3**, see Figure S11.

View Article Online
DOI: 10.1039/D0DT01366H

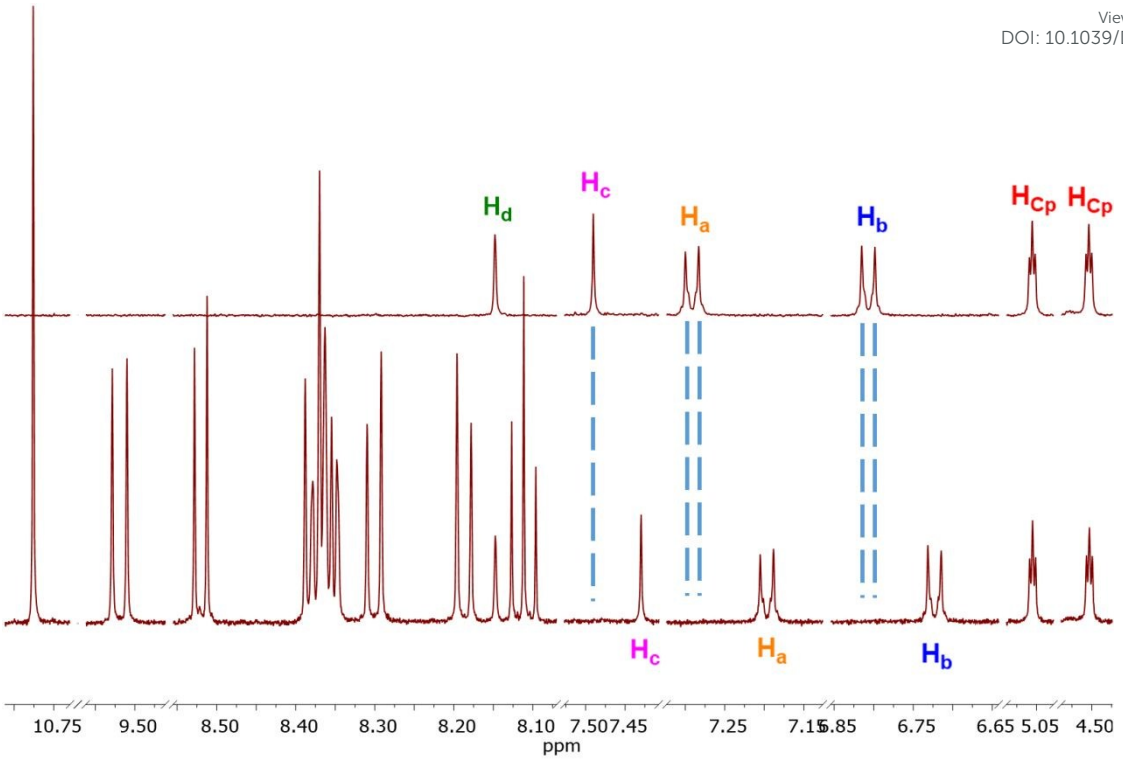

Figure S16. ^{1}H NMR (THF-d_8, 500 MHz) spectrum of cage **3** (**top**) and ^{1}H NMR (THF-d_8, 500 MHz) spectrum of cage **3** with 800 mol% of 1-pyrenecarboxaldehyde (**G-6**) added (**bottom**). For the atom labels of cage **3**, see Figure S11.

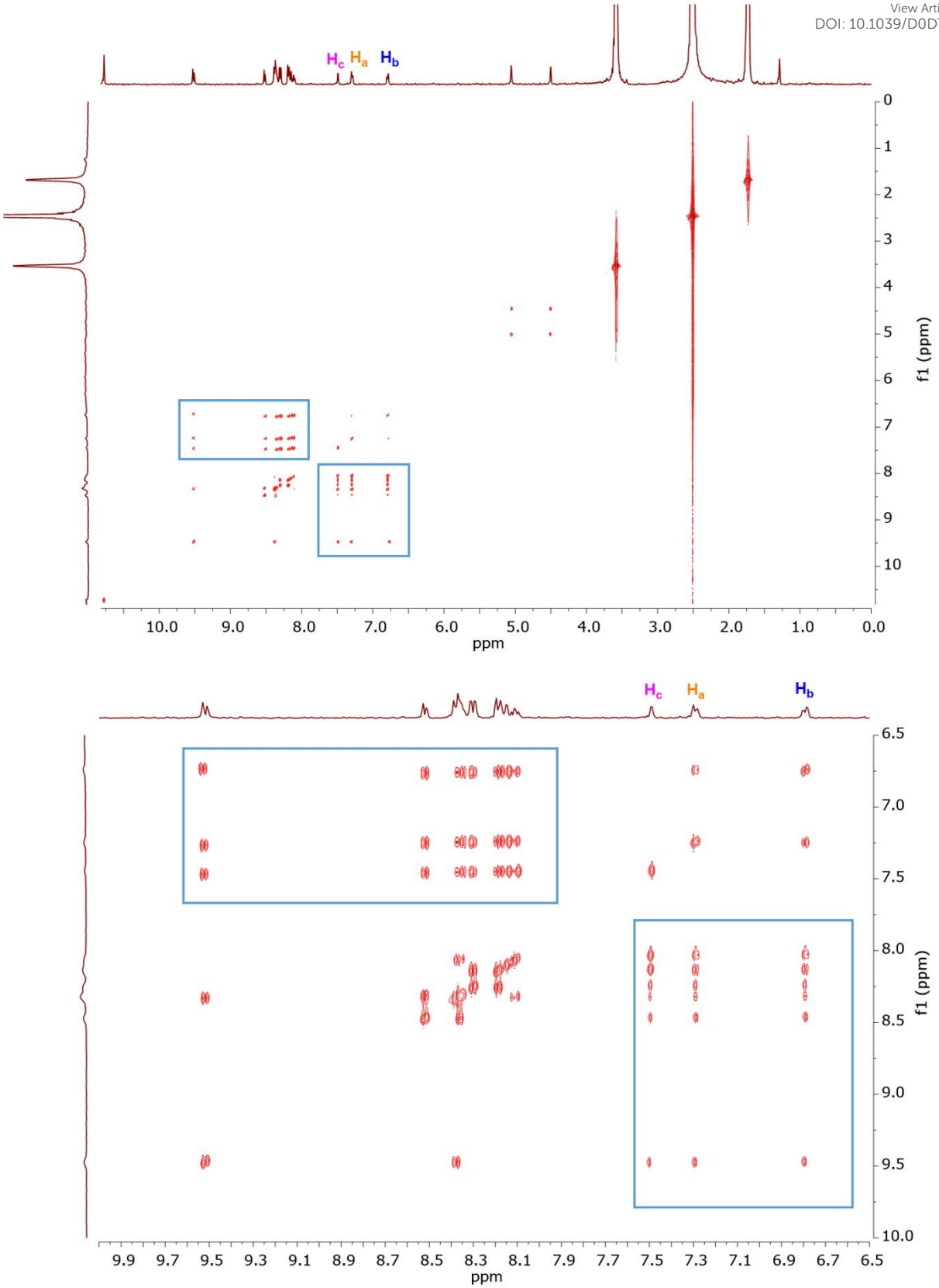

Figure S17. ^{1}H-^{1}H ROESY NMR (THF-d_8, 500 MHz) spectrum of cage **3** with 800 mol% of 1-pyrenecarboxaldehyde (**G-6**) added (top) and 10.00-6.50 ppm inset of this spectrum (**bottom**). The crucial cross-correlations are marked in blue. For the atom labels of cage **3**, see Figure S11.

View Article Online
DOI: 10.1039/D0DT01366H

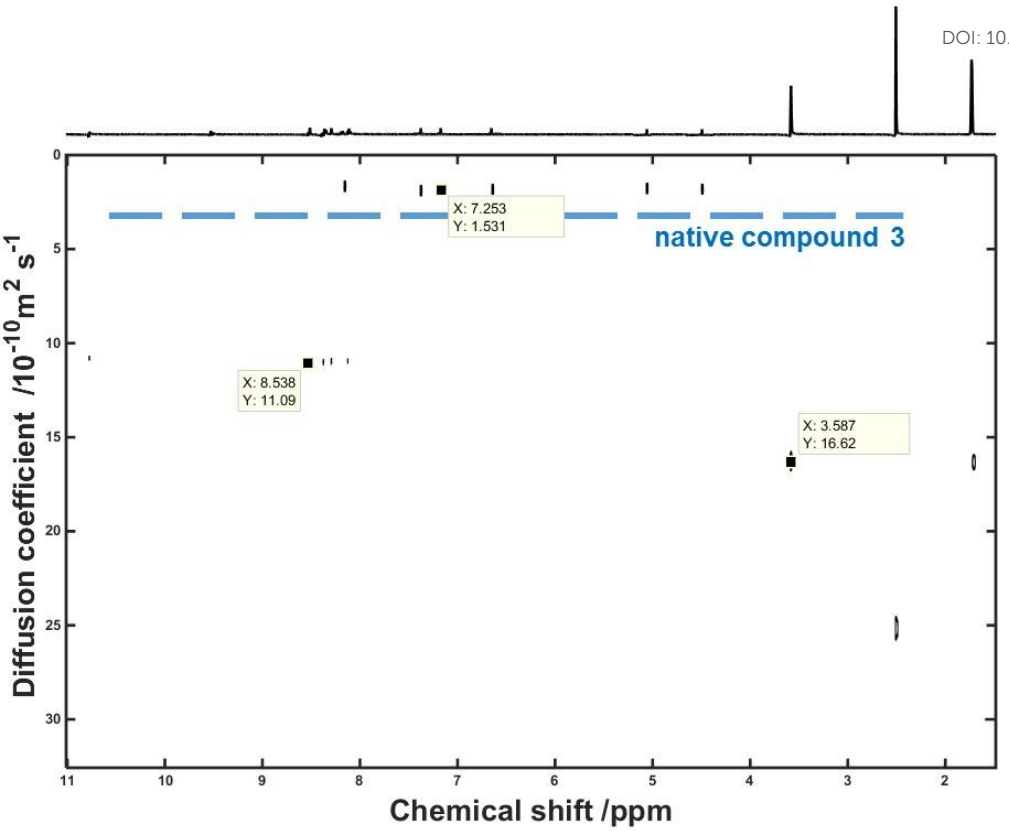

Figure S18. ^{1}H DOSY NMR (THF-d_8, 500 MHz) spectrum of cage **3** with 800 mol% of 1-pyrenecarboxaldehyde (**G-6**) added. The dashed blue line represents the diffusion coefficient value for the native cage **3**.

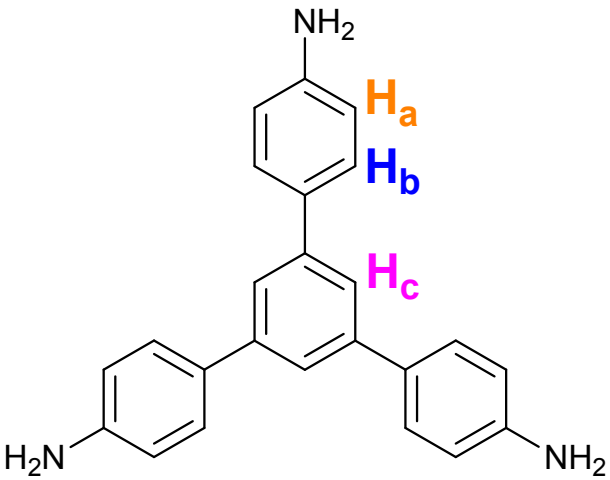

2

Figure S19. Structure of the compound **2** with the atom labels marked.

View Article Online
DOI: 10.1039/D0DT01366H

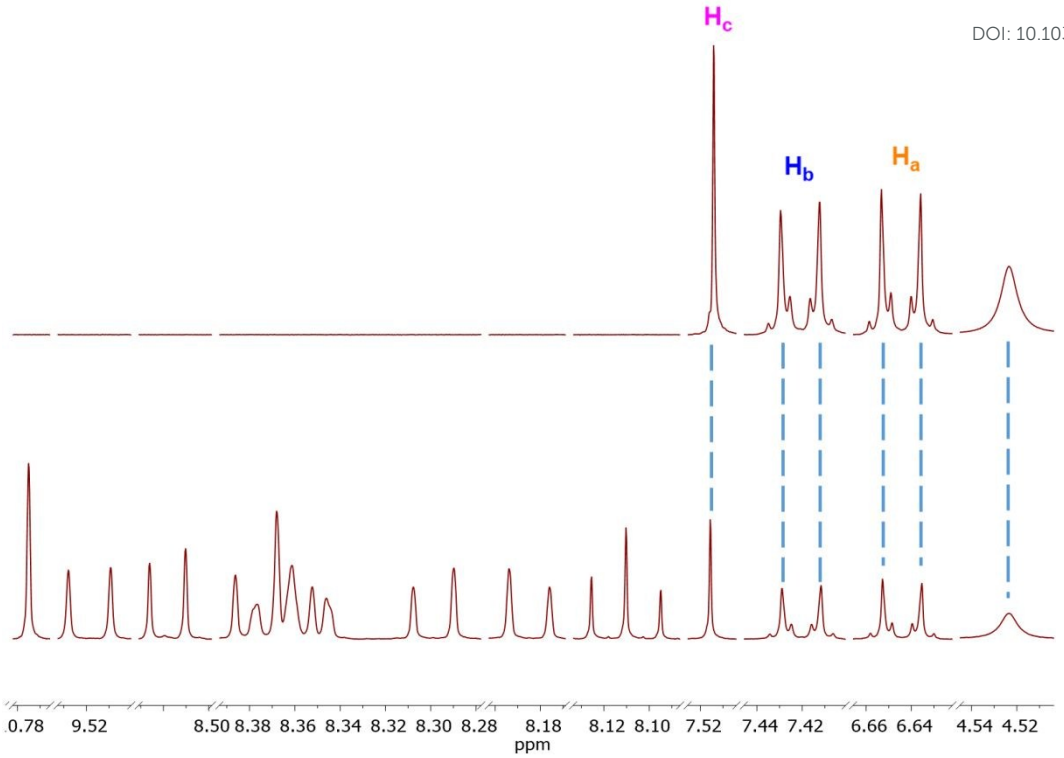

Figure S20. ^{1}H NMR (THF-d_8, 500 MHz) spectrum of compound **2** (**top**) and ^{1}H NMR (THF-d_8, 500 MHz) spectrum of compound **2** with 800 mol% of 1-pyrenecarboxaldehyde (**G-6**) added (**bottom**). For the atom labels of compound **2**, see Figure S19.

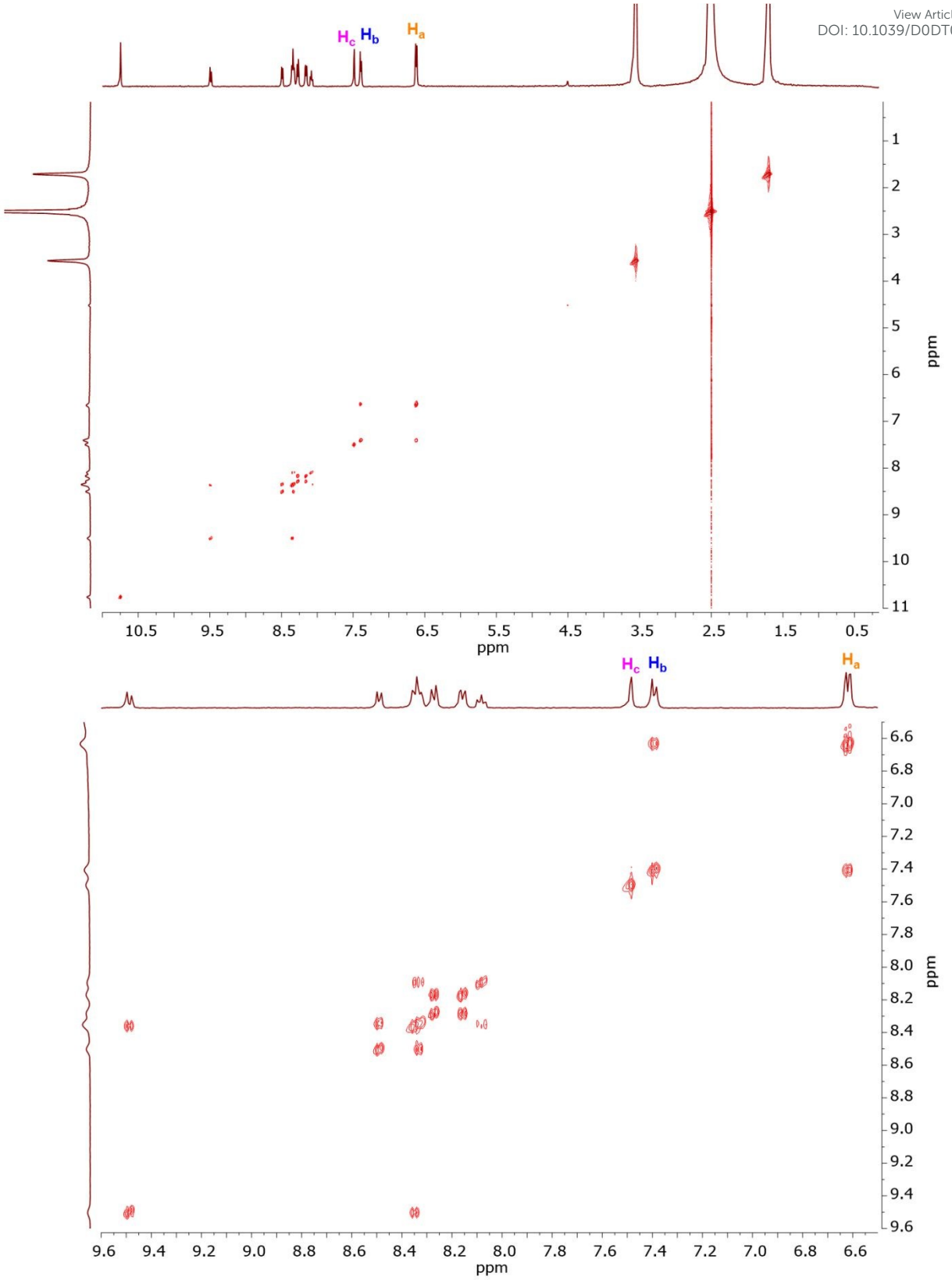

Figure S21. ^{1}H-^{1}H ROESY NMR (THF-d_8, 500 MHz) spectrum of compound **2** with 800 mol% of 1-pyrenecarboxaldehyde (**G-6**) added (**top**) and 9.60-6.50 ppm inset of this spectrum (**bottom**). For the atom labels of compound **2**, see Figure S19.

View Article Online
DOI: 10.1039/D0DT01366H

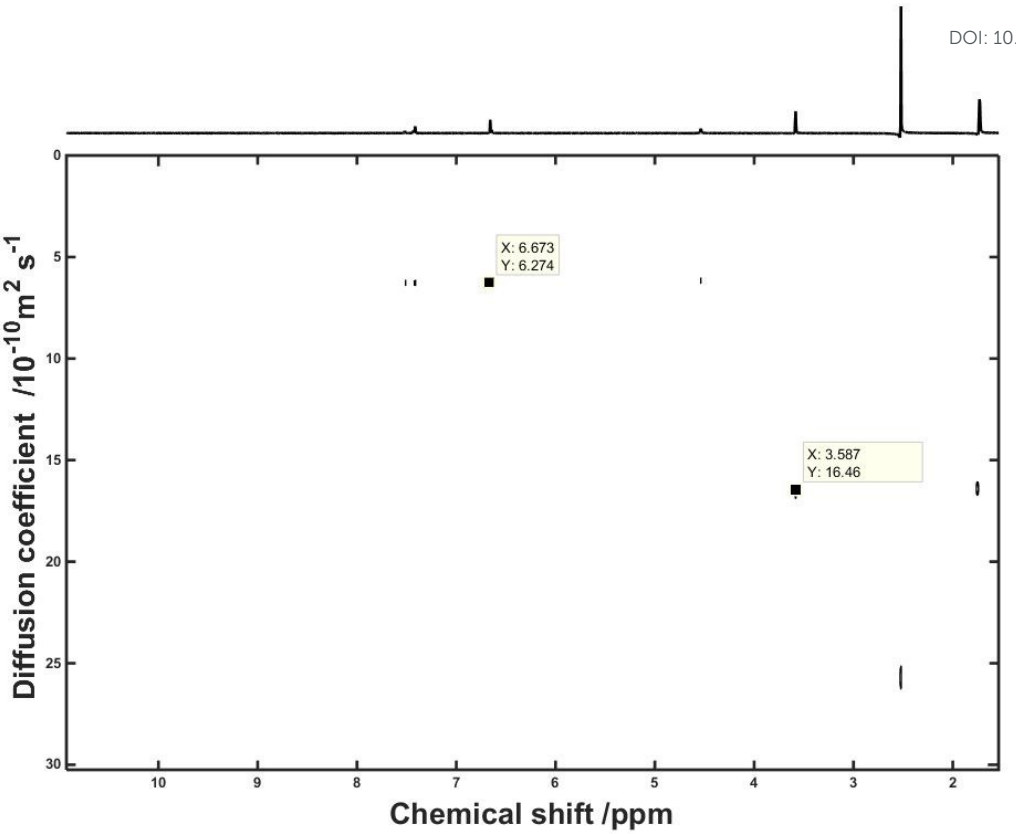

Figure S22. ^{1}H DOSY NMR (THF-d_8, 500 MHz) spectrum of compound **2**.

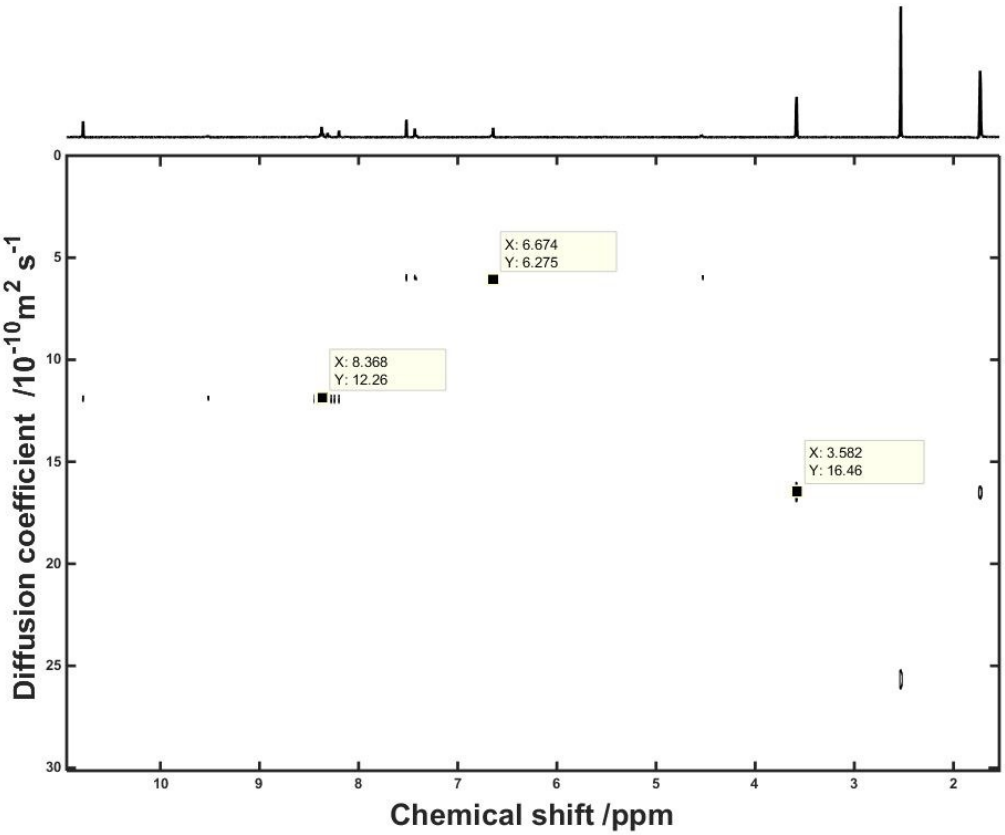

Figure S23. ^{1}H DOSY NMR (THF-d_8, 500 MHz) spectrum of compound **2** with 800 mol% of 1-pyrenecarboxaldehyde (**G-6**) added.

S7. Synthesis of 1,1′-biphenyls – ^{1}H NMR spectra

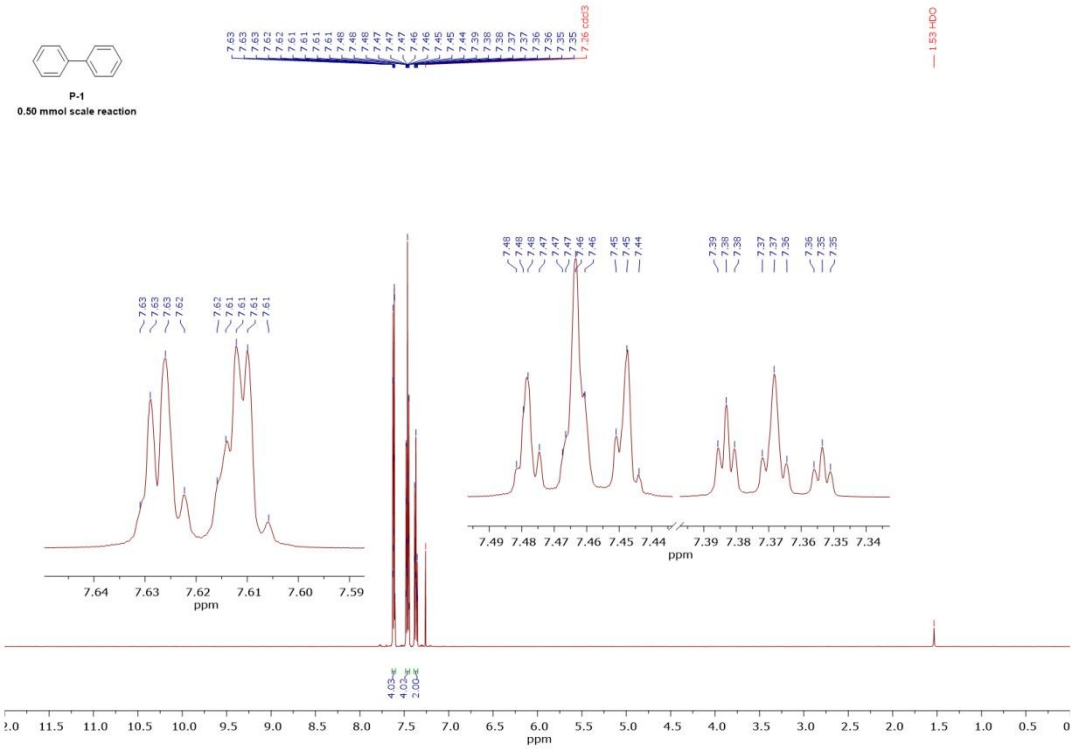

Figure S24. ^{1}H NMR ($CDCl_3$, 500 MHz) spectrum of 1,1′-biphenyl (**P-1**) obtained in a 0.50 mmol scale reaction.

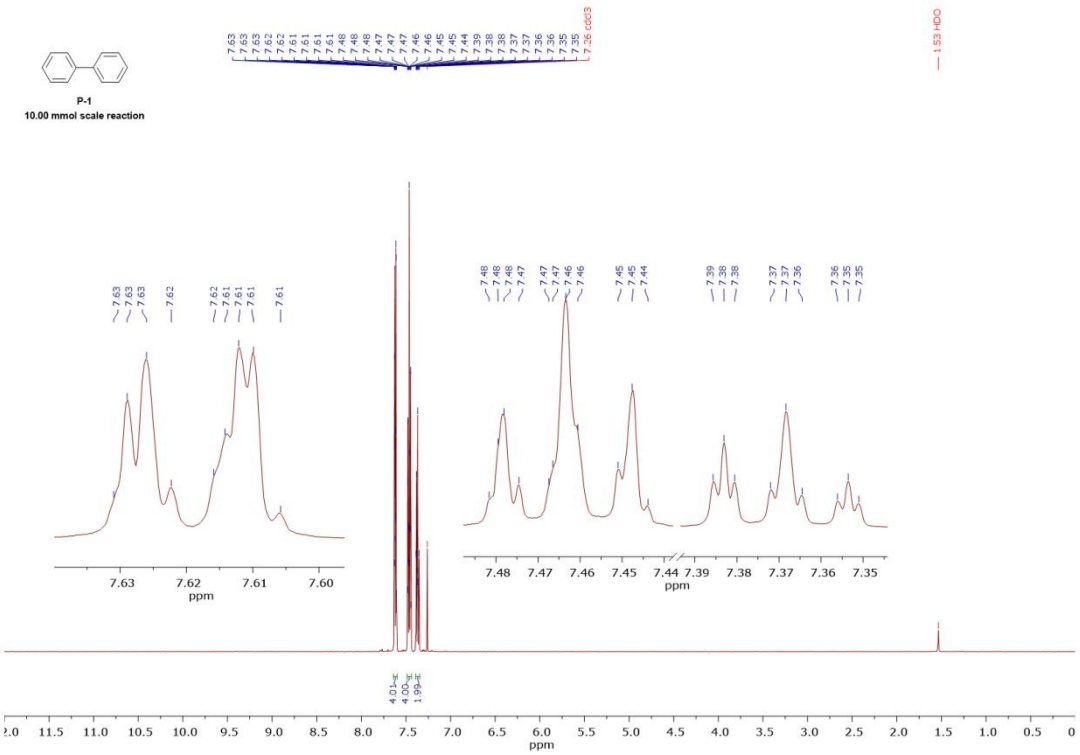

Figure S25. ^{1}H NMR ($CDCl_3$, 500 MHz) spectrum of 1,1′-biphenyl (**P-1**) obtained in a 10.00 mmol scale reaction.

View Article Online
DOI: 10.1039/D0DT01366H

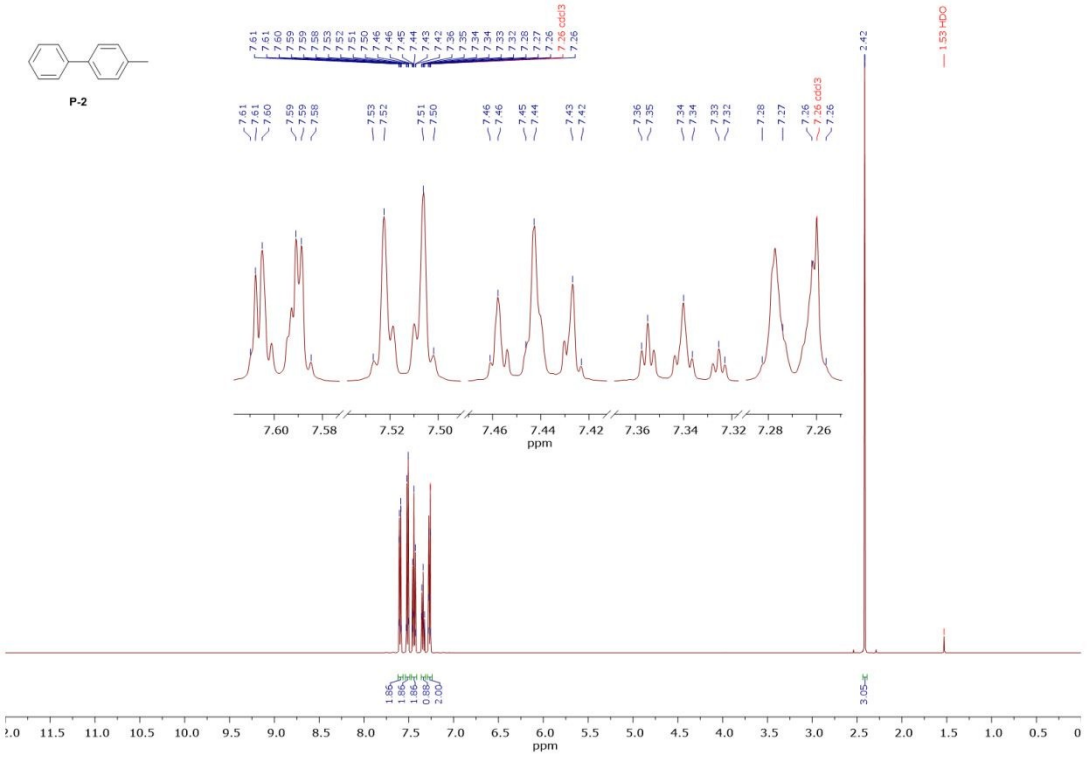

Figure S26. ^{1}H NMR ($CDCl_3$, 500 MHz) spectrum of 4-methyl-1,1′-biphenyl (**P-2**).

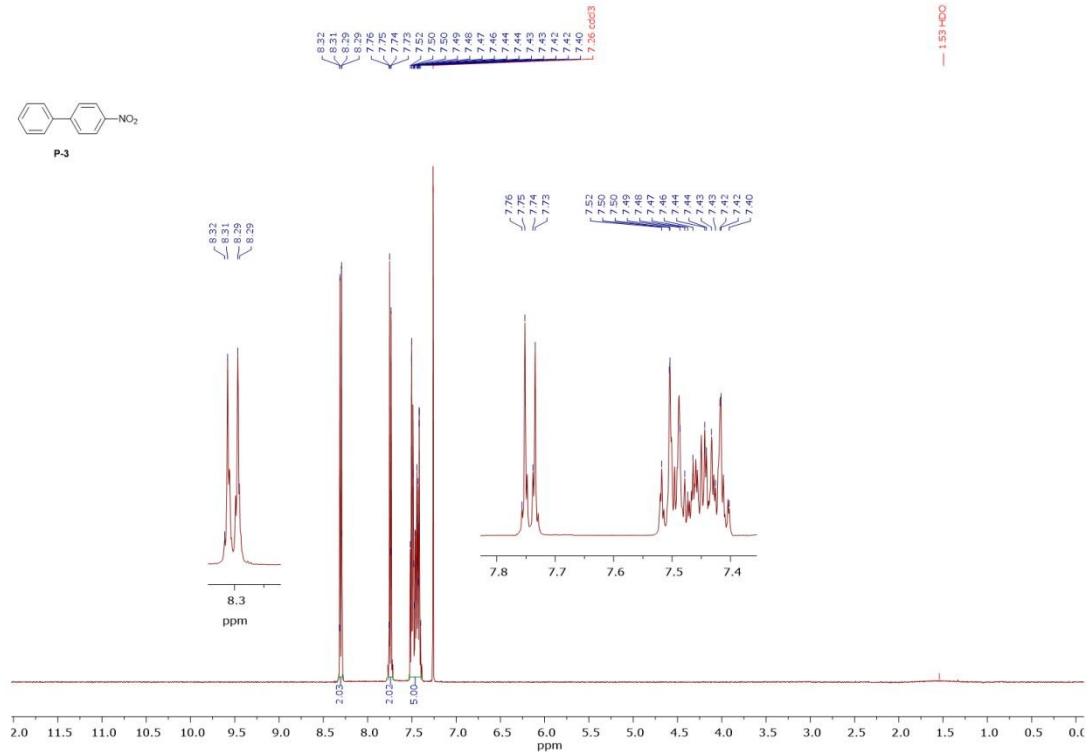

Figure S27. ^{1}H NMR ($CDCl_3$, 500 MHz) spectrum of 4-nitro-1,1′-biphenyl (**P-3**).

View Article Online
DOI: 10.1039/D0DT01366H

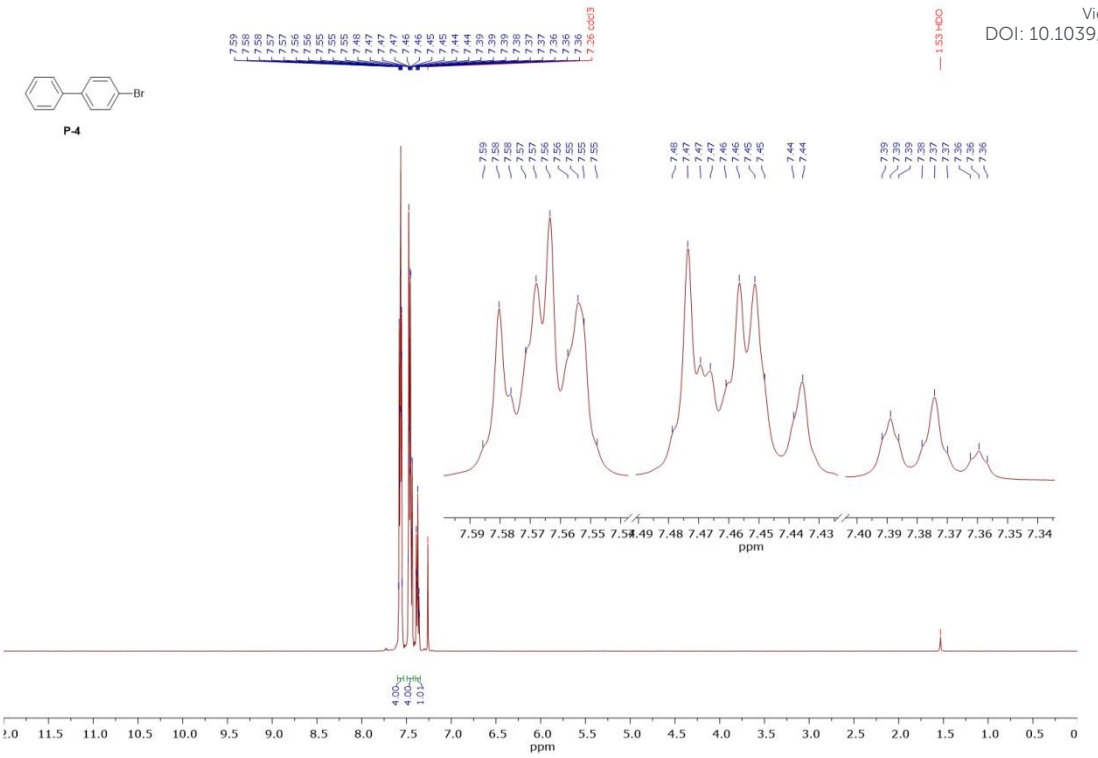

Figure S28. ^{1}H NMR ($CDCl_3$, 500 MHz) spectrum of 4-bromo-1,1′-biphenyl (**P-4**).

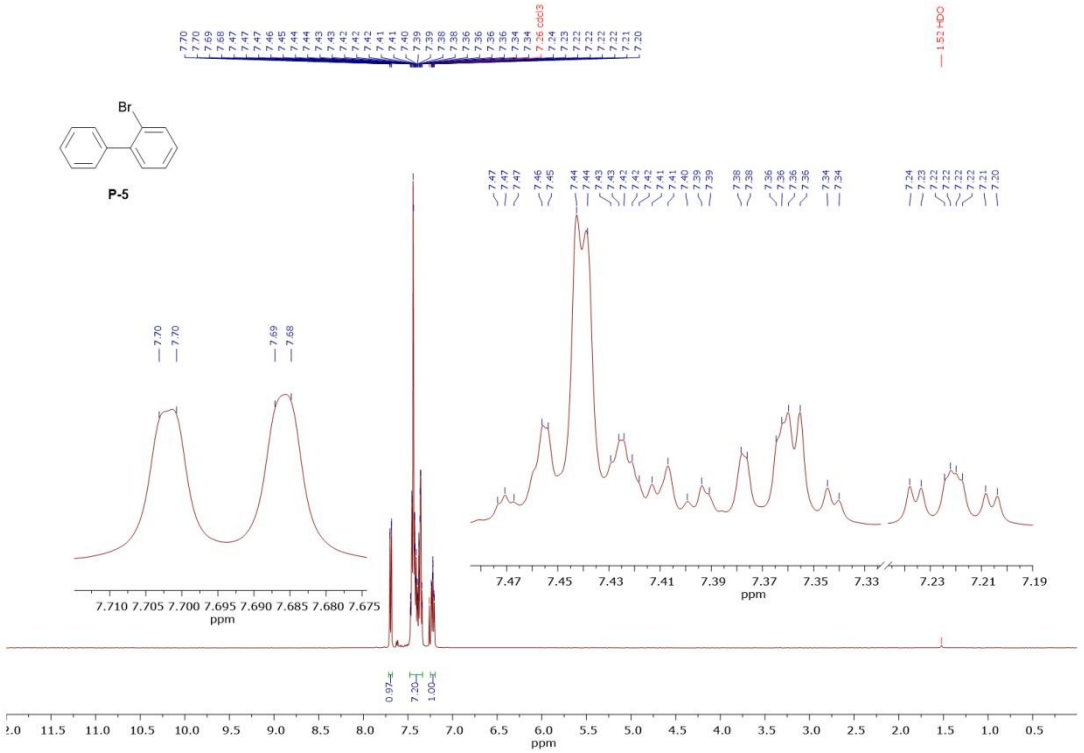

Figure S29. ^{1}H NMR ($CDCl_3$, 500 MHz) spectrum of 2-bromo-1,1′-biphenyl (**P-5**).

S8. Recyclability studies

a)

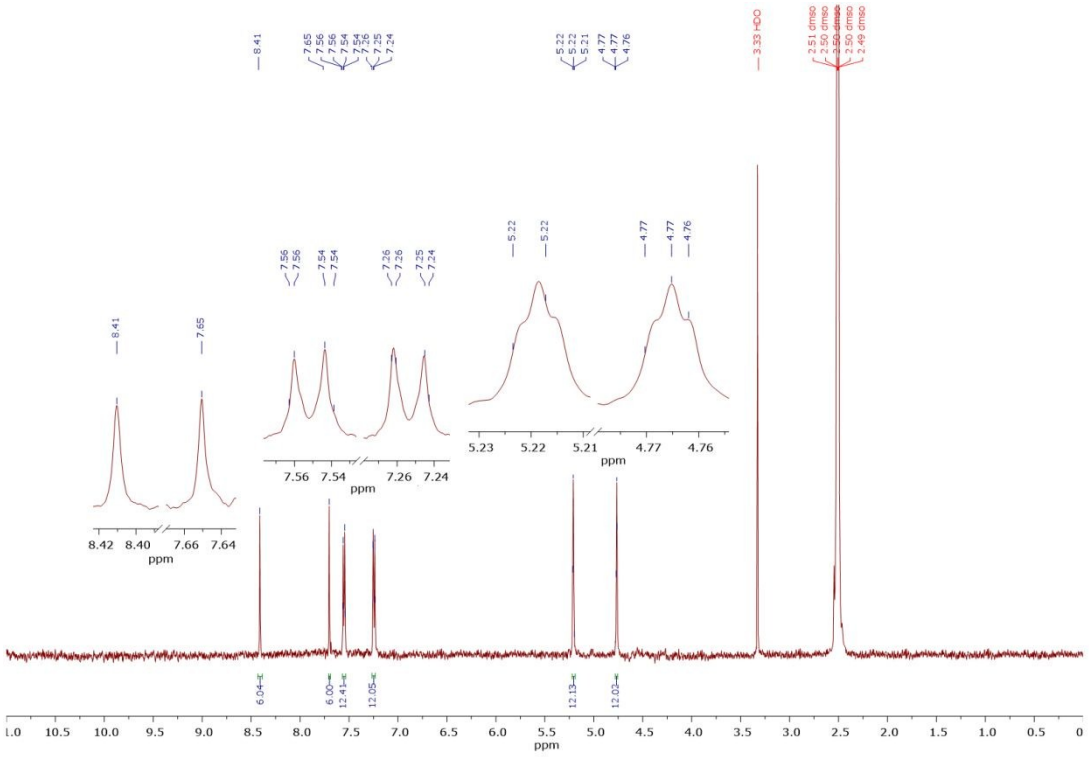

b)

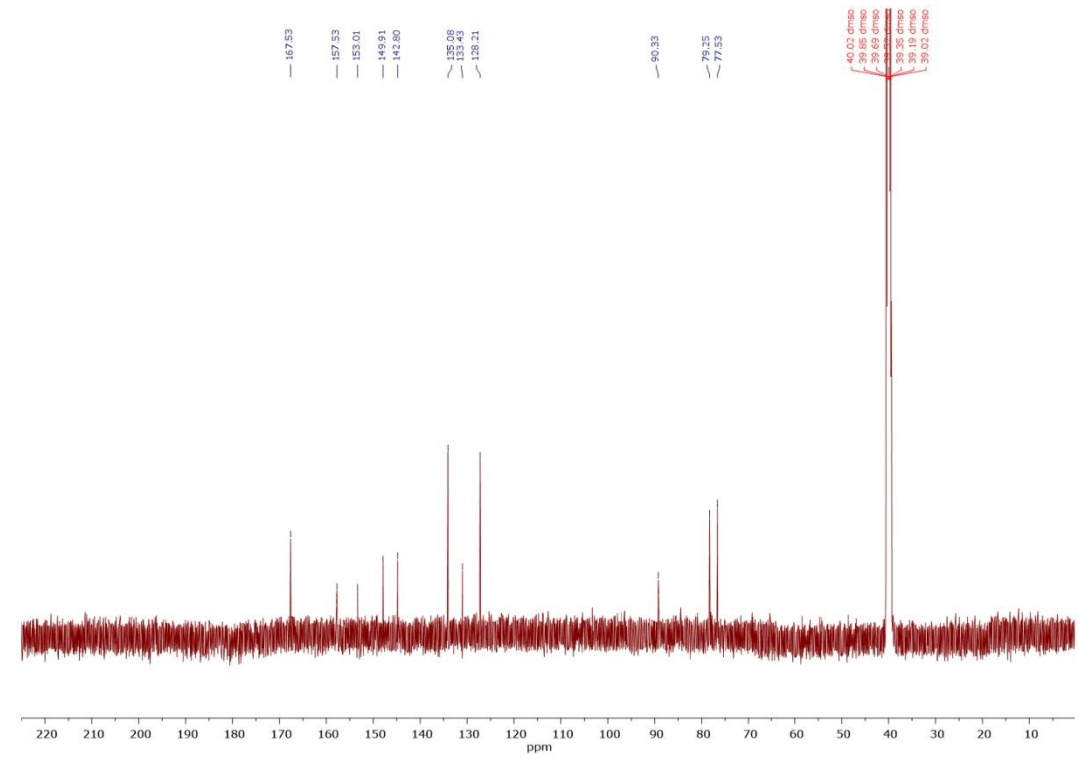

Figure S30. (**a**) ^{1}H NMR (DMSO-d_6, 500 MHz) and (**b**) ^{13}C NMR (DMSO-d_6, 125 MHz) spectra of a catalyst recovered after the catalytic reaction.

View Article Online
DOI: 10.1039/D0DT01366H

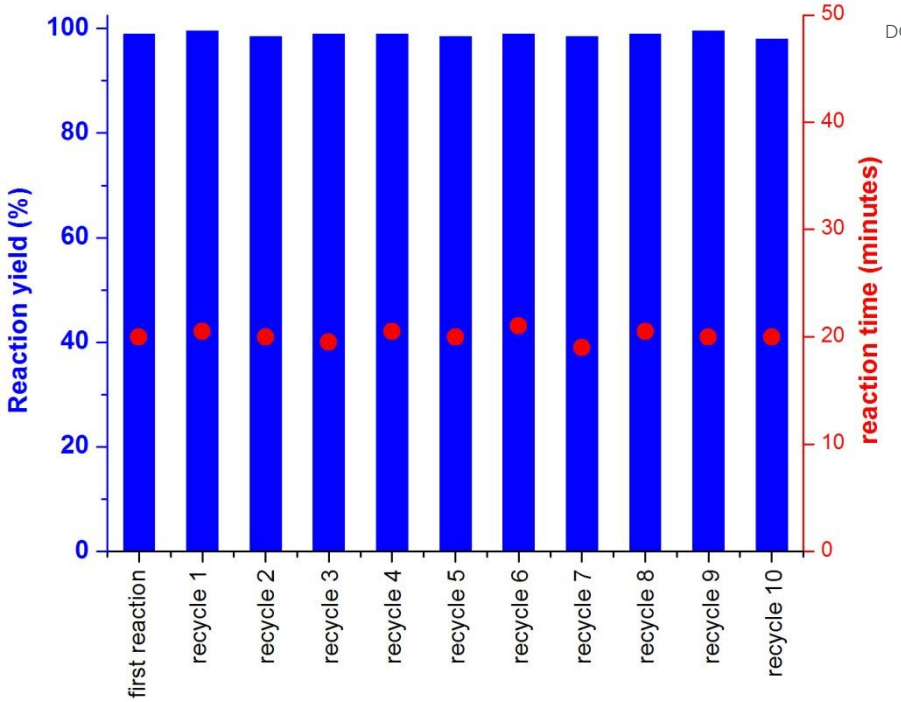

Figure S31. Reusability studies.

S9. UV-Vis titration, PL titration spectra, Job's plot analyses and calculation of binding parameters for the studied non-covalent systems

At first, the UV-Vis (Figure S32) and PL (Figure S33) titration spectra in THF were measured for cage **3** in the presence of representative **G-1**. Lowering of the absorption or emission intensity for cage **3** was observed after the addition of next portions of the **G-1**. PL titration method was found as the more sensitive technique for tracking the recognition. Then, PL titration spectra were measured for cage **3** in the presence of other aromatics (**G-2**-**G-6**; Figures S34-S38). Once again, the lowering of the emission intensity was observed after adding further portions of an aromatic molecule.

Continuous variation method was employed to estimate the system stoichiometry. The Job's plots related to the interactions between **3** and aromatics were constructed (Figures S39-S44). The system stoichiometry was estimated. Interactions of cage **3** with **G-1** or **G-2** featured system stoichiometry of 1:3, whilst for other aromatics (**G-3**-**G-6**) estimated stoichiometry was 1:1.

Calculations of the apparent binding constants (K_{app}) were based on the Stern-Volmer equation[15],[16]:

$$\frac{I_0}{I} = 1 + K_{\mathrm{app}} \cdot C_{\mathrm{ar}}$$

, where C_{ar} is the molar concentration of the aromatic molecule (**G-1** – **G-6**), I_0 and I are the fluorescence intensity of cage **3** in the absence and in the presence of the aromatic molecule, respectively. I_0/I = f(C_{ar}) dependencies were plotted for **G-1**-**G-6** (Figures S45-S50). All these dependencies were found to be linear. Therefore, K_{app} were calculated respectively using the Stern-Volmer method, see references [15] and [16] for details of this methodology.

Gibbs free energy values (free energies; ΔG) were calculated using the following equation:

$$\Delta G = -RT \ln K_{\mathrm{app}}$$

, where R stands for the gas constant (8.314 J·K^{-1}·mol^{-1}) and T is the temperature (298.15 K).

The calculated binding parameters (system stoichiometry, K_{app} and ΔG) are summarized in **Table 1** in the main article file.

For the representative aromatic molecule **G-6** (the highest K_{app} among the aromatics tested), the K_{app} and ΔG values evaluated from PL spectra titration method were also compared with the respective values obtained from ^{1}H DOSY NMR experiments. The method for calculation of these parameters employing the ^{1}H DOSY NMR procedure is described in detail elsewhere.[17]-[19] At first, the spectra for native **G-6** and 1:1 (mol:mol) mixture of cage **3** and **G-6**, were acquired (Figures S51-S52, $c_{cage3} = c_{G\text{-}6}$ = 0.5 mM). The diffusion coefficient for the free **G-6** was higher than the respective value for **G-6** in a presence of cage **3**. This feature was ascribed to the recognition feature of cage **3**.[17]-[19] K_{app} (658 M^{-1}) and ΔG (−16.1 kJ·mol^{-1}) values calculated employing the ^{1}H DOSY NMR method were highly consistent with the data obtained from PL experiments, see Table S4.

We would like note that, in general, the Stern-Volmer methodology is used to describe 1:1 models. However, I_0/I = f(C_{ar}) plots were linear for all studied systems. Therefore, this method was employed to calculate each K_{app}. For additional discussion, see for example: A. Kasprzak, H. Sakurai., *Dalton Trans*. **2019**, *48*, 17147;

View Article Online
DOI: 10.1039/D0DT01366H

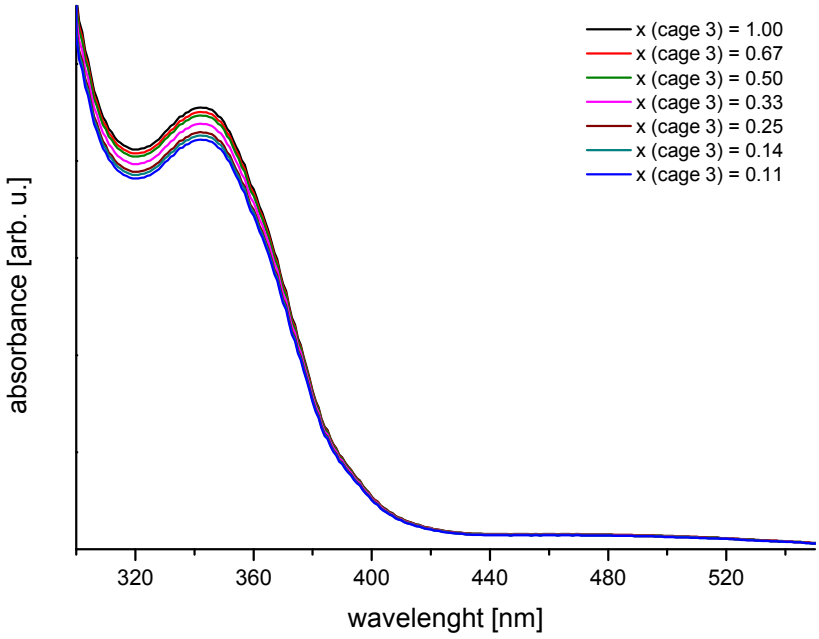

Figure S32. UV-Vis titration spectra of cage **3** in the presence of further portions of **G-1** (x stands for the molar fraction of **3**).

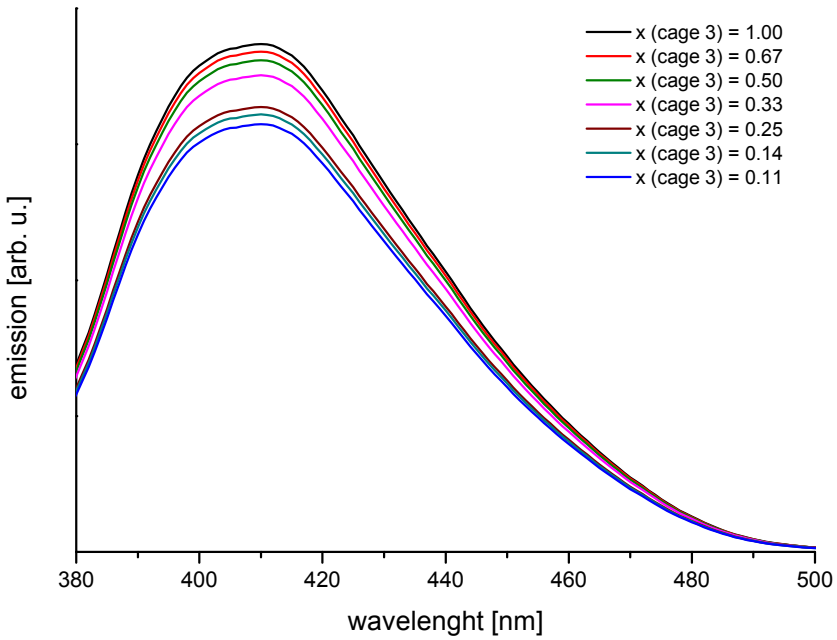

Figure S33. PL titration spectra of cage **3** in the presence of further portions of **G-1** (excitation wavelength: 335 nm; x stands for the molar fraction of **3**).

View Article Online
DOI: 10.1039/D0DT01366H

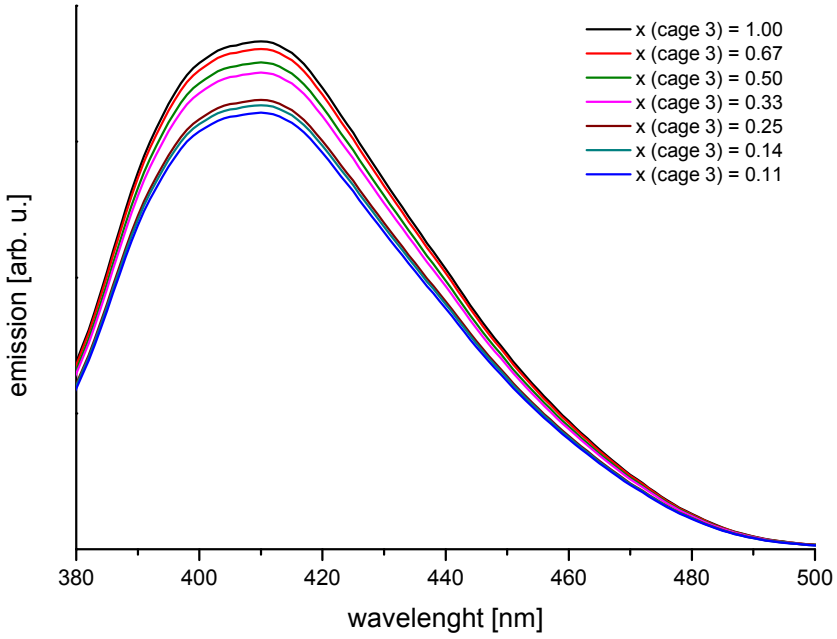

Figure S34. PL titration spectra of cage **3** in the presence of further portions of **G-2** (excitation wavelength: 335 nm; x stands for the molar fraction of **3**).

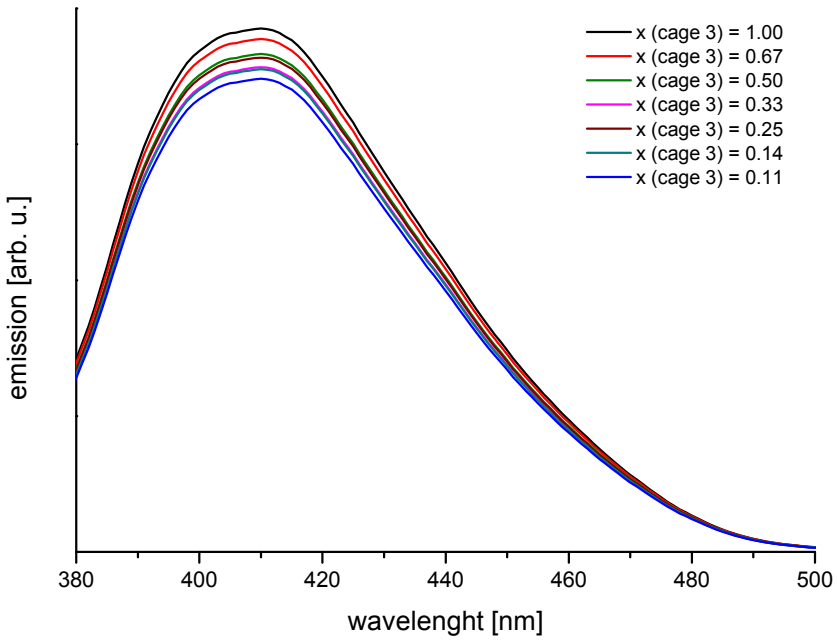

Figure S35. PL titration spectra of cage **3** in the presence of further portions of **G-3** (excitation wavelength: 335 nm; x stands for the molar fraction of **3**).

View Article Online
DOI: 10.1039/D0DT01366H

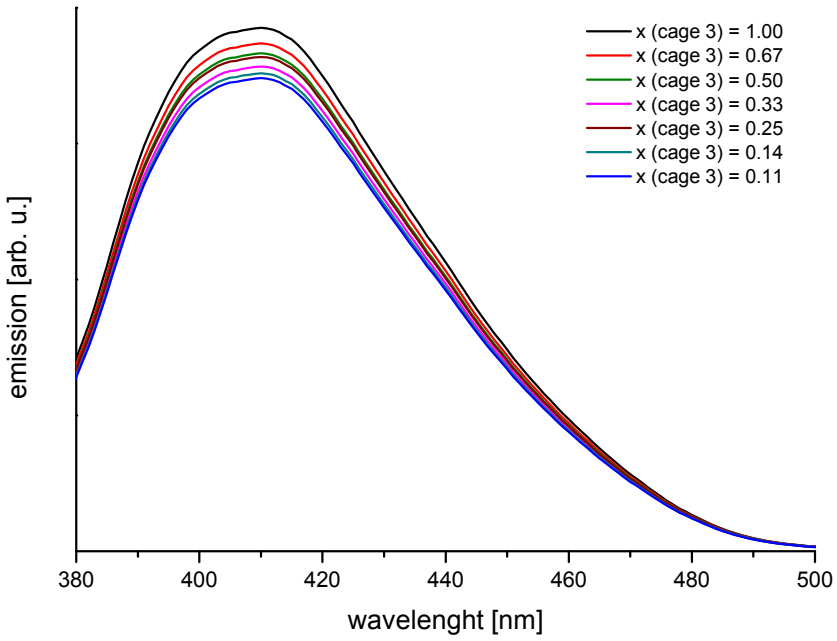

Figure S36. PL titration spectra of cage **3** in the presence of further portions of **G-4** (excitation wavelength: 335 nm; x stands for the molar fraction of **3**).

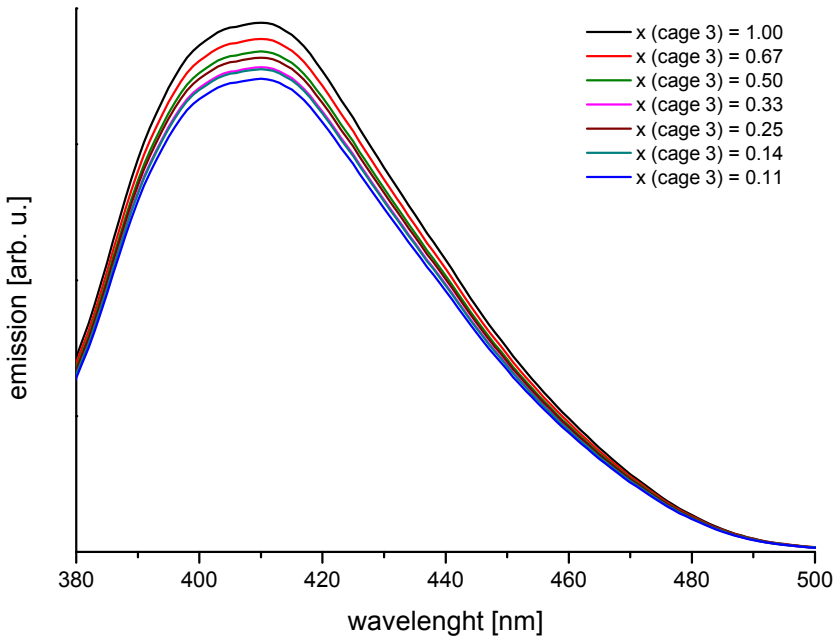

Figure S37. PL titration spectra of cage **3** in the presence of further portions of **G-5** (excitation wavelength: 335 nm; x stands for the molar fraction of **3**).

View Article Online
DOI: 10.1039/D0DT01366H

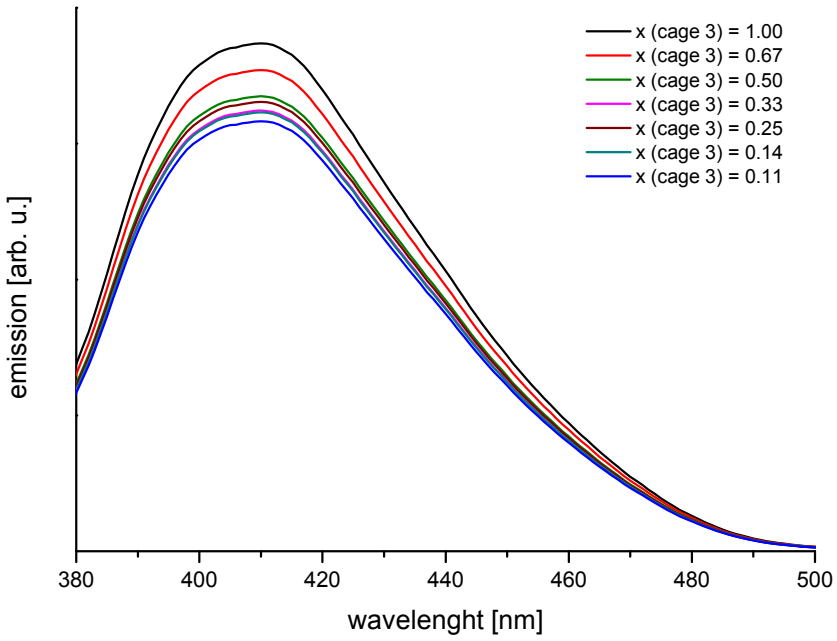

Figure S38. PL titration spectra of cage **3** in the presence of further portions of **G-6** (excitation wavelength: 335 nm; x stands for the molar fraction of **3**).

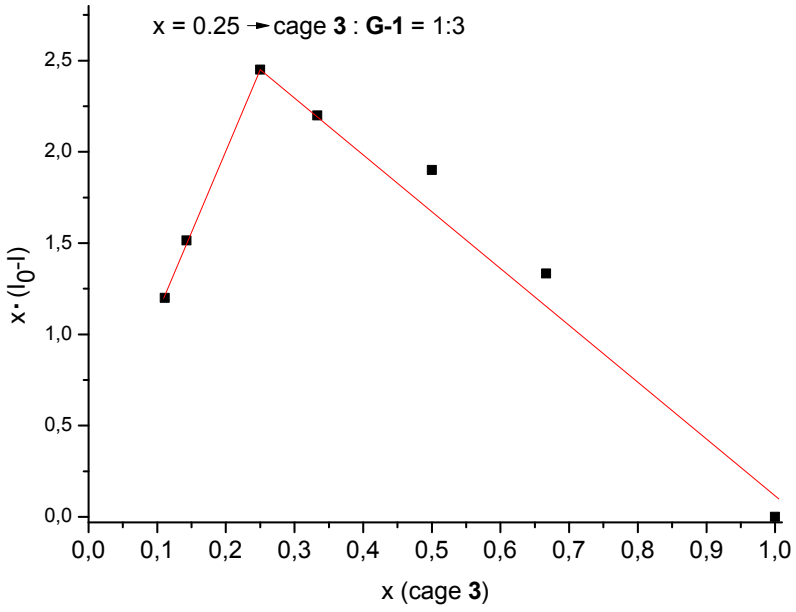

Figure S39. Job's plot regarding the interactions between cage **3** and **G-1** (obtained from the PL spectra titration data; x stands for the molar fraction of **3**, I_0 stands for the emission intensity of **3** without aromatic molecule added, I stands for the emission intensity of **3** with the given amount of aromatic molecule added).

View Article Online
DOI: 10.1039/D0DT01366H

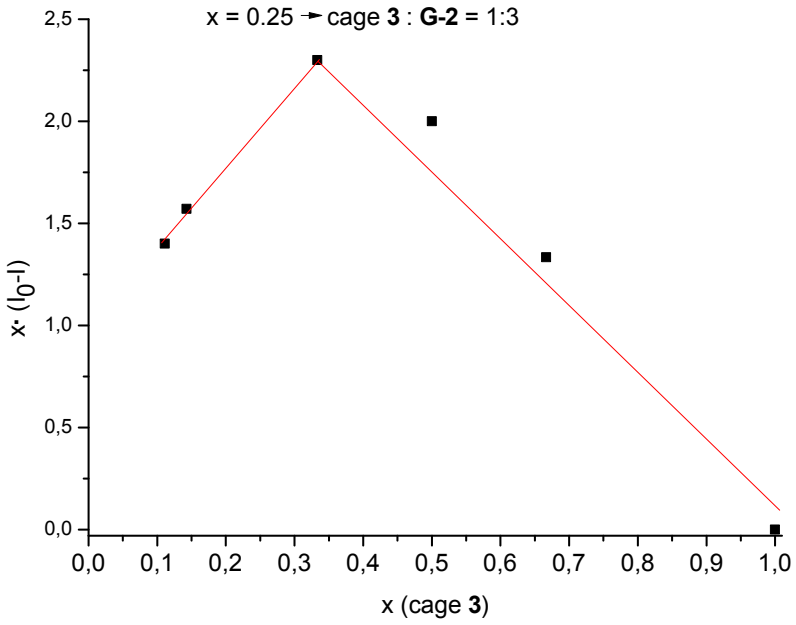

Figure S40. Job's plot regarding the interactions between cage **3** and **G-2**. (obtained from the PL spectra titration data; x stands for the molar fraction of **3**, I_0 stands for the emission intensity of **3** without aromatic molecule added, I stands for the emission intensity of **3** with the given amount of aromatic molecule added).

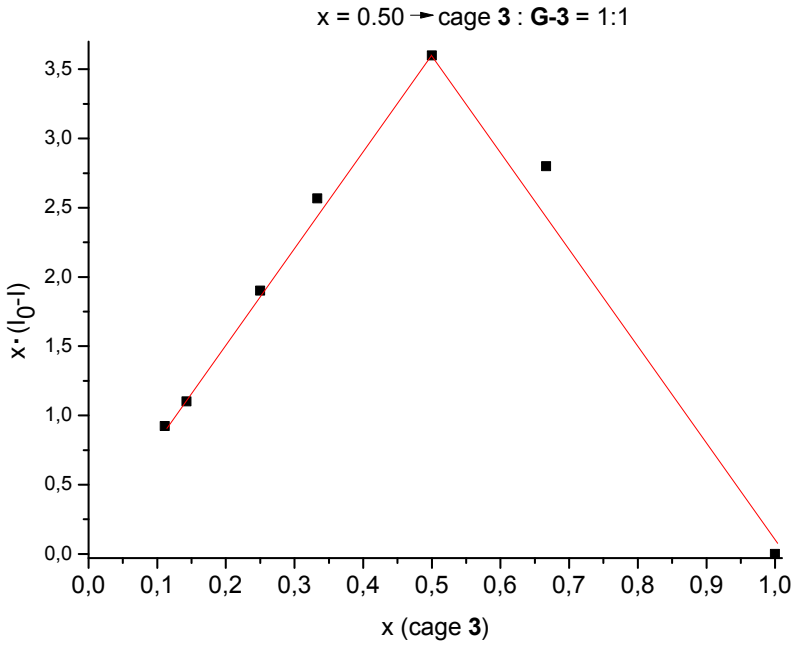

Figure S41. Job's plot regarding the interactions between cage **3** and **G-3**. (obtained from the PL spectra titration data; x stands for the molar fraction of **3**, I_0 stands for the emission intensity of **3** without aromatic molecule added, I stands for the emission intensity of **3** with the given amount of aromatic molecule added).

View Article Online
DOI: 10.1039/D0DT01366H

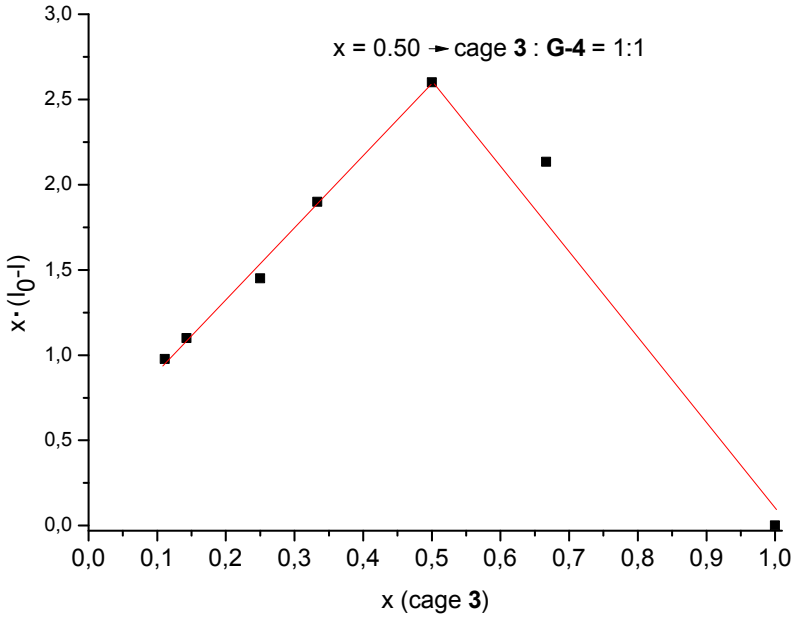

Figure S42. Job's plot regarding the interactions between cage **3** and **G-4**. (obtained from the PL spectra titration data; x stands for the molar fraction of **3**, I_0 stands for the emission intensity of **3** without aromatic molecule added, I stands for the emission intensity of **3** with the given amount of aromatic molecule added).

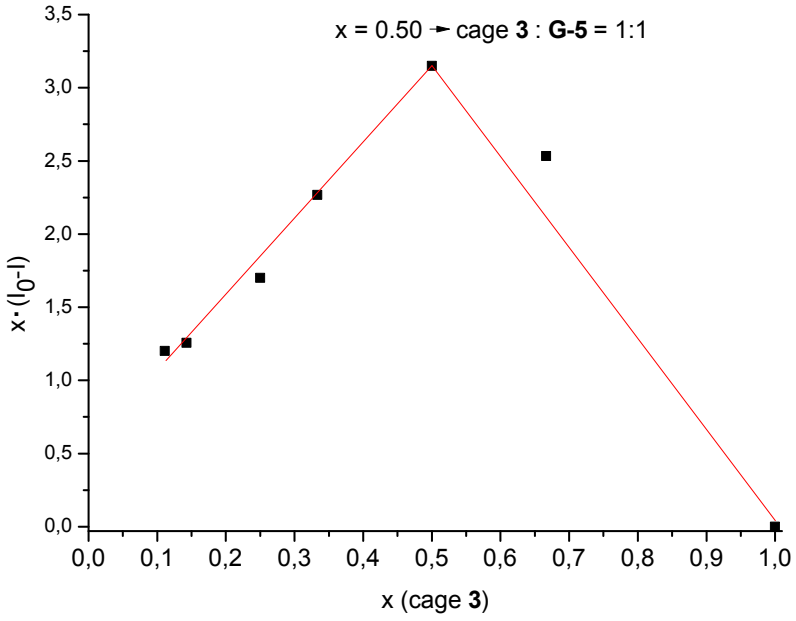

Figure S43. Job's plot regarding the interactions between cage **3** and **G-5**. (obtained from the PL spectra titration data; x stands for the molar fraction of **3**, I_0 stands for the emission intensity of **3** without aromatic molecule added, I stands for the emission intensity of **3** with the given amount of aromatic molecule added).

View Article Online
DOI: 10.1039/D0DT01366H

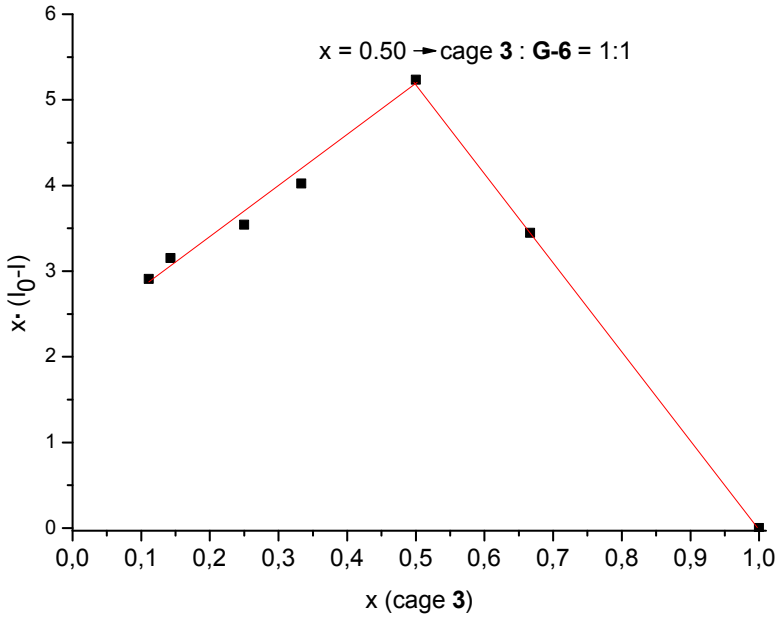

Figure S44. Job's plot regarding the interactions between cage **3** and **G-6**. (obtained from the PL spectra titration data; x stands for the molar fraction of **3**, I_0 stands for the emission intensity of **3** without aromatic molecule added, I stands for the emission intensity of **3** with the given amount of aromatic molecule added)

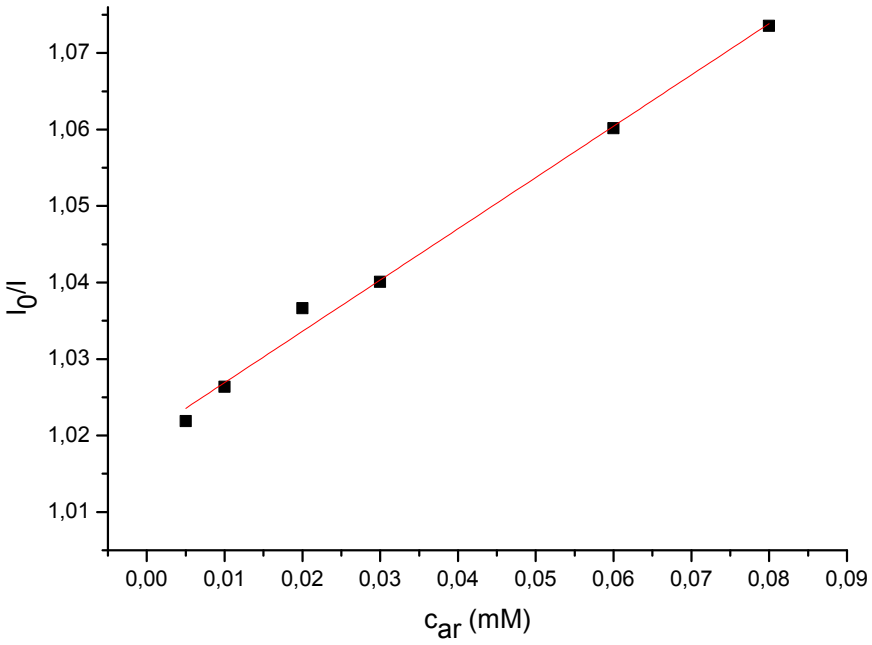

Figure S45. I_0/I = f(C_{ar}) plot regarding the interactions between **3** and **G-1**. R^2 = 0.9923.

View Article Online
DOI: 10.1039/D0DT01366H

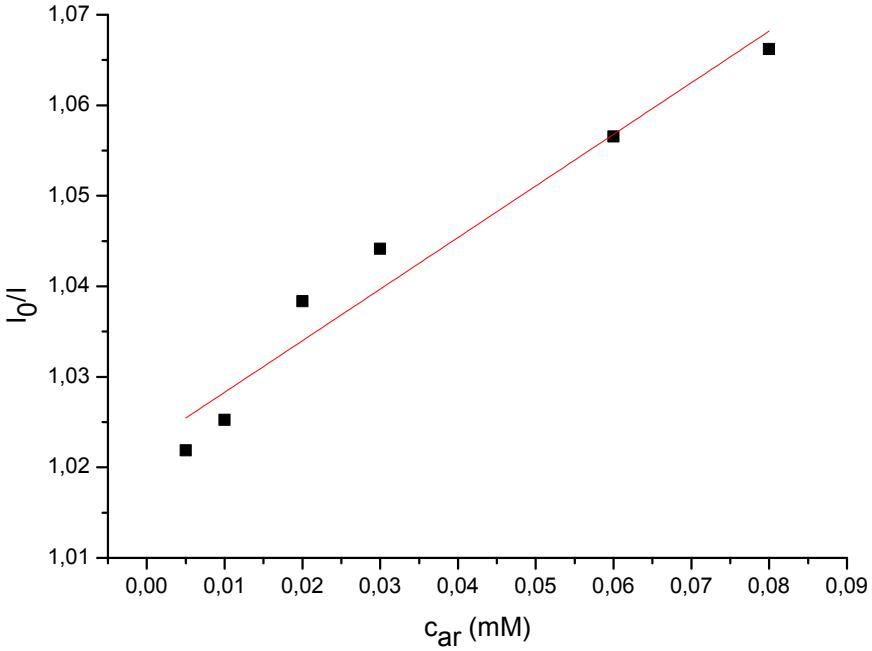

Figure S46. I_0/I = f(C_{ar}) plot regarding the interactions between **3** and **G-2**. R^2 = 0.9650.

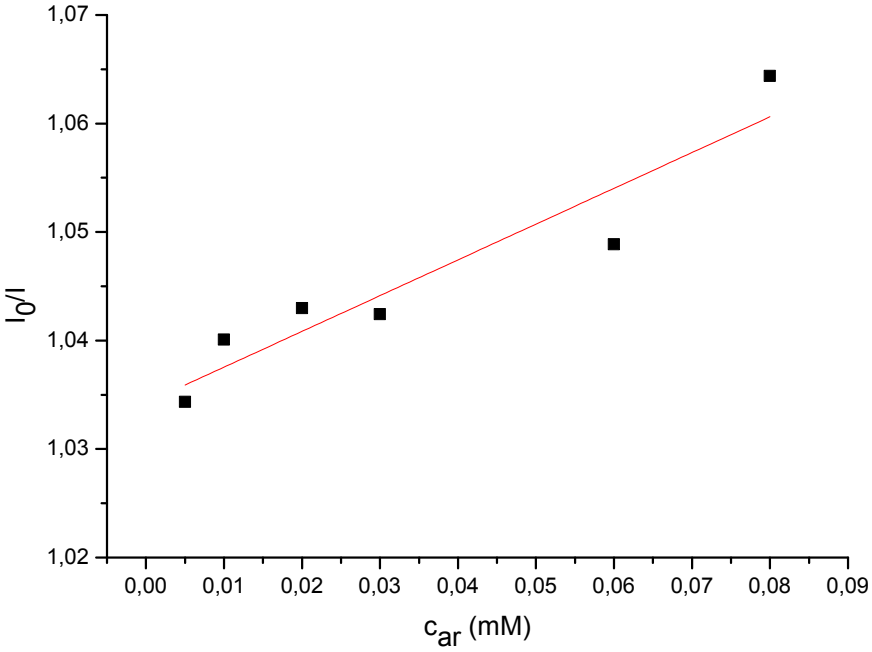

Figure S47. I_0/I = f(C_{ar}) plot regarding the interactions between **3** and **G-3**. R^2 = 0.9052.

View Article Online
DOI: 10.1039/D0DT01366H

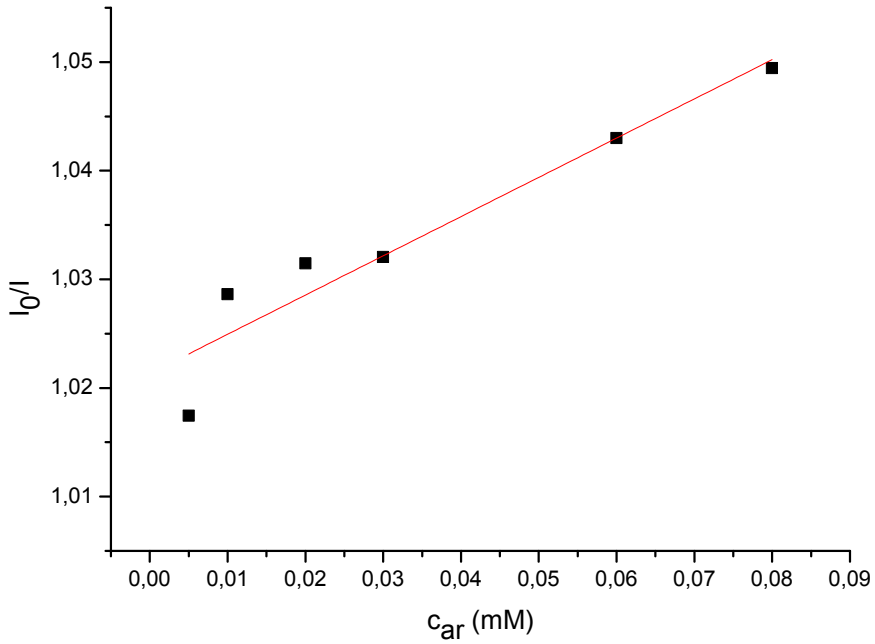

Figure S48. I_0/I = f(C_{ar}) plot regarding the interactions between **3** and **G-4**. R^2 = 0.9006.

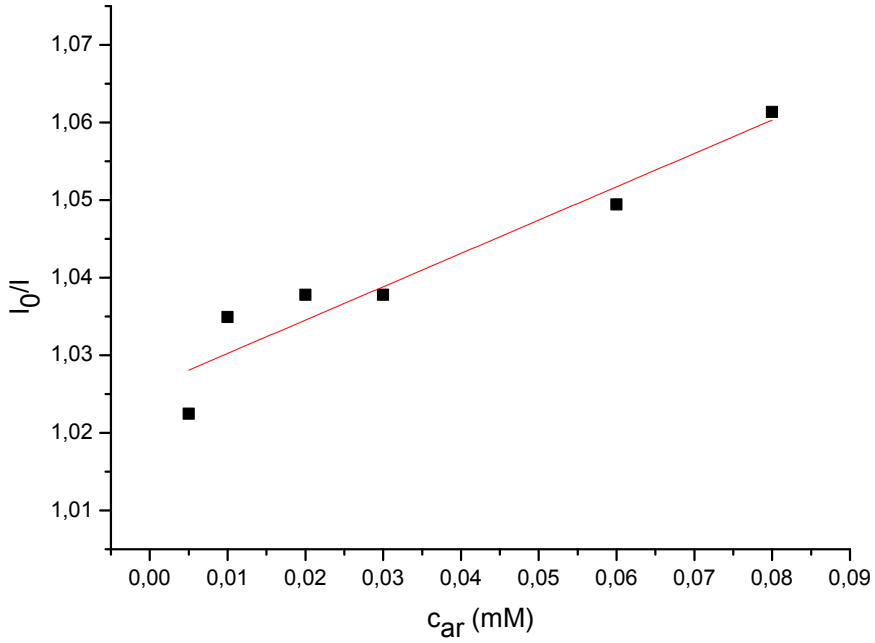

Figure S49. I_0/I = f(C_{ar}) plot regarding the interactions between **3** and **G-5**. R^2 = 0.9015.

View Article Online
DOI: 10.1039/D0DT01366H

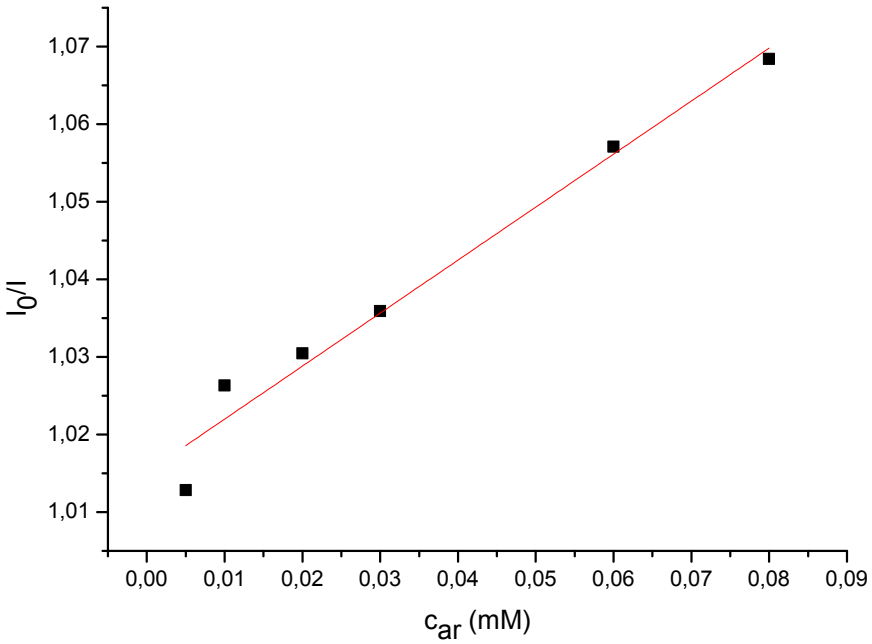

Figure S50. I_0/I = f(C_{ar}) plot regarding the interactions between **3** and **G-6**. R^2 = 0.9663.

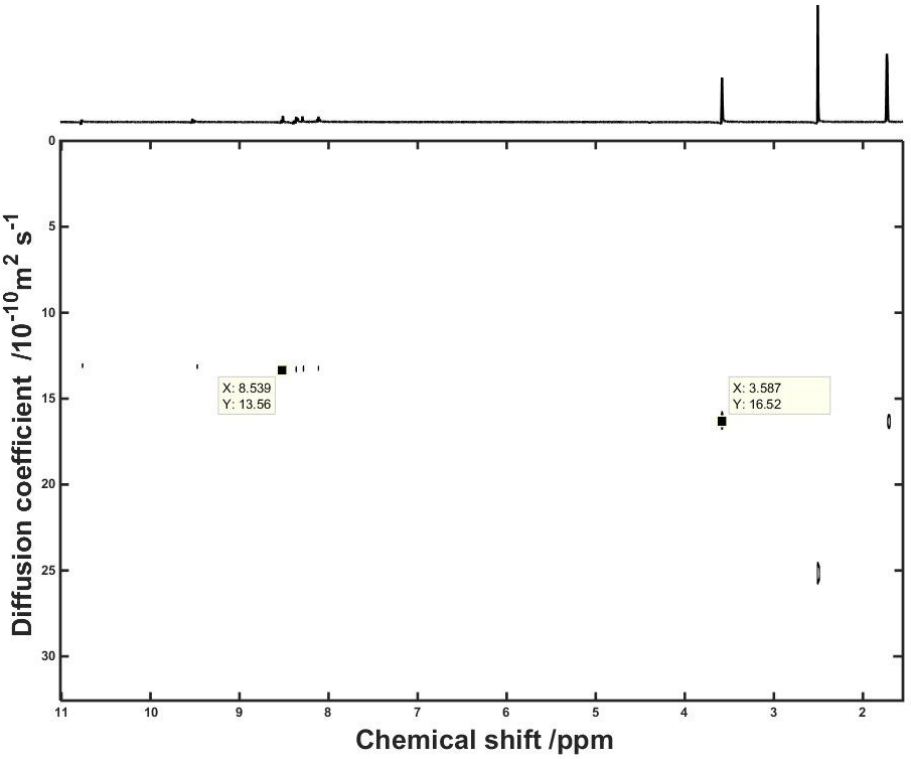

Figure S51. ^{1}H DOSY NMR (THF-d_8, 500 MHz) spectrum of native **G-6**.

View Article Online
DOI: 10.1039/D0DT01366H

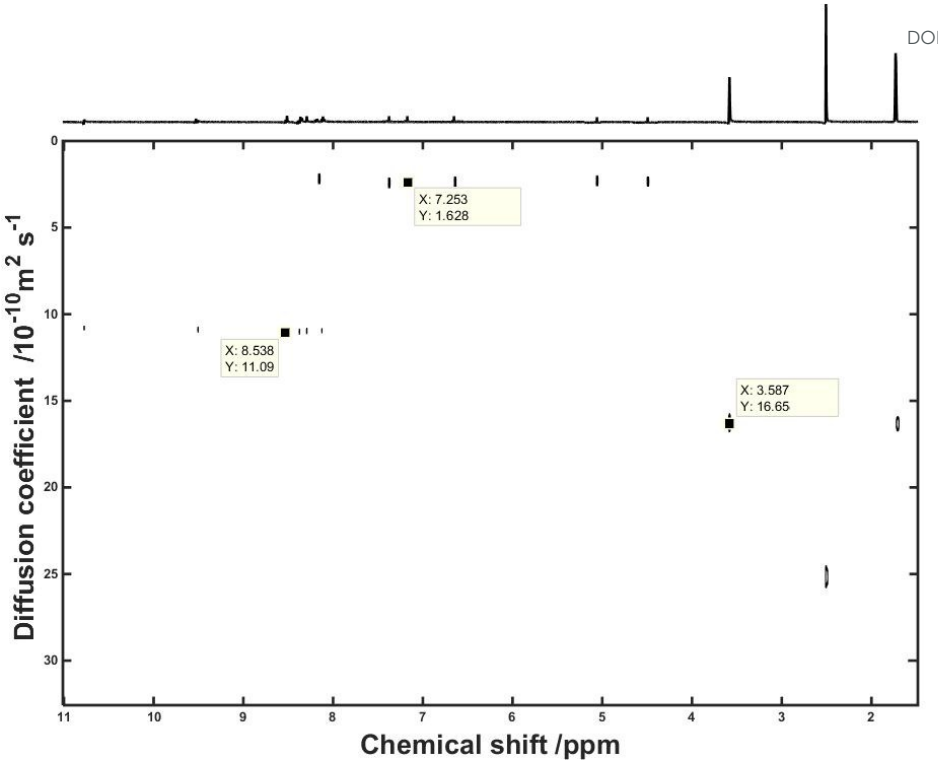

Figure S52. ^{1}H DOSY NMR (THF-d_8, 500 MHz) spectrum of 1:1 (mol:mol) mixture of cage **3** and **G-6**.

Table S4. K_{app} and ΔG values for the interactions between cage **3** and **G-6** calculated from ^{1}H DOSY NMR data. Diffusion coefficient values are given in 10^{-10} m^2 s^{-1}; x_b parameter was calculated as follows: $x_b = (D_{free} - D_{obs}) \cdot [(D_{free} - D_{bound})^{-1}]$, where D_{free} stands for the diffusion coefficient value for the native **G-6**, D_{obs} is the diffusion coefficient value for the **G-6** in the system, D_{bound} is the diffusion coefficient value for cage **3** in the system; K_{app} values were calculated as follows: $K_{app} = x_b \cdot [(1 - x_b) \cdot (0.5\ mM - x_b \cdot 0.5\ mM)]^{-1}$. The respective K_{app} and ΔG values evaluated from PL titration experiments are also shown.

Component	D_{free}	D_{obs}	D_{bound}	x_b	K_{app} /M^{-1} (K_{app} value calculated based on PL experiments data)	ΔG /kJ·mol^{-1} (ΔG value calculated based on PL experiments data)
Cage **3**	N/A	N/A	1.628	0.207	**658**	**−16.1**
G-6	13.560	11.090	N/A		(650)	(−16.1)

View Article Online
DOI: 10.1039/D0DT01366H

S10. Kinetic studies

^{1}H NMR spectra were measured in DMSO-d_6 in time intervals (2 minutes, 5 minutes, 10 minutes, 15 minutes and 20 minutes). Phenylboronic acid (**G-1**) and chlorobenzene (**G-2**) were used as the reactants. The reactions monitored by ^{1}H NMR were conducted on the basis of the designed general procedure for the synthesis of 1,1′-biphenyls presented in Section S1.6, ESI. The spectra were measured (i) in the absence of the catalyst (Figure S53), (ii) in the presence of 0.5 mol% of the cage **5** as the catalyst (Figure S54), or (iii) in the presence of cage **5** (0.5 mol%) as catalyst and **G-6** (100 mol%) as the competing aromatic molecule (Figure S55). Kinetic curves constructed based on the Michaelis-Menten model and the respective Lineweaver-Burk plots are presented in Figures S56-S57. For the details of this methodology, see for example reference [20].

View Article Online
DOI: 10.1039/D0DT01366H

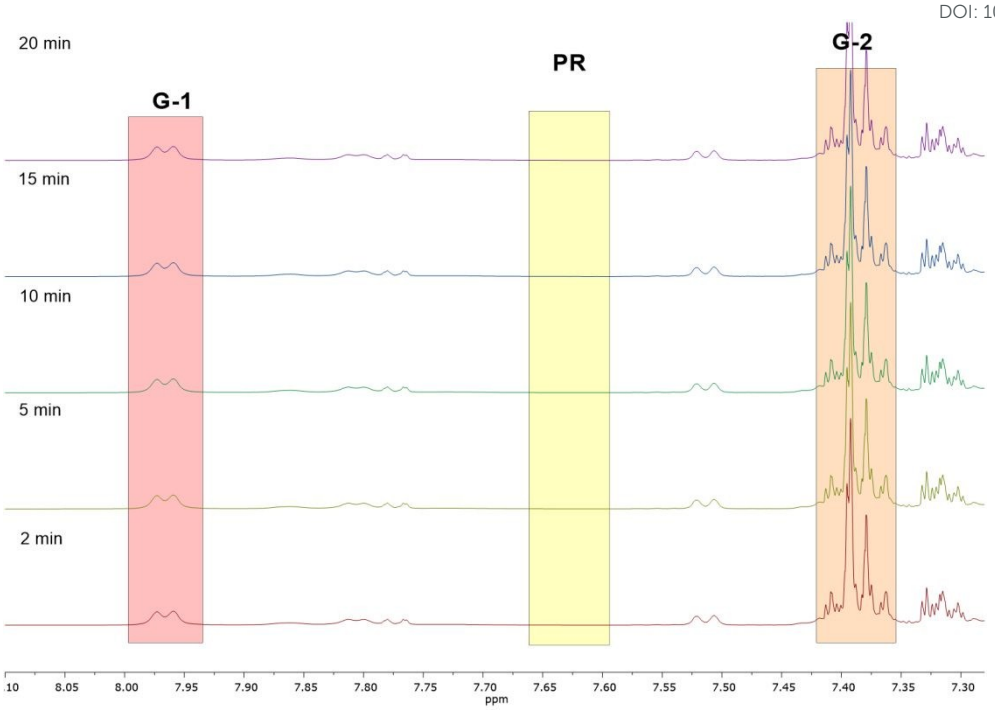

Figure S53. Evolution of ^{1}H NMR spectra during the reaction between phenylboronic acid (**G-1**) and chlorobenzene (**G-2**) without catalyst added. **PR** = product (1,1′-biphenyl). The crucial inset of the spectra is presented. The representative signals' locations for **G-1**, **G-2** and **PR** are marked with colours.

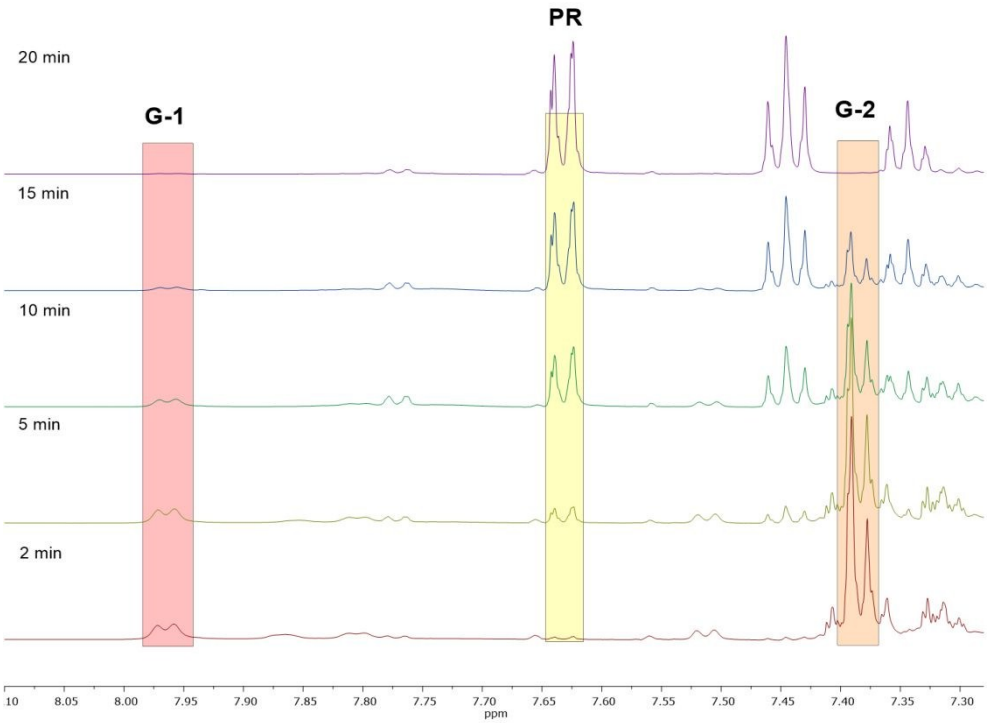

Figure S54. Evolution of ^{1}H NMR spectra during the reaction between phenylboronic acid (**G-1**) and chlorobenzene (**G-2**) in the presence of cage **5** (0.5 mol%) as catalyst. **PR** = product (1,1′-biphenyl). The crucial inset of the spectra is presented. The representative signals' locations for **G-1**, **G-2** and **PR** are marked with colours.

View Article Online
DOI: 10.1039/D0DT01366H

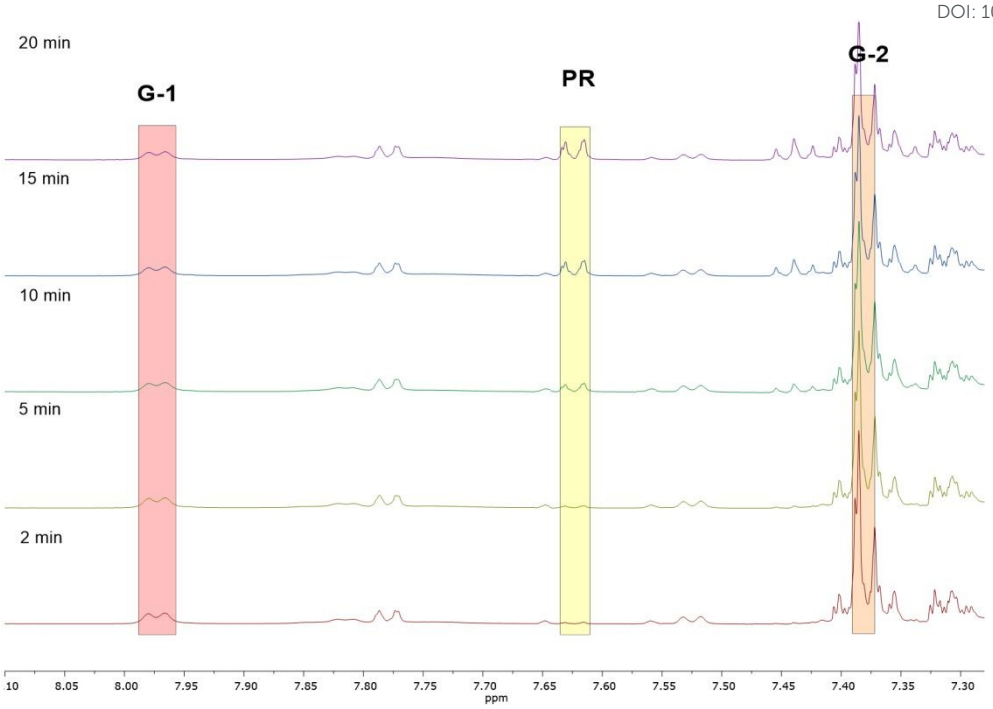

Figure S55. Evolution of ^{1}H NMR spectra during the reaction between phenylboronic acid (**G-1**) and chlorobenzene (**G-2**) in the presence of cage **5** (0.5 mol%) as catalyst and 1-pyrenecarboxaldehyde (**G-6**) as the competing aromatic molecule. **PR** = product (1,1′-biphenyl). The crucial inset of the spectra is presented. The representative signals' locations for **G-1**, **G-2** and **PR** are marked with colours.

View Article Online
DOI: 10.1039/D0DT01366H

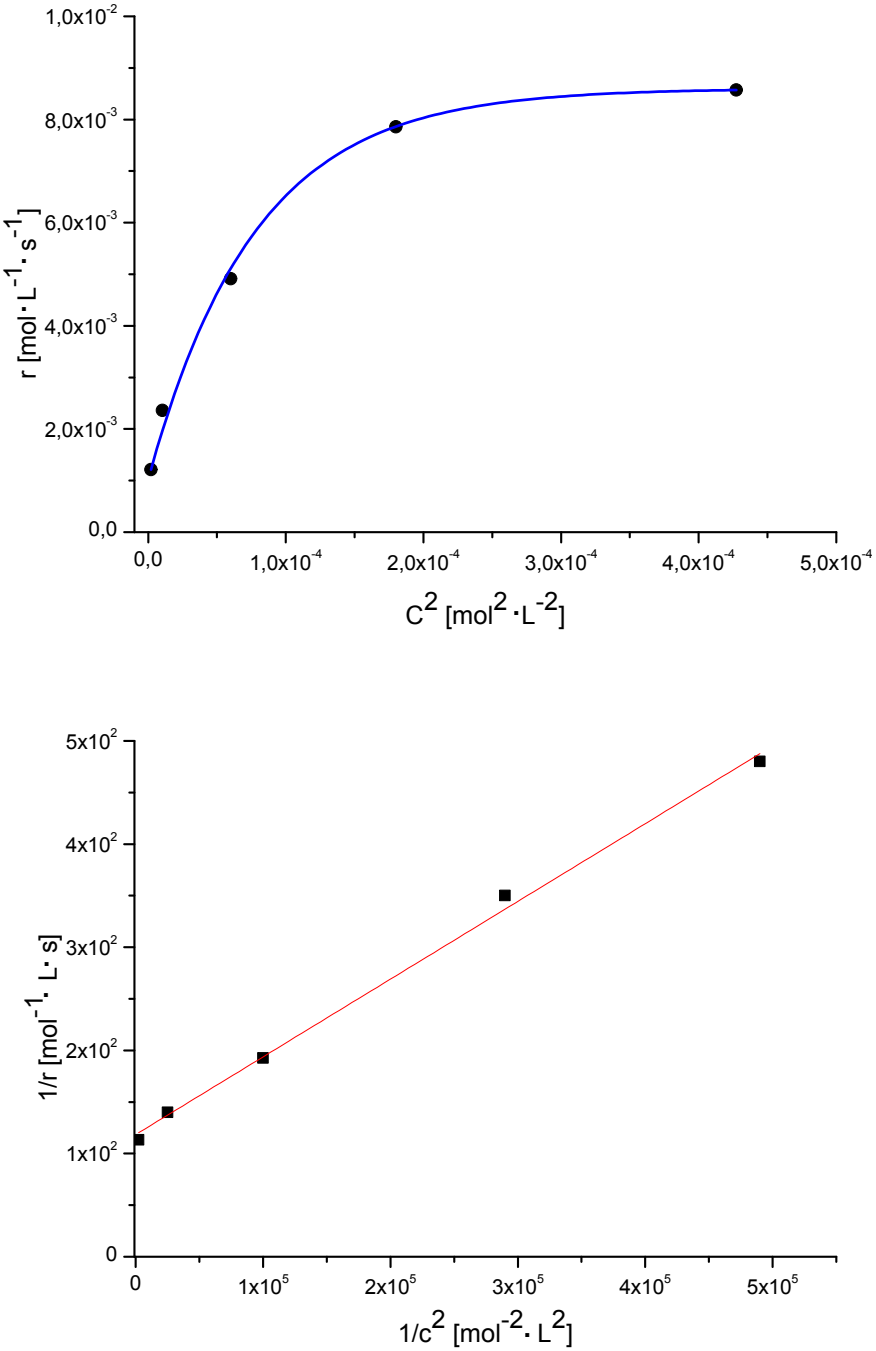

Figure S56. Kinetic plot constructed based on the Michaelis-Menten model (**top**) and the respective Lineweaver-Burk plot (**bottom**) for the reaction in the presence of cage **5** (0.5 mol%) as catalyst (Figure S53), R^2 = 0.9961.

View Article Online
DOI: 10.1039/D0DT01366H

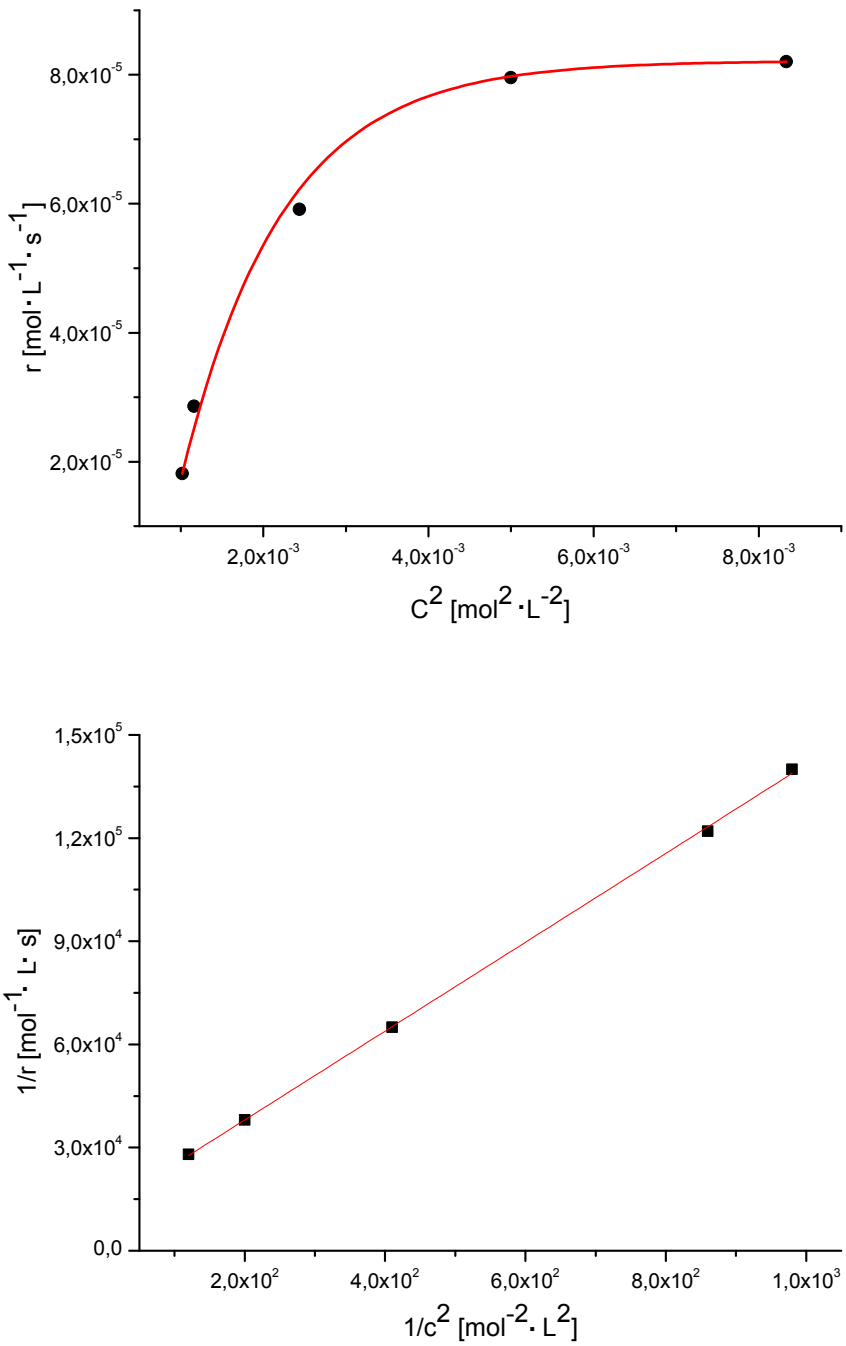

Figure S57. Kinetic plot constructed based on the Michaelis-Menten model (**top**) and the respective Lineweaver-Burk plot (**bottom**) for the reaction in the presence of cage **5** (0.5 mol%) as catalyst and 1-pyrenecarboxaldehyde (**G-6**) as the competing aromatic molecule (Figure S54), R^2 = 0.9996.

S11. ESI-MS spectra of the mixtures of 3 with G-1–G-6

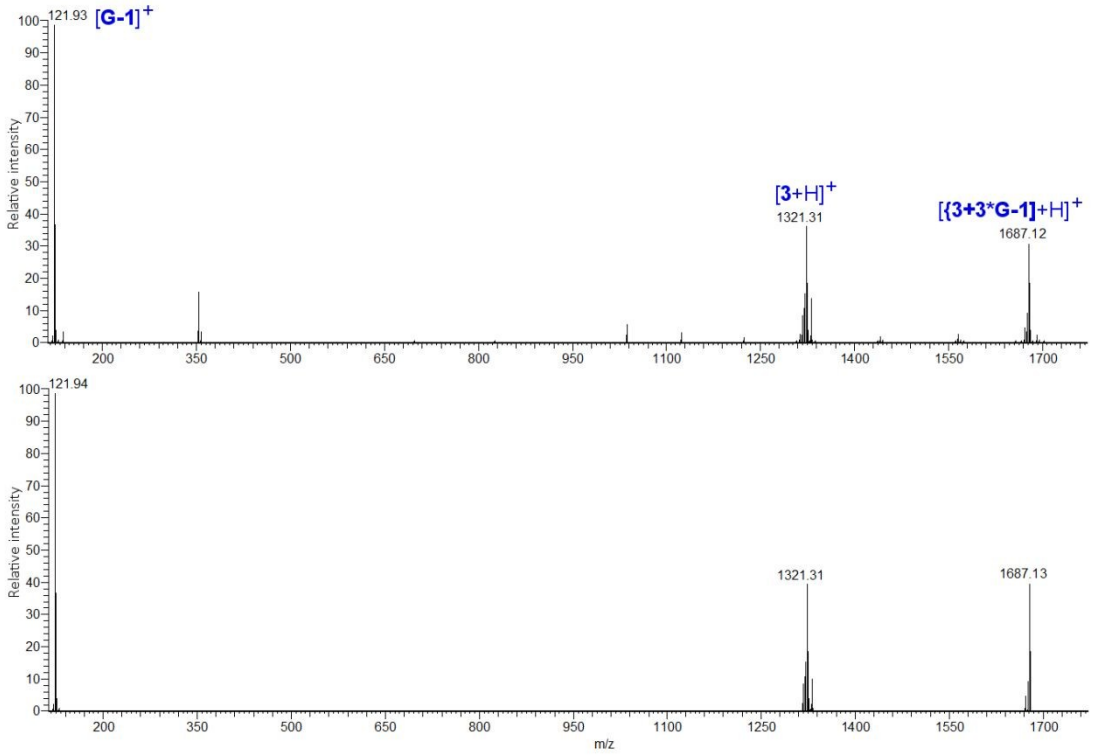

Figure S58. ESI-MS spectrum of 1:3 mol/mol mixture of **3** and **G-1**: top – measured, bottom – calculated (for the mixture comprising 1:3 non-covalent system). The peak of m/z = 1687.12 resembles to the non-covalent system (**3+3*G-1**).

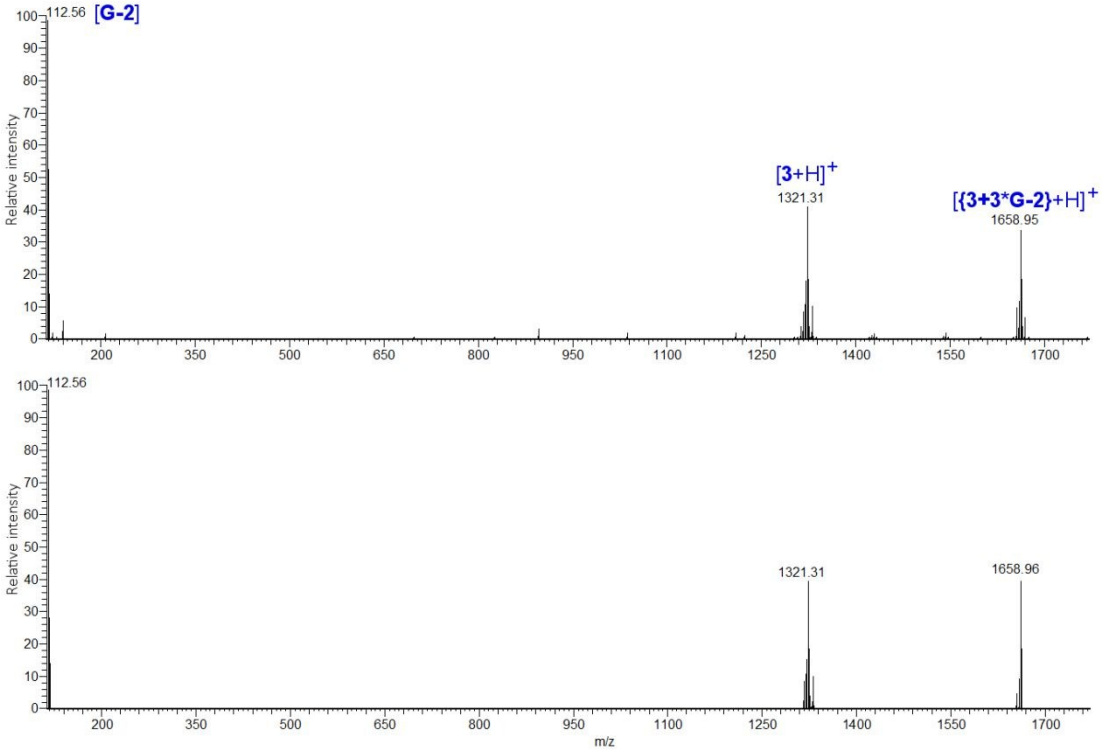

Figure S59. ESI-MS spectrum of 1:3 mol/mol mixture of **3** and **G-2**: top – measured, bottom – calculated (for the mixture comprising 1:3 non-covalent system). The peak of m/z = 1658.95 resembles to the non-covalent system (**3+3*G-2**).

View Article Online
DOI: 10.1039/D0DT01366H

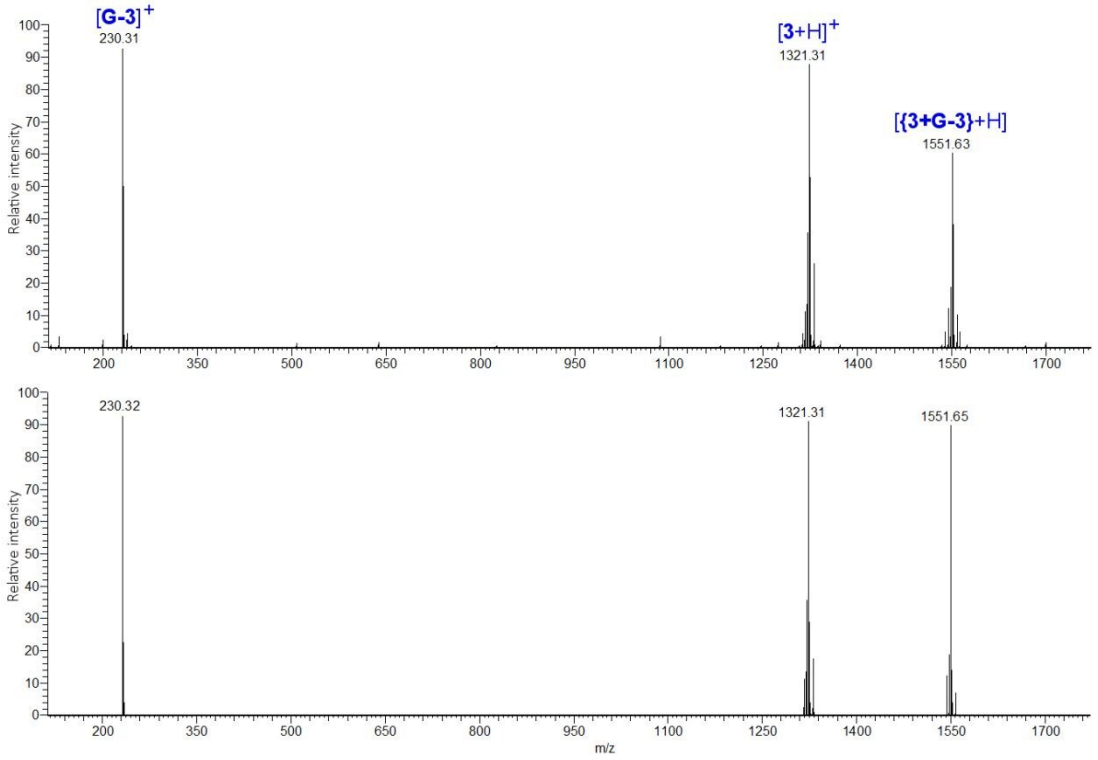

Figure S60. ESI-MS spectrum of 1:1 mol/mol mixture of **3** and **G-3**: top – measured, bottom – calculated (for the mixture comprising 1:1 non-covalent system). The peak of m/z = 1551.63 resembles to the non-covalent system (**3+G-3**).

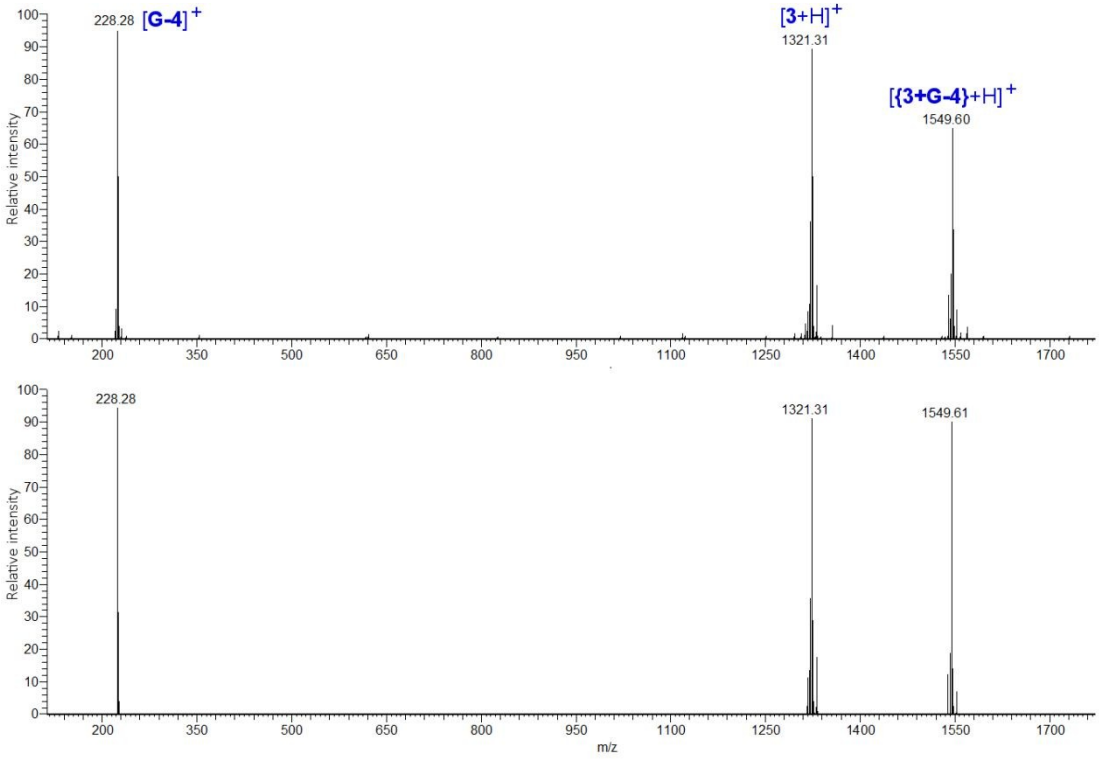

Figure S61. ESI-MS spectrum of 1:1 mol/mol mixture of **3** and **G-4**: top – measured, bottom – calculated (for the mixture comprising 1:1 non-covalent system). The peak of m/z = 1549.60 resembles to the non-covalent system (**3+G-4**).

View Article Online
DOI: 10.1039/D0DT01366H

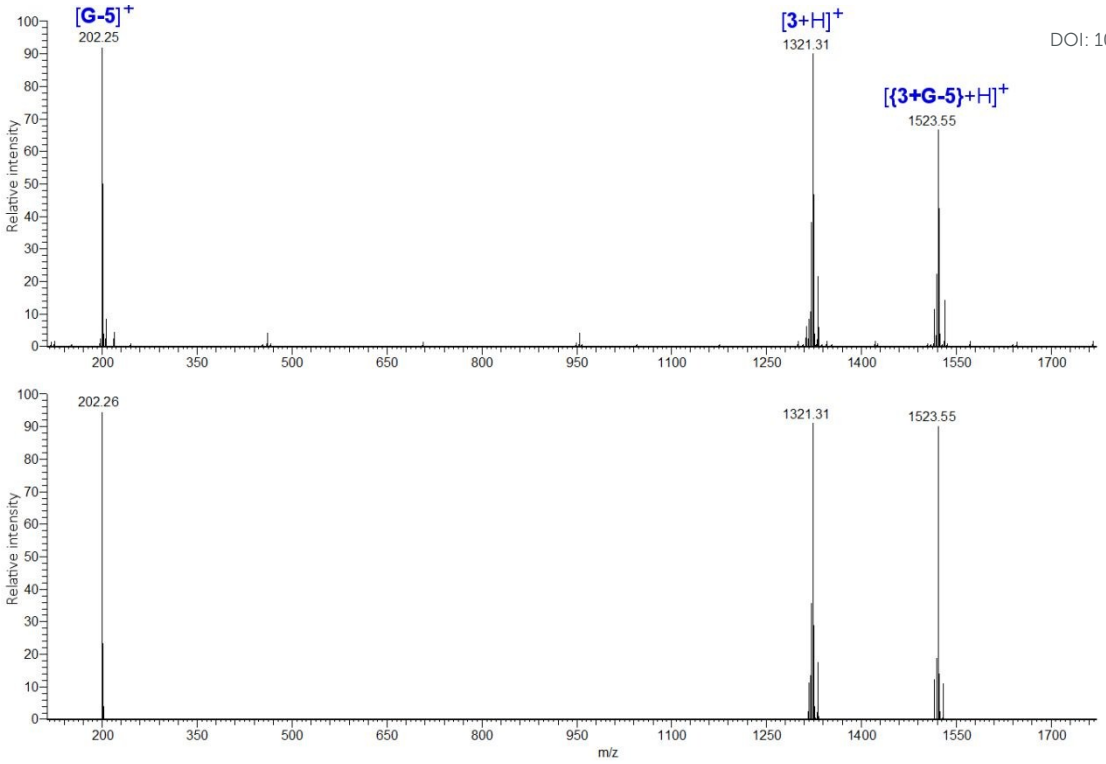

Figure S62. ESI-MS spectrum of 1:1 mol/mol mixture of **3** and **G-5**: top – measured, bottom – calculated (for the mixture comprising 1:1 non-covalent system). The peak of m/z = 1523.55 resembles to the non-covalent system (**3+G-5**).

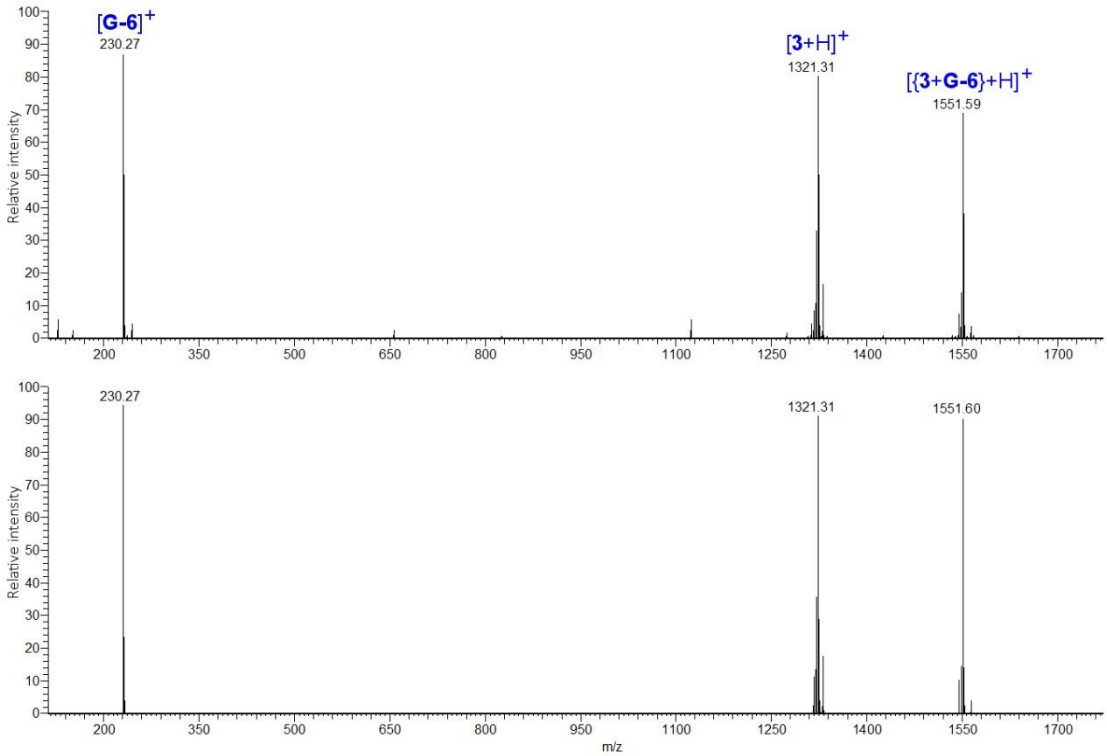

Figure S63. ESI-MS spectrum of 1:1 mol/mol mixture of **3** and **G-6**: top – measured, bottom – calculated (for the mixture comprising 1:1 non-covalent system). The peak of m/z = 1551.59 resembles to the non-covalent system (**3+G-3**).

View Article Online
DOI: 10.1039/D0DT01366H

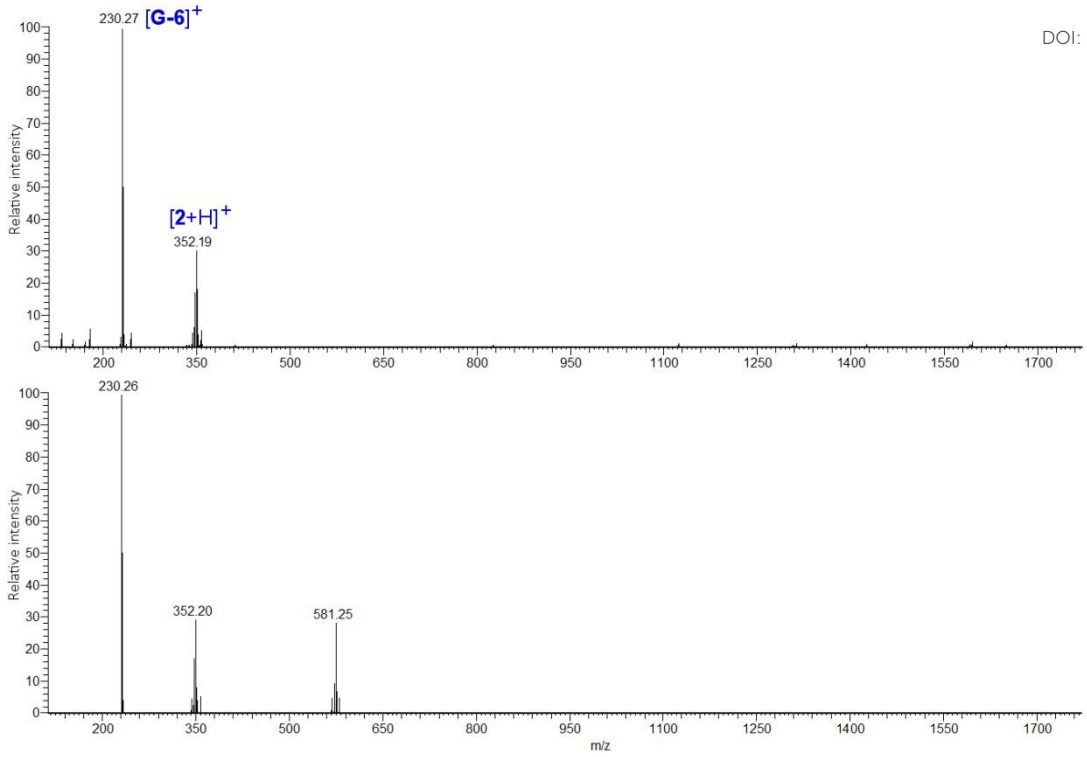

Figure S64. ESI-MS spectrum of 1:3 mol/mol mixture of **2** and **G-6**: top – measured, bottom – calculated (for the mixture comprising potential 1:1 non-covalent system: m/z = 581.25).

S12. References

[1] Wu, D. H.; Chen, A.; Johnson, C. S. *J. Magn. Reson. Ser. A* **1995**, *115*, 260–264.
[2] Jerschow, A.; Müller, N. *J. Magn. Reson.* **1997**, *125*, 372–375.
[3] Xu, W.-Q.; Fan, Y.-Z.; Wang, H.-P.; Teng, J.; Li, Y.-H.; Chen, C.-X.; Fenske, D.; Jiang, J.-J.; Su, C.-Y. *Chem. Eu. J.* **2017**, *23*, 3542-3547.
[4] Luu, H.-T.; Wiesler, S.; Frey, G.; Streuff, J. *Org. Lett*. **2015**, *17*, 2478-2481.
[5] (**a**) see data in Figure S31; (**b**) see data on reactions yields and times in Table 1, main text; (**c**) Steinborn, D. *Fundamentals of Organometallic Catalysis*; Wiley VCH, Weinheim, 2011, ISBN: 978-3-527-32717-1.
[6] Pereira, R.; Cvengroš, J. *J. Organomet. Chem.* **2013**, *729*, 81–85.
[7] *SDBSWeb: Https://Sdbs.Db.Aist.Go.Jp (National Institute of Advanced Industrial Science and Technology, Date of Access – 22.11.2019)*.
[8] Isolated yield.
[9] *CrysAlisPro Software System Ver. 171.40.53*; Rigaku OD: Oxford, UK, 2019.
[10] Sheldrick, G. M. *Acta Crystallogr. Sect. A* **2015**, *71*, 3–8.
[11] Sheldrick, G. M. *Acta Crystallogr. Sect. C* **2015**, *71*, 3–8.
[12] Dolomanov, O. V.; Bourhis, L. J.; Gildea, R. J.; Howard, J. A. K.; Puschmann, H. *J. Appl. Crystallogr.* **2009**, *42*, 339–341.
[13] Spek, A. L. *J. Appl. Crystallogr.* **2003**, *36*, 7–13.
[14] Spek, A. L. *Acta Crystallogr. Sect. C* **2015**, *71*, 9–18.
[15] Pyle, A. M.; Rehmann, J. P.; Meshoyrer, R.; Kumar, C. V.; Turro, N. J.; Barton. *J. Am. Chem. Soc*. **1989**, *111*, 3051-3058.
[16] Kasprzak, A.; Sakurai, H. *Dalton Trans*. **2019**, *48*, 17147-17152.
[17] Jullian, C.; Miranda, S.; Zapata-Torres, G.; Mendizábal, F.; Olea-Azar, C. *Bioorganic Med. Chem.* **2007**, *15*, 3217–3224.
[18] Bakkour, Y.; Vermeersch, G.; Morcellet, M.; Boschin, F.; Martel, B.; Azaroual, N. *J. Incl. Phenom.* **2006**, *54* (1–2), 109–114.
[19] Kasprzak, A.; Koszytkowska-Stawinska, M.; Nowicka, A. M.; Buchowicz, W.; Poplawska, M. *J. Org. Chem*. **2019**, *84*, 15900-15914.
[20] Jiao, J.; Li, Z.; Qiao, Z.; Li, X.; Liu, Y.; Dong, J.; Jiang, J.; Cui, Y. *Nat. Commun.* **2018**, *9*, article number 4423, 8 pages.